RCA REVIEW

a technical journal

RADIO AND ELECTRONICS
RESEARCH • ENGINEERING

VOLUME XII JUNE 1951 NO. 2

RCA REVIEW

GEORGE M. K. BAKER
Manager

CHAS. C. FOSTER, JR.
Editorial Manager

THOMAS R. ROGERS
Business Manager

SUBSCRIPTIONS:

United States, Canada, and Postal Union: One Year $2.00, Two Years $3.50, Three Years $4.50
Other Countries: One Year $2.40, Two Years $4.30, Three Years $5.70

SINGLE COPIES:

United States: $.75 each. Other Countries: $.85 each

Published quarterly in March, June, September, and December by RCA Laboratories Division, Radio Corporation of America, Princeton, New Jersey

Entered as second class matter July 3, 1950, at the Post Office at Princeton, New Jersey, under the act of March 3, 1879

PRINTED IN U.S.A.

RCA REVIEW

a technical journal

RADIO AND ELECTRONICS
RESEARCH • ENGINEERING

Published quarterly by
RADIO CORPORATION OF AMERICA
RCA LABORATORIES DIVISION
in cooperation with

RCA VICTOR DIVISION
RADIOMARINE CORPORATION OF AMERICA
RCA INTERNATIONAL DIVISION
RCA COMMUNICATIONS, INC.
NATIONAL BROADCASTING COMPANY, INC
RCA INSTITUTES, INC.

VOLUME XII JUNE, 1951 NUMBER 2

CONTENTS

PAGE

Practical Considerations in the Use of Television Super Turnstile and Super-Gain Antennas 159
H. E. GIHRING

A Diversity Receiving System for Radio Frequency Carrier Shift Radiophoto Signals 177
J. B. ATWOOD

Rapid Determination of Gas Discharge Constants from Probe Data.. 191
L. MALTER AND W. M. WEBSTER

A New Television Studio Audio Console 211
R. W. BYLOFF

A Storage Oscilloscope 220
L. E. FLORY, J. E. DILLEY, W. S. PIKE AND R. W. SMITH

Graphechon Writing Characteristics 230
A. H. BENNER AND L. M. SEEBERGER

Methods to Extend the Frequency Range of Untuned Diode Noise Generators 251
H. JOHNSON

High-Speed Ten-Volt Effect 258
R. M. MATHESON AND L. S. NERGAARD

Direct-Reading Noise-Factor Measuring Systems 269
R. W. PETER

RCA TECHNICAL PAPERS 282
CORRECTIONS 284
AUTHORS 285

RCA Review is regularly abstracted and indexed by *Industrial Arts Index Science Abstracts* (I.E.E.-Brit.), *Engineering Index, Electronic Engineering Master Index, Abstracts and References (Wireless Engineer*-Brit. and *Proc. I.R.E.)* and *Digest-Index Bulletin*.

RCA REVIEW

PRACTICAL CONSIDERATIONS IN THE USE OF TELEVISION SUPER TURNSTILE AND SUPER-GAIN ANTENNAS*

By

H. E. Gihring

Engineering Products Department, RCA Victor Division,
Camden, N. J.

Summary—*Some general considerations with respect to gain, patterns, diplexing and bandwidth of television broadcasting antennas are presented. Applications of the Super Turnstile and Super-Gain antennas are discussed. A special application of the Super-Gain antenna as used in the new Empire State antenna is presented in detail.*

Introduction

SINCE the power level of transmitters usually is established on an industry-wide basis and since the effective radiated power required by different stations varies widely depending on a number of factors, the antenna system must in many cases be tailored to fit the specific requirements of a given installation. Some of the factors that influence the choice of a television antenna system are:

1. The effective radiated power (ERP) required.
2. The shape of the service area to be covered.

The ERP required depends upon the size of the area to be covered and the height above average terrain that can be achieved by means of towers or mountain top locations. Tower heights in turn depend upon the location of airways, the availability of land for a tall guyed structure, and cost. The shape of the service area is determined by its geography, including the proximity of large bodies of water, and sometimes by the presence of an existing transmitter plant which may dictate a directional pattern for best coverage.

While it is usually desirable, from a cost angle, to use available standard types of antennas, such an investment is a poor one if coverage requirements are not fulfilled. It is the purpose of this article to present some of the possibilities that exist and some of the more recent trends in television antennas.

Theory

A review of some of the fundamental theory involved in television

* Decimal Classification: R326.6.

antennas may be helpful. Some of the factors involved are discussed below.

A. Gain

The gain of omnidirectional linear arrays which are uniformly illuminated by a continuous current sheet can be reduced to a fairly simple expression.[1] For sufficiently tall antennas, the gain approaches the asymptotic expression, $G = 1.22\,D$, where D is the aperture in wavelengths and gain is expressed relative to a half-wave dipole. When N equal, properly designed, discrete elements are evenly spaced at intervals of S wavelengths, the same formula becomes $G = 1.22\,SN$.

Since these formulas are asymptotic expressions, the calculated gains can be only approached in practice. The closest approach is for current sheet type of radiators many wavelengths high. Variations below the values given can be attributed to non-uniform illumination and practical tolerances due to mechanical dissymmetries which affect current distribution and phasing.

While the above expression will give a maximum value for a given aperture, actual values must be computed taking non-uniform illumination into account. In practical antennas constructed to date like the Pylon, the Super Turnstile and the Super-Gain, fairly uniform illumination has been possible so that the practical values are within 5 to 10 per cent of the asymptotic expression: $G = 1.22D$. These computations can be checked against the actual antenna or a scale model by various methods, as follows:

1. **Absolute field strength determination**—This is the least satisfactory method since field strengths in the television band cannot usually be determined closer than ±20 per cent because of calibration errors and local effects. This will result in a power-gain determination which is accurate by about 2:1. An additional disadvantage is that a normal field must be calculated from FCC curves or by some other method which can be done with reasonable accuracy only for smooth terrain with no obstructions. Hence, this method, in general, is not very satisfactory for the determination of power gain.

2. **Standard dipole comparison**—In this method, a calibrated dipole is placed at the center of the antenna and power is fed alternately into the antenna and the dipole while comparative readings are taken. This method is better than the first method, but unless a number of radials are carefully taken in a number of directions for each condition, results are likely to be inaccurate, especially if the local terrain is rough or if there are many obstructions. A complete survey with both

[1] R. W. Masters, "Special Antenna Considerations", unpublished report, October 13, 1948.

the dipole and the complete antenna is necessary to obtain a fair degree of accuracy.

3. **Vertical pattern determination**—Since gain is really a function of the vertical directivity of the antenna, determination of the vertical pattern is the best method of determining gain. This can be accomplished either by the use of a complete antenna or a scale model, since pattern work can usually be scaled quite accurately. In this method, the antenna is mounted on its side and pivoted about its mid point. The antenna is then energized at the frequency at which the pattern is desired. A receiving point is located far enough away so that the length of the antenna is negligible compared to the distance to the receiving point. The antenna is then rotated and a determination of the amplitude and angle of all the lobes is made. This information can be plotted and a gain determination made by means of a planimeter. This method has the additional advantage that the location and amplitude of the lobes are known which is often a factor in determining the value of the antenna for a given application.

Obviously, this method cannot be applied after the antenna is installed. In many cases, it cannot even be applied on the actual antenna since the rotation of a Super-Gain antenna 200 feet in length becomes a major engineering feat. Hence, such work is usually done by means of scale models. There is under construction a huge turntable which will make it possible to rotate antennas up to 140 feet in length.

The gain measurement obtained by this method is known as the directivity gain and takes no losses of any kind into account. Antenna gain has not been too strictly defined. However, here it has been taken to mean that figure by which the transmitter power can be multiplied to obtain the ERP of the station, taking only the main transmission line losses into account. All other losses must be reflected in the antenna gain figure. Some of these losses are:

1. Feedline losses, which are the losses between the junction box and the radiators themselves.
2. Diplexer losses.
3. Power equalizer losses.

As a typical example, suppose that the directivity gain is 12.5 as determined by actual calculations. The asymptotic gain as determined from $G = 1.22\ \lambda$ in this particular case was 13.2 indicating that uniform illumination was achieved within a few per cent. If the feedline losses are 10 per cent, the power equalizer loss 2 per cent, and the diplexer loss 2 per cent, the net gain would be 11.1. This is the figure quoted in the specifications.

B. Horizontal Pattern

As will become apparent when diplexing and power equalizing are discussed, the use of quadrature feed, or turnstiling, is a highly desirable feature. In this arrangement, the north-south and east-west radiators are fed with currents phased 90 degrees apart. If the field is unity in the north-south and east-west directions, the value of the field from each radiator at 45 degrees from the normal to the tower will be .707. Hence, at 45 degrees there will be two values of .707 from the two adjacent faces added in quadrature which will give a value of unity. This is true at all angles at which radiation is received from both sets of radiators since the resultant field of two fields having cosine distribution added in quadrature is unity. This consideration is true for point sources. In a practical case, radiation usually does not emanate from point sources and hence the horizontal pattern is circular within ±1.5 decibels for the Super Turnstile type of antenna and ±2 decibels for the Super-Gain antenna. Advantage can be taken of these slight variations in orienting the antenna to obtain better coverage in certain directions.

C. Vertical Pattern

The vertical pattern was discussed above. The angle between the half-power points of the main beam can be determined from the formula

$$a = \frac{61}{G},$$

where a is the total angle between half-power points, and G is the directivity gain of the antenna (not net gain). This formula, again, assumes uniform current distribution although values obtained with ordinary antennas are accurate enough for the usual type of calculation. In mountain top locations where coverage is desired close to the base of the mountain, this vertical angle must be taken into account in specifying an antenna. Where the angle required is quite broad thus limiting the gain, it is possible to tilt the vertical beam downward by small amounts which will help this situation. This beam tipping can be accomplished by feeding the upper and lower parts of the antenna separately. The phasing of one of these groups can be arranged to provide a slight change in vertical angle without any material sacrifice in gain.

D. Bandwidth

In order to avoid reflections from the antenna, a voltage-standing-

wave ratio measured at the input should not exceed 1.1 over the visual band. There are two basic methods of obtaining bandwidth.

1. The use of inherently broad-band radiators which depend upon complementary reactance slopes. For instance, a combination of a parallel resonant and series resonant circuit will give a reactance slope which tends to remain constant over a fairly wide frequency band. See Figure 1. A dipole with a stub is such a device. The reactance slope of the dipole is similar to a series resonant circuit while the stub behaves like a parallel resonant circuit.

2. When the radiator itself has been made as wide as possible by the above means, power equalizing[2] is a means of obtaining even greater bandwidths, or of using antennas whose bandwidth is otherwise too narrow. The action of the power equalizer can be seen from Figure 2. This figure depicts two basic systems which may be employed in feeding an antenna. Figure 2a makes use of a bridge type diplexer and a notch type power equalizer.

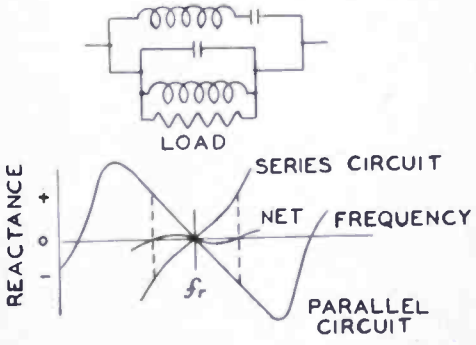

Fig. 1—Parallel resonant circuit and series resonant circuit adjusted to obtain complementary impedances to increase bandwidth.

Power equalizing makes use of the fact that the N-S and E-W elements of an antenna can usually be made symmetrical. Hence, the reflection from both halves of the antenna will be equal. However, the reflected components on the righthand side of Figure 2a will pass through the 90-degree phasing loop twice and thus be retarded 180 degrees. Since the reflected components are now out of phase because of the 180 degrees phase difference, they will not re-enter the picture transmitter but pass on down the sound line. Due to the frequency difference between the picture and sound transmitters, the reflected energy can be trapped out by a suitable notch power equalizer. Figure 2a is the system normally employed with a two-line feed. Figure 2b shows how the same principle can be applied to a single-line feed. In this case, picture and sound carriers are combined by means of a notch-type diplexer and transmitted over one line to the antenna. At

[2] R. W. Masters, "A Power Equalizing Network for Antennas", *Proc. I.R.E.*, Vol. 37, No. 7, p. 735, July 1949.

this point, a bridge-type power equalizer is inserted which functions in the same fashion in that reflections are delayed 180 degrees and enter the resistor instead of traveling back down the line.

While it may seem that the loss of this reflected energy is undesirable, the effect is negligible when the standing-wave ratios are of a reasonable value. The power dissipated in the resistor is proportional to the square of the reflection coefficient. For instance, if the

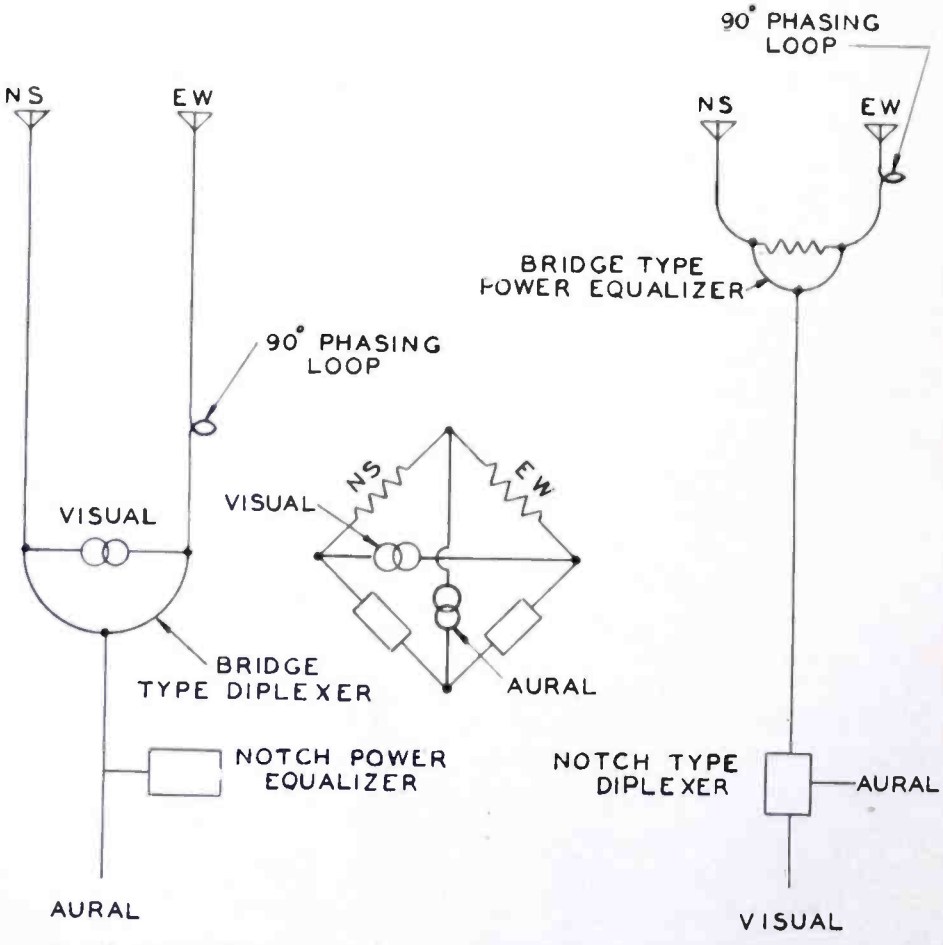

Figs. 2a (left) and 2b (right)—Two methods of "power equalizing" an antenna using double-line or single-line feed.

standing wave ratio is 1.22, the reflection coefficient is 10 per cent, and only 1 per cent of the power is lost in the power equalizing resistor.

An additional advantage of power equalizing is the fact that it forces equal power into the north-south and east-west elements thus maintaining a circular pattern. For instance, if the standing wave ratio were 1.2 on the north-south radiators, it would be .8 on the east-west radiators. By reason of the phase delay in the 90-degree section,

this difference in voltage-standing-wave ratio would cause a difference in pattern of over 2.1 in the north-south and east-west directions if it were not corrected by the power equalizer.

E. Diplexing

As shown above, two methods of introducing picture and sound carriers on one antenna are possible. The first is known as bridge diplexing and the second as notch diplexing. Bridge diplexing is so called because it has the characteristics of a Wheatstone bridge which is obvious from an inspection of Figure 2a. The isolation between picture and sound is a function of the similarity between the north-south and east-west antenna elements. An isolation of 20 to 30 decibels usually can be achieved. This has been shown in practice to be more than adequate.

In order to combine picture and sound carriers and feed them to the antenna by means of a single transmission line, a notch diplexer is required. In this method, a notch is placed in the picture bass band centered about the sound carrier and the elements of the filter are so constructed that there is negligible mutual interaction between picture and sound carriers. A new type of notch diplexer has been developed which presents a constant impedance to the transmitter over the entire television band.

The above principles constitute the theoretical background of the more important principles used in our antenna designs and are valuable in understanding the applications of the antennas.

Television Antennas

Both Super Turnstile and Super-Gain antennas have been used commercially. The present television spectrum can be covered with three Super Turnstile types; namely, 54-66 megacycles, 66-88 megacycles, and 174-216 megacycles. The low-band types (54-88 megacycles) have been built using 3, 4, and 5 bays. 6-bay antennas are contemplated and can be built. In the high band (174-216 megacycles) about 30 of the 6-bay antennas are in use commercially. An additional feature of the low-band antennas in the 66-88 megacycle band is that they can be triplexed with a frequency-modulation (FM) carrier with up to 10 kilowatts of power. This requires an additional unit known as a triplexer. The present units are suitable for only 5 kilowatts of television power.

For the range of sizes listed, it is felt that the Super Turnstile antenna provides the most gain for the minimum cost. As the height

of the antenna increases, however, other types may become more desirable. In order to permit much higher gain and other special applications, the Super-Gain antenna was developed. The Super-Gain antenna has been described in the literature.[3]

It consists basically of a dipole in front of a screen ½ wavelength wide. The dipole is spaced in front of the screen for maximum bandwidth considerations. Four of these screens can be fastened on the four faces of the tower to obtain an omnidirectional pattern. The advantage of this arrangement is that a tower type structure can be used with a cross-sectional area great enough so that fairly high structures can be accommodated. Super-Gain antennas do not materially extend coverage if the lowest bay is too close to the ground since the center of radiation is thus lowered. As a general rule, the center of the antenna should be above ground by twice the aperture of the antenna.

The Super-Gain antenna also has other important advantages. One of these is its ability to give a variety of directional patterns. While the Super Turnstile antenna is limited basically to figure-of-eight, or peanut-shaped patterns, a wide variety of patterns can be obtained from the Super-Gain antenna by energizing 1, 2, 3 or 4 faces of the tower with currents of various phases and amplitudes. Figures 3 and 4 show some practical patterns that have been calculated for installations requiring directional patterns. In both cases, the antennas were situated adjacent to a large body of water. The service area extended along this body of water and inland. Hence a specially shaped pattern was indicated to obtain the maximum results from the power used.

The Super-Gain antenna is the only commercially available television antenna which can give directional patterns. The antenna can be installed with an omnidirectional pattern and later changed to a directional pattern if that should become desirable.

It is felt that one of the most important features of the Super-Gain antenna is the fact that a number of antennas may be stacked at a single location. An excellent example of this is the Empire State multiple antenna system which will be discussed in more detail below. Because of the relatively large cross-section required for the Super-Gain antenna, substantial towers can be built which can accommodate five antennas or even more if desired. In the case of the Empire State antenna, a Super Turnstile antenna was combined with the Super-Gain. In other cases, FM antennas such as the Pylon can be placed on

[3] L. J. Wolf, "High Gain and Directional Antennas for TV Broadcasting," *Broadcast News*, Vol. 58, March-April, 1950.

top of such a stack, or the FM antennas can be worked into the Super-Gain array. The system is extremely flexible.

The importance of a single television center in metropolitan dis-

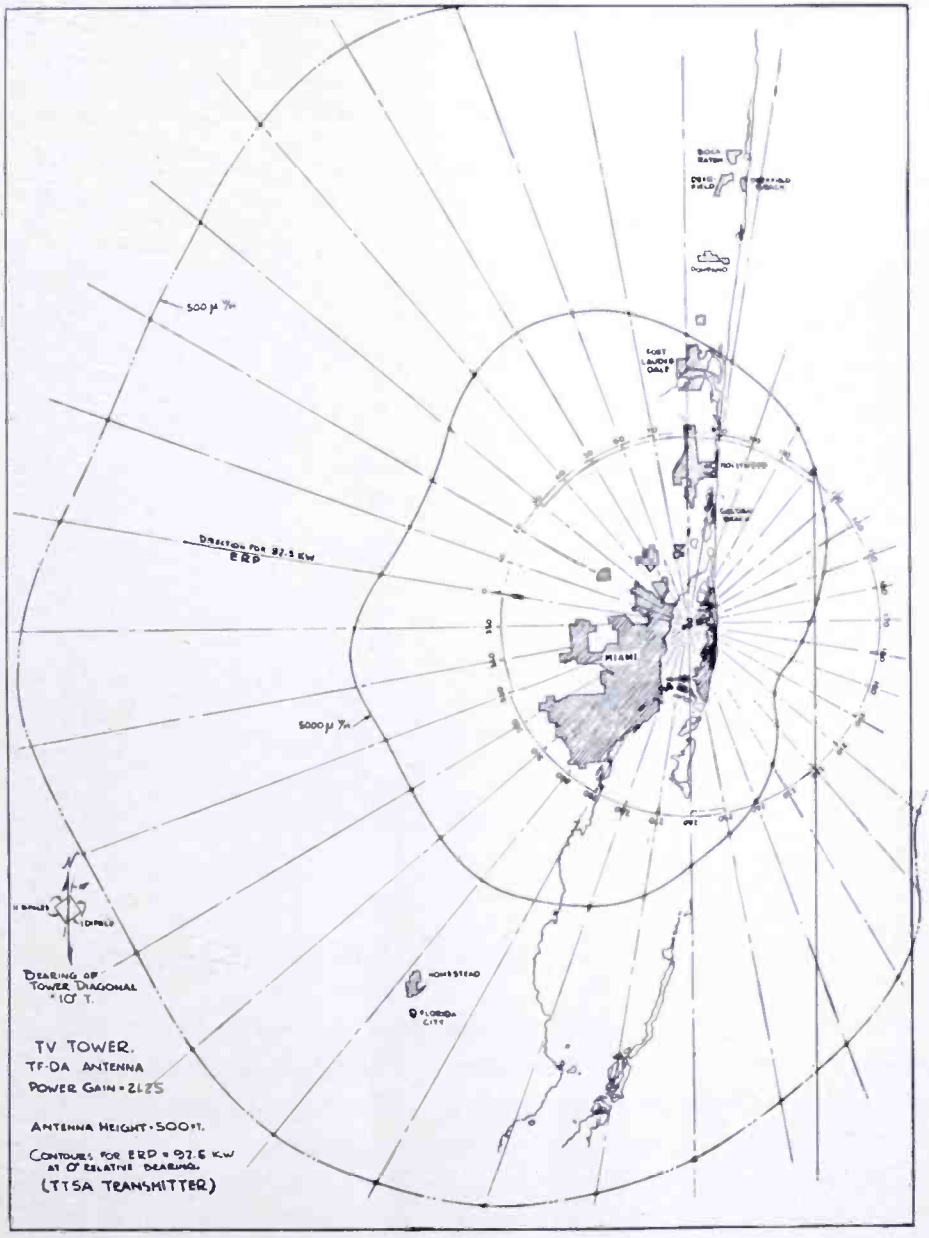

Fig. 3—Directional pattern employed to obtain optimum results with available power when station is adjacent to large body of water.

tricts is fast becoming apparent. It has many advantages, but the greatest is that all of the receiving antennas in the service area can be oriented in one direction. In an area where there is no single television center, compromises are often necessary in the orientation of

receiving antennas. If two or more stations start broadcasting from a central location, the probability is that most of the receiving antennas will be oriented in that direction. Hence, the service rendered by stations not in this central location may be degraded at a sizeable number of receiver locations.

Empire State Antenna

Formerly, only one television antenna was located atop the Empire State Building. Six other stations were located in various parts of the metropolitan area. All except two were located in Manhattan. Most

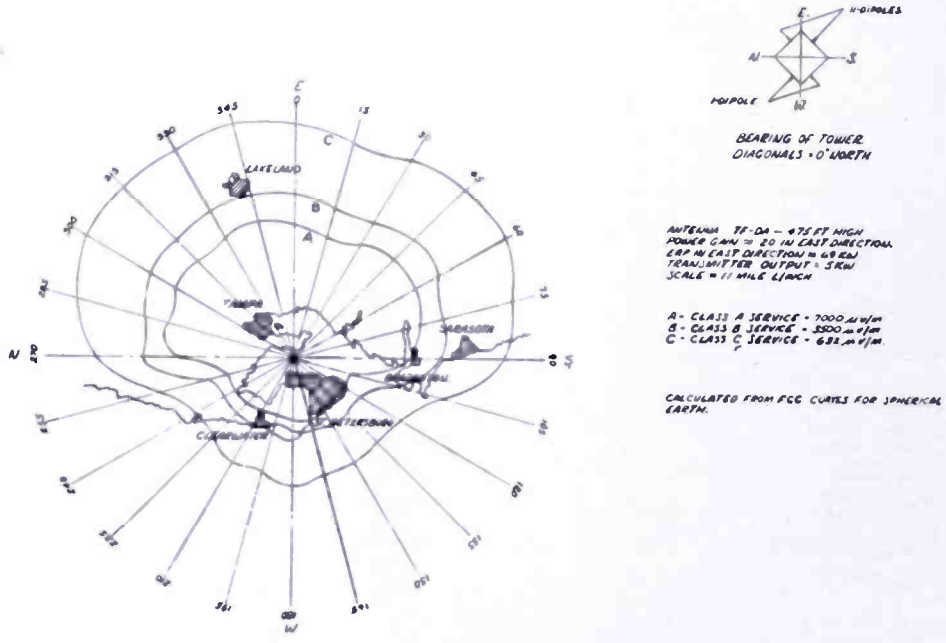

Fig. 4—Directional pattern—same problem as Figure 3.

of these latter stations gave poor signals in certain areas, either because of ghosts from some of the larger buildings such as Empire State and Radio City or because of shadows. Hence, consideration was given to locating other stations on the Empire State Building. At the present time, provision is being made for a Super Turnstile antenna on Channel 4, and four stacked Super-Gain antennas on Channels 11, 7, 5 and 2. Besides these main television antennas, a number of emergency and FM antennas are contemplated.

Specifications included a voltage-standing-wave ratio (VSWR) of 1.1 over the visual band and 1.5 over the aural band; a circularity of ±2 decibels, a power handling capacity of 100 kilowatts ERP; a directivity gain of 4 for the low band stations and 5 for the high band stations; and a decoupling between antennas of 26 decibels. The first

two requirements are those normally encountered in any Super-Gain antenna design. The third requirement necessitated the design of a special feed system utilizing RG-35/U cable. This turned out to be a much larger job than had been anticipated because of the problems involved in the connectors. The junction boxes required a design which would receive these special connectors and also maintain the proper impedance without discontinuities. Considerable experimental work was necessary to accomplish this requirement. Figure 5 depicts a junction box and feed cable. The order of gain required for the Empire State installation is normally covered by the Super Turnstile an-

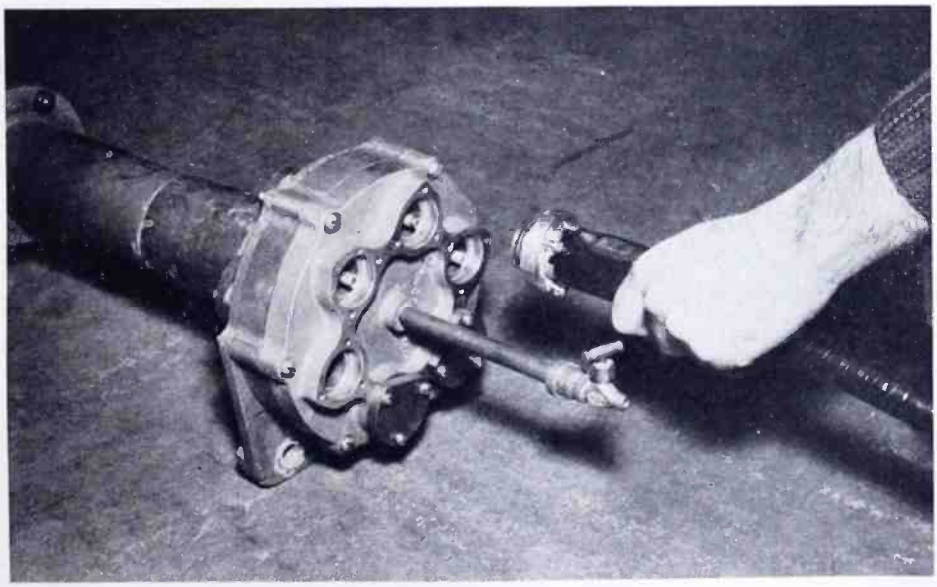

Fig. 5—Junction box and feedline for Empire State antennas.

tenna. Hence, some special work was necessary to determine the maximum amount of gain that could be achieved in the aperture permitted on top of the building. It was determined by the structural people, after considerable calculation, that 217 feet was the limit to which the tower could be safely built. Hence, this limited the aperture for each antenna. Determination of gains was done on Channel 7 by obtaining the vertical patterns as described above. Since gain information can be readily scaled, this information was scaled to the other antennas involved. It was found that the specifications for gain could be met.

Since little previous experience was available with reference to coupling between antennas, considerable thought was given to this aspect of the problem. Coupling between stations was broken down into antenna to antenna, antenna to transmitter, and transmitter to trans-

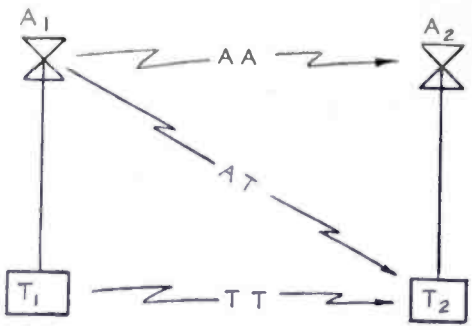

Fig. 6—Possible types of interference in multiple antenna systems.

mitter types as shown on Figure 6. Obviously the antenna design cannot take account of the first or last types since these are the function of shielding the transmitter or transmitter room. Neither can the antenna design take account of harmonics since harmonics are generated in the transmitter and must be attenuated to a non-interfering level at that point. Hence, the only type of interference considered was antenna to antenna interference between carriers.

In order to approach the coupling problem, single screens and dipoles were placed adjacent to each other as shown in Figure 7. A signal was fed from an oscillator into A in series with the measuring line. The product of the maximum and minimum voltage readings established a relative power level which was held constant throughout the measurement. At first, the output of the measuring line was fed directly into the field intensity meter for calibration purposes as shown by the dotted line. Then, the output was connected back into

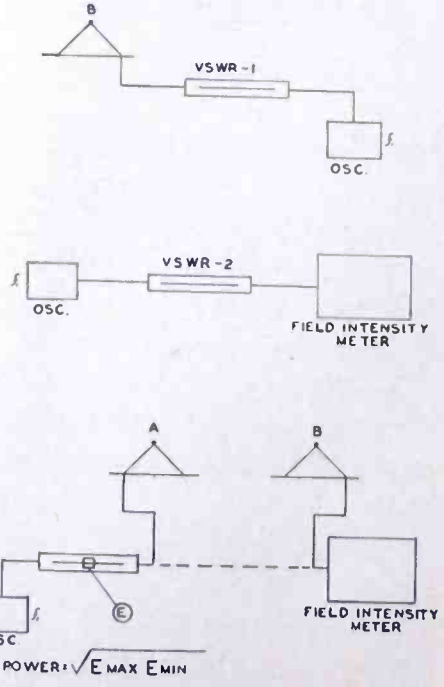

Fig. 7—Method of making coupling tests.

antenna A, and the field intensity meter to antenna B, and the drop, in decibels, between these two readings was determined. This value must be reduced by two additional values which represent the mismatch loss as a result of VSWR 1 and 2 as shown on the diagram. In this way, the worst condition is assumed; namely, that the receiving impedance (which would normally consist of a transmitter) is the conjugate of the sending impedance.

The result of these tests with single screens indicated that the proper order of decoupling could be achieved. Accordingly, plans were

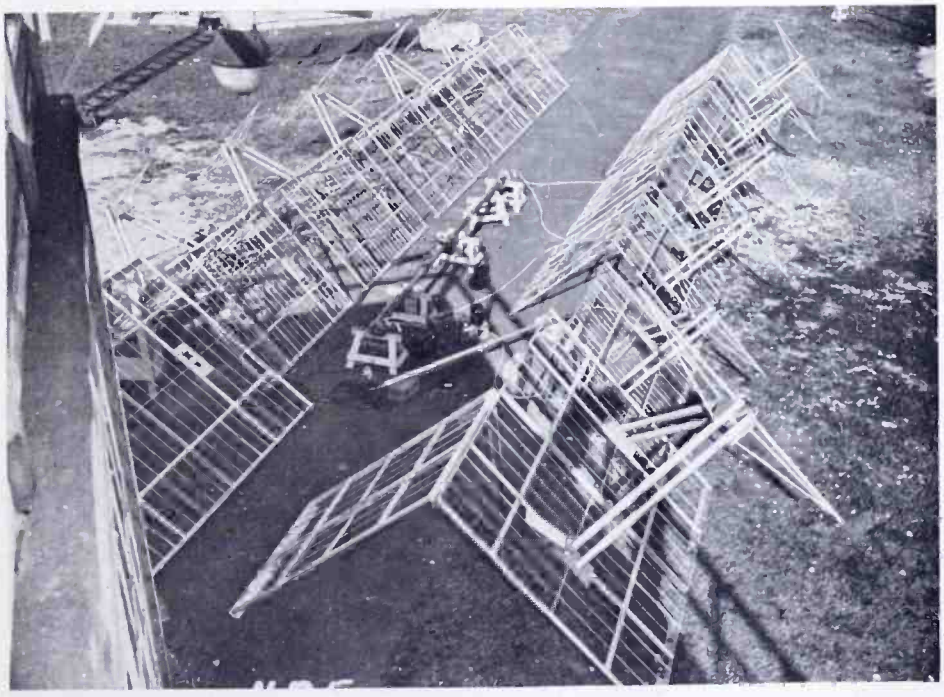

Fig. 8—Tests of Channel 5 Empire State antenna on ground to determine VSWR over the band.

made to proceed with the balance of the work. The final antennas, screens and feed systems were obtained and were first tested on the ground (see Figure 8) to determine that impedances over the band were within the specifications. Meanwhile, four towers were erected for each adjacent pair of antennas. Thus, there is one tower for Channels 4 and 11, one for 11 and 7, one for 7 and 5, and one for 5 and 2 (see Figures 9 and 10). Adjacent antennas were placed on these towers and tests were repeated for standing-wave ratio over the band to determine any discrepancies between these tests and the ground tests. After this, the coupling measurements were made by the same method as described above. The actual assembly on the tower was also a mechanical assembly and weathering test intended to weed

out as many problems as possible in advance of the actual installation on the Empire State Building.

Since each of the broadcasters owns his own antenna, as much flexibility as possible was permitted in determining his particular system. Figures 11 and 12 are systems diagrams for a low- and high-band antenna showing the various components used. Two of the low-band stations chose to split up the bays into 2 and 3 bays respectively, thus creating substantially two separate antennas which are fed separately from the transmitter room. At the transmitter room, a wye connector is used which consists of three transformers in a branch

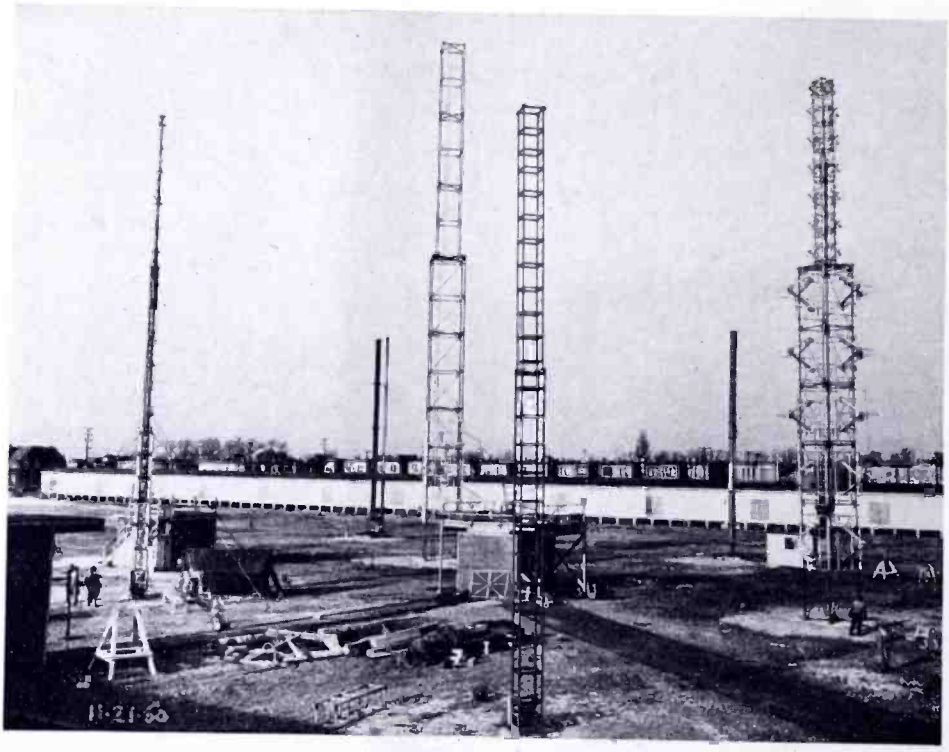

Fig. 9—General view of test towers used for Empire State antennas. Each tower accommodates two adjacent antennas.

circuit so that each antenna receives its proper amount of power and so that the impendance presented to the transmitter is 51.5 ohms. The purpose of this split feed is to provide for an emergency antenna since the likelihood that both halves will fail at the same time is very remote. A simple manual switching arrangement permits either one or the other antenna to be used. It will be noted that the other stations elected not to use this arrangement since they have other emergency provisions.

It will also be noted that Channels 2 and 5 use the notch diplexing arrangement, while the high-band stations use bridge diplexing. When

the bridge diplexer is used, a notch power equalizer is required in the sound transmitter line in order to prevent reflected energy from radiating and also to stay within a pattern circularity of ±2 decibels.

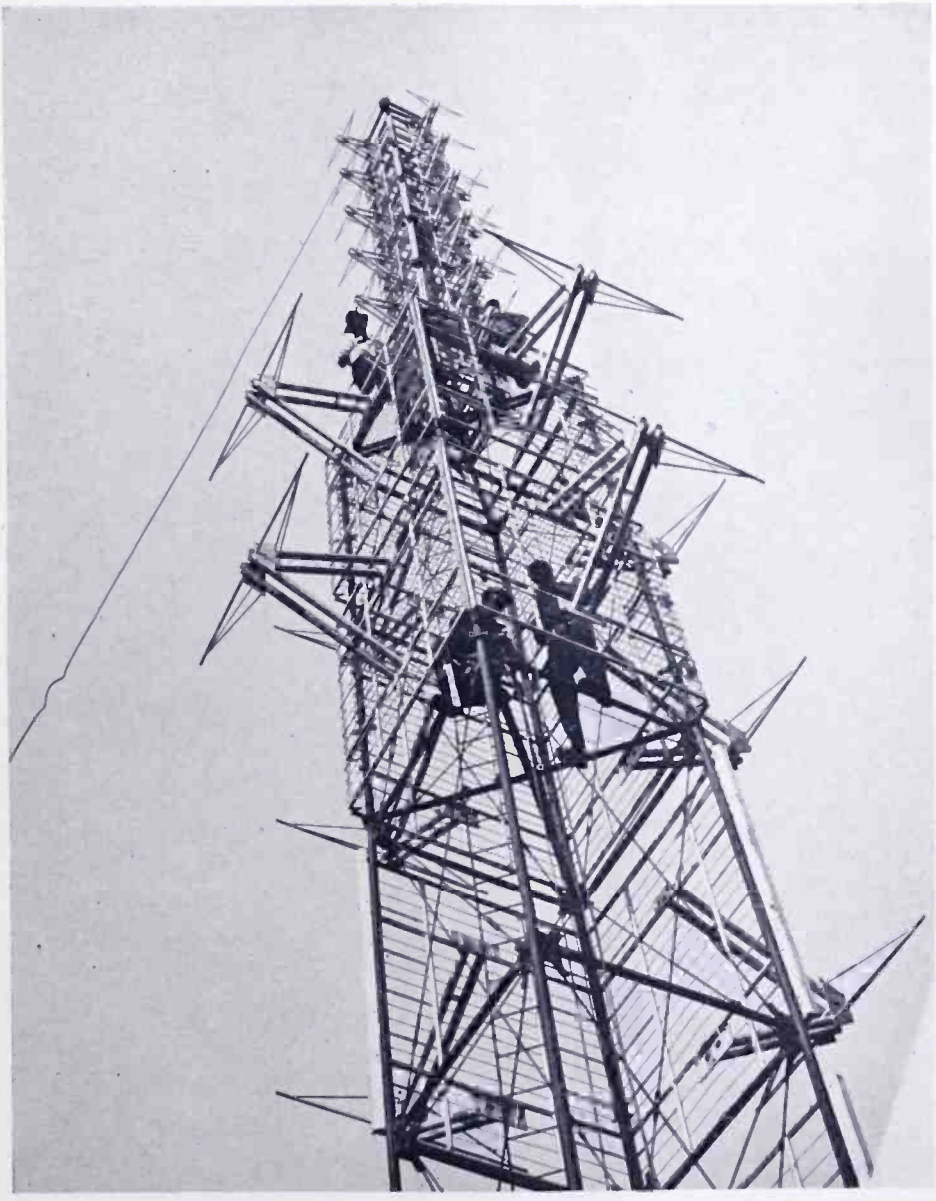

Fig. 10—View of Channel 5 and 7 antennas mounted on test tower.

In all of these installations, much of the operation with respect to power equalizing and diplexing depends on the inherent symmetry on the north-south and east-west sides which includes the transmission line when bridge diplexing is used. Hence, extreme care must be exercised in making a symmetrical installation all the way into the sta-

tion. Much thought and care were given to this phase of the planning. Since mechanical requirements inside the tower and electrical requirements usually are not compatible, considerable liaison and successive approximations were necessary to arrive at a suitable plan. As nearly as possible, all of the line runs are kept absolutely straight down the

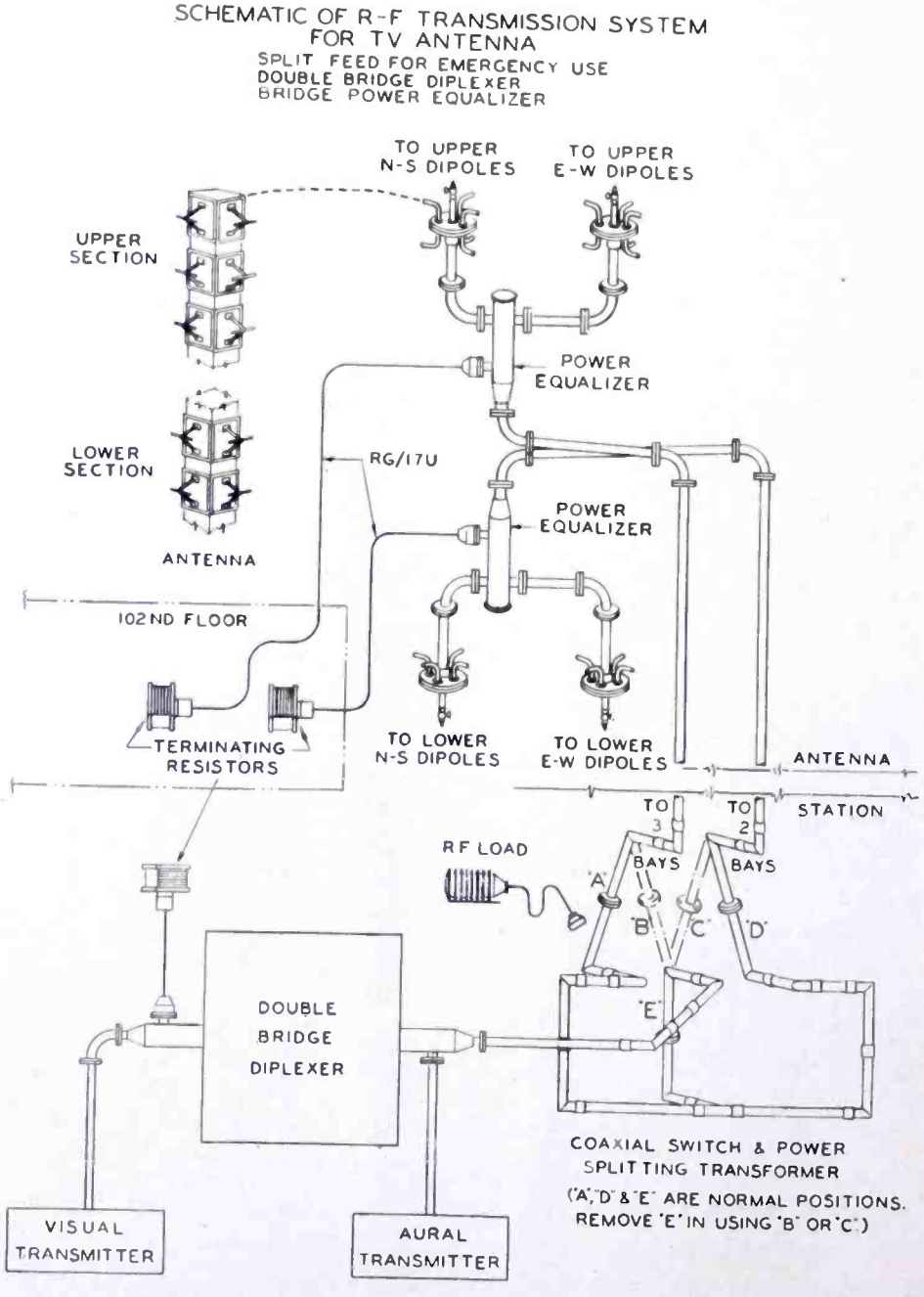

Fig. 11—Systems diagram showing components and connections for low-band Empire State stations.

middle of the tower. A multiplicity of elbows, especially near the antenna will introduce minor reflections and if the effect is cumulative, may cause difficulty. Hence, careful attention to detail is necessary in this part of the layout.

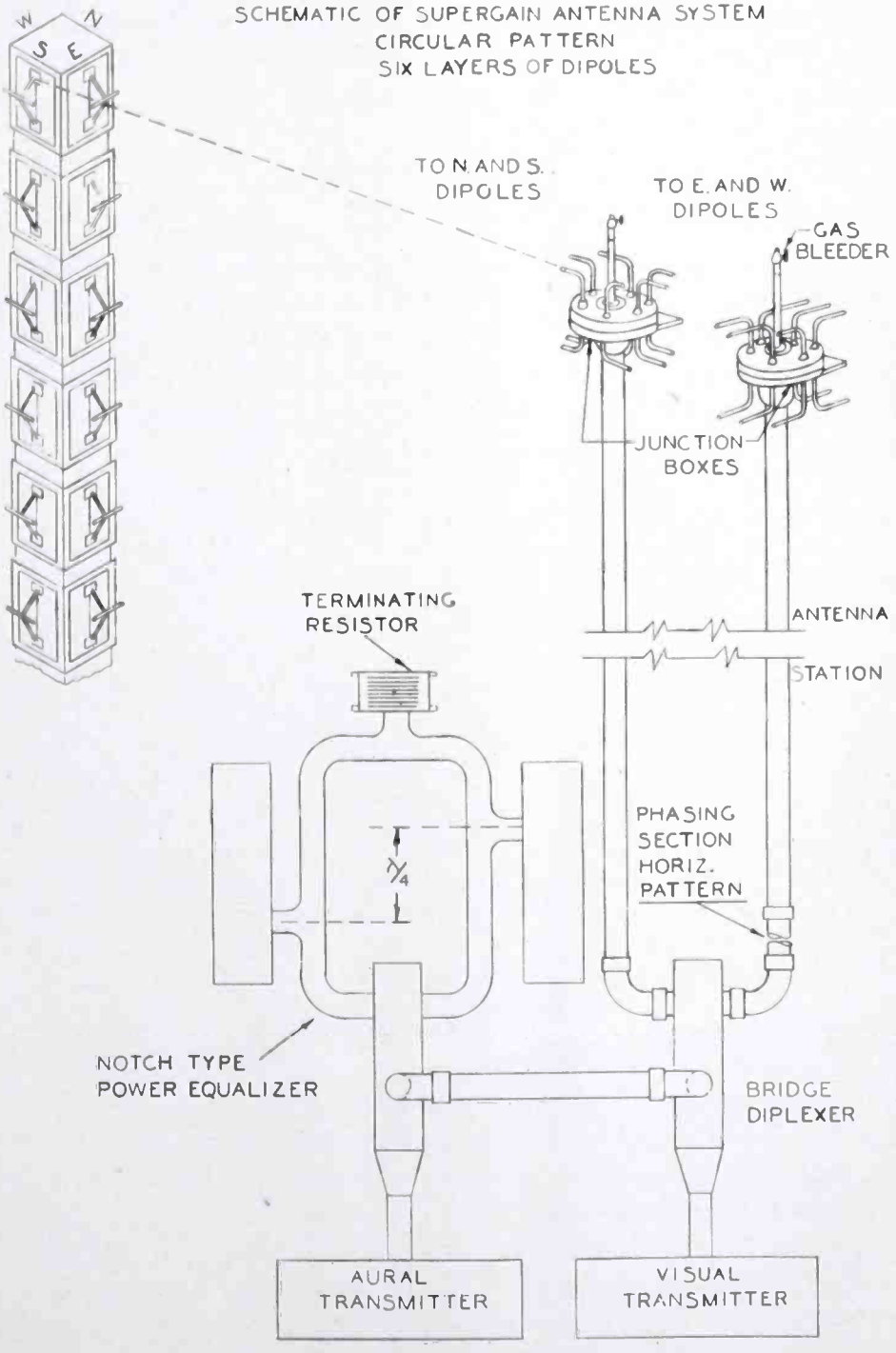

Fig. 12—Systems diagram showing components and connections for high-band Empire State antennas.

Conclusions

The Super Turnstile and Super-Gain antennas each have important features which render them suitable for given applications. The Super-Gain antenna especially can be used for a multiplicity of purposes including high gain, directional antennas, and stacking. Stacking of antennas exemplified by the Empire State antenna may be an important factor in new television areas.

Acknowledgment

The work described herein especially, on the Empire State antennas, is the work of many men. L. J. Wolf is responsible for much of the supervision and planning. R. W. Masters, formerly associated with RCA and presently engaged as a consultant to RCA for this project, is responsible for the basic theoretical work on Super Turnstile and Super-Gain antennas. In addition, 14 other engineers are engaged on various parts of the project.

A DIVERSITY RECEIVING SYSTEM FOR RADIO FREQUENCY CARRIER SHIFT RADIOPHOTO SIGNALS*

By

JOHN B. ATWOOD

Research Department, RCA Laboratories Division,
Riverhead, N. Y.

Summary—*A diversity receiving system for radiophoto signals transmitted by the radio frequency carrier shift (RFCS) method is described and the results of tests made on the system are presented. Included in the tests was a comparison between the RFCS method and the subcarrier frequency modulation (SCFM) method. A further test of the diversity-combining equipment was made by applying it to two single-sideband (SSB) receivers to form an SSB diversity receiving system for radiophoto signals transmitted by the SCFM method on an SSB transmitter.*

The tests showed:

1. The RFCS system used in these tests gave an improved signal-to-noise ratio over SCFM.

2. RFCS signals having a shift of 800 cycles could be received using an intermediate-frequency amplifier bandwidth of 1.3 kilocycles with practically no loss of picture detail. The narrow bandwidth provided a marked reduction of interference.

3. A definite improvement was obtained on RFCS by using space diversity.

4. The SSB system of receiving SCFM showed a definite improvement when space diversity was added.

5. A common high-frequency oscillator was not necessary when two SSB receivers were used in diversity with the RFCS combining equipment.

6. Operating experience in receiving one sideband of SCFM signals as an RFCS signal has shown a marked reduction in interference and noise and an indication that there may be a reduction in stagger.

INTRODUCTION

THE purpose of this paper is to describe a diversity receiving system for radiophoto signals transmitted by the radio frequency carrier shift (RFCS) method. Preliminary tests on the system were conducted over a short path from Rocky Point to Riverhead, New York. More extensive tests on the system were conducted over a longer path from Bolinas, California to Riverhead from July 8 to July 21, 1948. Included in the latter tests was a comparison between the RFCS method and the subcarrier frequency modulation (SCFM) method. A further test of the diversity-combining equipment was made by applying it to two single-sideband (SSB) receivers to form

* Decimal Classification: R 581.

an SSB diversity receiving system for radiophoto signals transmitted by the SCFM method on an SSB transmitter. This system was tested on September 16 and 17, 1948 between Bolinas and Riverhead.

Requirements of System

The requirements of a receiving system for the reception of radiophoto signals transmitted by the RFCS method may be summarized as follows:

1. The SCFM method is in common use at the present time with standardization taking place for 2300 cycles as the black frequency and 1500 cycles as the white frequency. This is a shift of 800 cycles. It would be desirable to use as much of the central office equipment as possible for the new system and hence the receiver should supply these same frequencies for a shift on the received signal of 800 cycles.

2. There should be no controls or adjustments on the receiver which could cause the signal shift on the output of the receiver to differ from the shift on the received signal. Practically, this means a heterodyne system.

3. A maximum drift of 50 cycles in the black frequency can be tolerated provided that it is spread out uniformly over the whole picture and that the black frequency is within plus or minus 25 cycles of the correct frequency at the beginning and end of the picture. Small frequency drifts should not occur at a rate exceeding about 1 cycle per second. This imposes a high order of frequency stability on the receiver and requires the use of automatic frequency control (AFC).

4. The top keying speed will be about 850 cycles.

5. Provision should be made to obtain the benefits of space diversity.

Description of Receiving System

A block diagram of the receiving system is shown in Figure 1. It consists of two radio-frequency (r-f) amplifiers having a common high-frequency oscillator which is used to convert the received signal to the first intermediate frequency (i-f). The r-f amplifiers are followed by two i-f amplifiers having a common oscillator which is used to convert to the second intermediate frequency of 50 kilocycles. This oscillator is operated on by the AFC so as to maintain the black frequency at its correct value of 2300 cycles at the audio output of the receiver.

The two 50-kilocycle outputs from the i-f amplifiers are then separately amplified, limited, converted to 10 kilocycles and fed through

a series of multipliers whose purpose will be described later. At this point (gates), the receiver automatically selects the stronger of the two signals and passes it on to the rest of the circuit.

The automatic selector (gate control) consists of a pair of differentially connected diodes which rectify the amplified 50-kilocycle outputs from the two i-f amplifiers. The differential voltage developed is used to trip a double trigger which in turn operates the gating circuit.

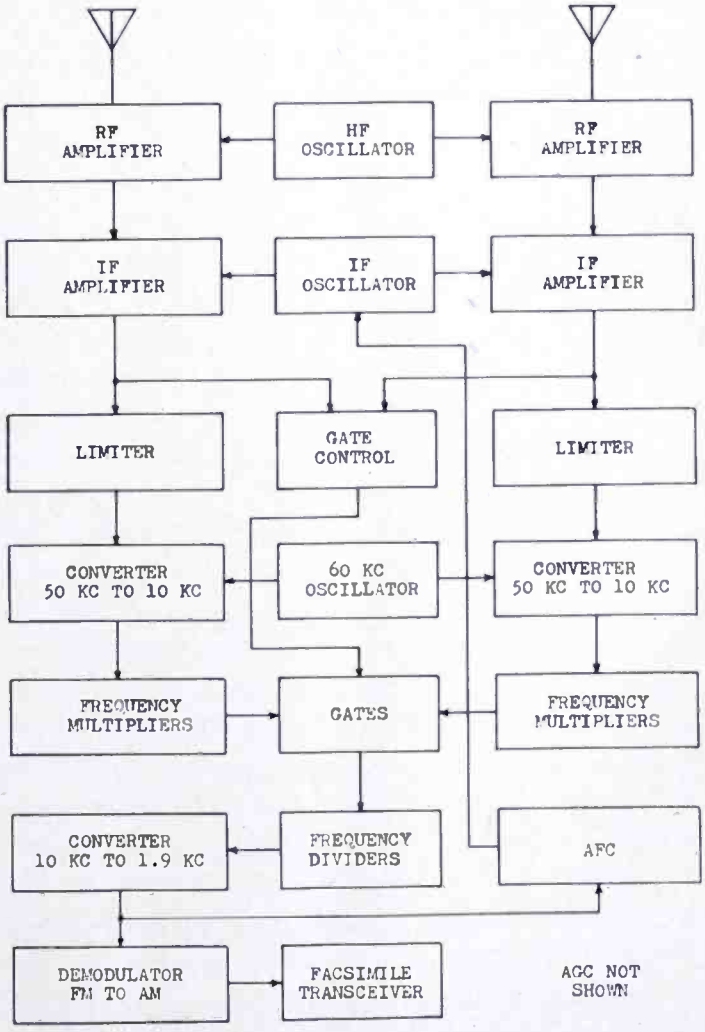

Fig. 1 — Block diagram of RFCS diversity receiving equipment.

The gate control will switch the gates from one signal to the other with a difference in level of about 3 decibels. The actual switching time is about 0.2 microsecond, but the decision to switch takes about 150 microseconds.

Following the gates, the selected signal goes through a frequency divider which brings the frequency back down to 10 kilocycles. It is then heterodyned down to a center frequency of 1900 cycles. The frequency-modulated audio tones are then converted by the demodulator to amplitude modulation and fed to the facsimile transceiver.

An automatic frequency control is provided to maintain the black frequency in the audio output at its proper value of 2300 cycles. A tuning meter is also incorporated as a part of the AFC circuit.

The complications in the system just outlined are caused by the desirability of providing space diversity. For a single receiver, it would only be necessary to heterodyne the received signal to the proper audio frequency, provide limiting to maintain the output at constant level, and supply AFC.

With two receivers, it is essential that each oscillator in the system be common to the two receivers to prevent sudden frequency changes in the output when diversity switching occurs. Even with common oscillators, this switching cannot take place directly at the output of the i-f amplifiers since the two outputs may be out of phase. A sudden phase change produces a transient whose size is proportional to the amount of the phase change and which reaches a maximum at 180 degrees. The sudden phase change is equivalent to a momentary frequency change and hence shows up in the picture as either a black or white dot depending upon the direction of phase reversal. The density of these dots is proportional to the phase change.

If the two signals are fed through frequency multipliers and then switched, the maximum transient-producing phase change that can take place due to switching is still 180 degrees. If the switched signal is now fed through a series of frequency dividers, any phase change will be reduced by a factor equal to the amount of frequency division employed. Thus, if a factor of 16 is used, a 180 degree phase change will be reduced to 11.25 degrees. The amount of multiplication used should be the same as the amount of division; otherwise, the shift on the output signal will differ from the shift on the received signal. It should be pointed out that a maximum 180 degree phase change is not encountered at every switchover, but large phase changes are encountered frequently enough that the above steps are necessary. One purpose of the tests which were made on the system was to determine the amount of frequency division required to reduce the density of the switching transients to a point where they would not be visible in the picture.

The time required for the switching to take place should be short compared to the time of one cycle of the frequency to be switched or phase shifts in excess of 180 degrees can occur and neutralize the benefits obtained from the frequency division. In this system, the frequency which is switched is 160 kilocycles so that the length of one cycle is 6.25 microseconds. The switching time of 0.2 microsecond is 12 degrees at this frequency and, if a division factor of 16 is used,

it is reduced to only 0.75 degree. Adding this to the 11.25 degrees resulting from a 180 degree change of phase gives a maximum phase change in the output of 12 degrees.

Description of the Test Circuits

Bolinas-Riverhead Circuit

A block diagram of the transmitting end of this circuit is shown in Figure 2. The facsimile transceiver and modulator were located at San Francisco, the output of the modulator being fed over about 30

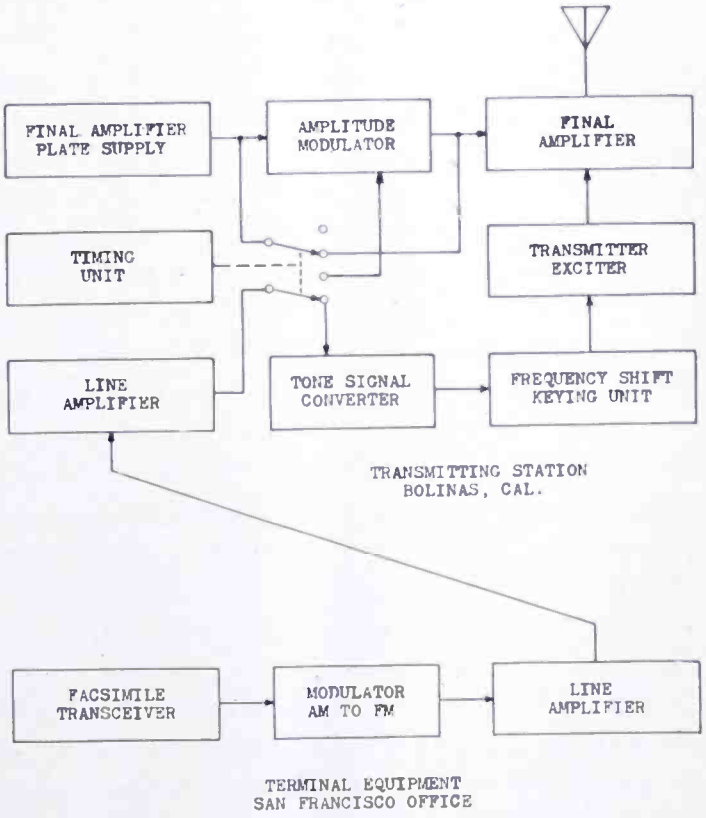

Fig. 2 — Block diagram of transmitter as arranged for the Bolinas - Riverhead tests.

miles of cable to the transmitter at Bolinas. The facsimile transceiver produced an audio-frequency carrier amplitude modulated in accordance with the shading of the picture on its drum. The picture used was a portion of a facsimile test sheet. The transceiver was followed by a modulator which converted the amplitude-modulated carrier to a frequency-modulated (FM) audio signal. The percentage modulation from the transceiver was adjusted so that the modulator would produce a 2300-cycle tone for black and a 1500-cycle tone for white. At Bolinas, these FM tones were fed to a tone signal converter which converted the tones to a variable amplitude dc voltage. The dc voltage was

then used to control a reactance tube in the frequency shift keying unit to produce the frequency-shifted r-f carrier. The frequency shift of the r-f carrier was adjusted to be the same as that of the output of the modulator. The output of the frequency shift keying unit was fed to a transmitter which was connected to a rhombic antenna having a power gain of about 10 decibels. The transmitter operated on a frequency of 13,720 kilocycles with a power input to the final amplifier of 703 watts.

The transmitter could also be switched over rapidly to transmit pictures by the SCFM method. This was accomplished by means of switches operated from a motor driven timing unit. An oil switch was used to insert an amplitude modulator in series with the final amplifier plate supply and an additional switch transferred the FM radiophoto tones from the tone signal converter to the input of the amplitude modulator. In this condition, the power input to the final amplifier was 462 watts using 85 per cent modulation.

Various arrangements were used at the receiver which was located at Riverhead, a distance of 2644 miles from Bolinas. In one arrangement, the receiver was as shown in Figure 1 using rhombic antennas.

A second arrangement was used for receiving SCFM. This is not shown as it was merely a two-receiver diversity system arranged for the reception of double-sideband audio signals in the normal manner. The changeover from RFCS to SCFM was easily made by means of switches on the receiver control panel.

One hundred and three pictures were received over the Bolinas-Riverhead circuit during the period from July 8 to July 21, 1948.

Some time later, a further test of the diversity-combining equipment was made by applying it to two SSB receivers to form an SSB diversity receiving system for radiophoto signals transmitted by the SCFM method on an SSB transmitter.

For this test, the FM radiophoto tones were used to modulate a type D-156000 single-sideband transmitter which was connected to a rhombic antenna having a power gain of about 10 decibels. The transmitter operated on a frequency of 13,720 kilocycles with a signal-on power input to the final amplifier of 2728 watts. The carrier suppression was 10 decibels.

A block diagram of the receiving system is shown in Figure 3. Two radio telephone receivers, type D-99945, were connected to rhombic antennas. These are single-sideband receivers, each having its own high-frequency oscillator and its own AFC system. The FM radiophoto signals from the audio outputs of the two receivers were converted to a center frequency of 50 kilocycles by means of two converters

having a common oscillator. Each of these converters contained a 50-kilocycle band-pass filter having a bandwidth of approximately 1300 cycles.

The outputs from the two converters were fed to a signal selector. This signal selector was the same equipment shown in Figure 1 following the i-f amplifiers except that the AFC was not used. The output of the selector circuit was fed through a demodulator to a facsimile transceiver located in the darkroom. Also located in the darkroom was a headset connected to the audio output of one of the receivers. This was for the purpose of monitoring the voice transmissions at the commencement of each picture since these would not pass through the narrow-band portion of the system.

A short test of this system was conducted on September 16 and 17, 1948.

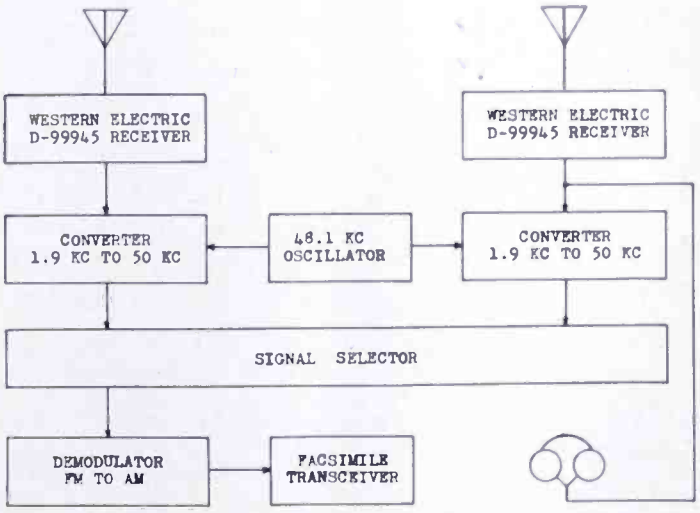

Fig. 3 — Block diagram of receiving equipment for SSB diversity tests.

Rocky Point-Riverhead Circuit

The preliminary testing of the RFCS system was done over a 15 mile path from Rocky Point to Riverhead. The transmitting arrangement was essentially the same as that of Figure 2 except that the equipment was all at one location and there was no provision for amplitude modulating the transmitter. The transmitter operated on a frequency of 6425 kilocycles with a power input to the final amplifier of about 500 watts. The transmitter was connected to a doublet antenna located about a quarter wavelength above ground to provide high-angle radiation.

The receiving equipment was as shown in Figure 1 using half-wave doublets located about a quarter wavelength above ground. The object of accentuating the high-angle radiation was to provide as much multipath as possible over the short distance.

Twenty-four pictures were sent over this circuit from March 31 to June 17, 1948.

Test Procedure

No special procedure was followed for the tests over the Rocky Point-Riverhead circuit since both ends of the circuit were under local control. However, these tests showed the desirability of following a fixed procedure for the Bolinas-Riverhead tests which came later since no cue circuit was available.

The AFC on the receiver is designed to maintain the black frequency of 2300 cycles. Accordingly, it is necessary that black frequency be transmitted continuously if the transmitting picture drum is not rotating, and at least once each drum revolution while the drum is rotating.

The actual procedure used for the Bolinas-Riverhead RFCS tests was as follows:

1. The drum on the transmitting radiophoto machine was modified by having a strip of non-reflecting black material attached to the gripper bar and an additional black strip attached around the raised left hand side of the drum. These black strips were cut from the black paper which comes with the recording film and they were held in place with rubber cement.

2. A picture transmission was started every 15 minutes from 1830 to 2100 inclusive, Greenwich Mean Time. The transmitting drum was allowed to rotate in the idle position at the extreme left until time to start the picture. The drum was then moved over, so that steady black was transmitted from the black strip around the raised left hand side of the drum, and the clutch engaged. The steady black provided notice at the receiver that the picture was about to start. At the receiving end, the drum on the receiving machine was started when the steady black tone was received and synchronized as soon as the gripper bar pulses were received from the picture. At the end of the picture, the transmitting drum was allowed to rotate in the idle position until time for the next transmission. A pulse of black frequency was thus transmitted each drum revolution from the gripper bar.

3. While the picture was being transmitted, the receiver was alternated between two test conditions with about one minute being allowed for each condition. Where this could not be done, as was the case when comparing RFCS and SCFM, the test conditions at the receiver were alternated each picture.

4. For the SSB-SCFM test, it was not necessary to leave the drum rotating at the end of the picture because the AFC was obtained

from the suppressed SSB carrier and not from the black frequency. Voice announcements were used just before the start of each picture to indicate the beginning of the phasing pulses and the engagement of the clutch on the lead screw.

5. All transmissions were recorded using Kodak Type A Transmission film. The film was developed in Dektol developer diluted 1:2 and the developing time was varied with the temperature of the developer. After a water rinse, the films were fixed in an F-5 fixing bath.

Fig. 4—3× enlargement of a portion of a picture showing transients resulting from i-f switching when frequency division is not used.

RESULTS

1. *Switching Transients, RFCS*

One of the objects of the tests made on the system was to find out how much division (and corresponding multiplication) would be required to reduce the switching transients to a point where they would not be visible in the picture. Division factors of 1, 2, 4, 8, 16, and 32 were tried and it was found that a factor of 16 was sufficient.

Figure 4 is a 3× enlargement of a portion of a picture showing how the switching transients record as black and white dots if division is not used. This picture was received from Rocky Point using a division factor of 1 (direct i-f switching) at the receiver. These transients cannot be detected on the negative if the division factor is increased to 16.

2. Picture Detail versus Intermediate-Frequency Bandwidth, RFCS

The normal bandwidth which would be used to receive pictures by the RFCS method would be the shift plus twice the maximum keying speed, or 2.5 kilocycles. The i-f amplifiers which were used did not have this bandwidth available. Comparisons were made between i-f bandwidths of 4 kilocycles and 1.3 kilocycles and it was found that there was very little loss of detail when using the narrower bandwidth.

3. Noise versus Intermediate-Frequency Bandwidth, RFCS

The improvement which can be obtained on noise in the picture by reducing the i-f bandwidth is shown in Figure 5. The left hand

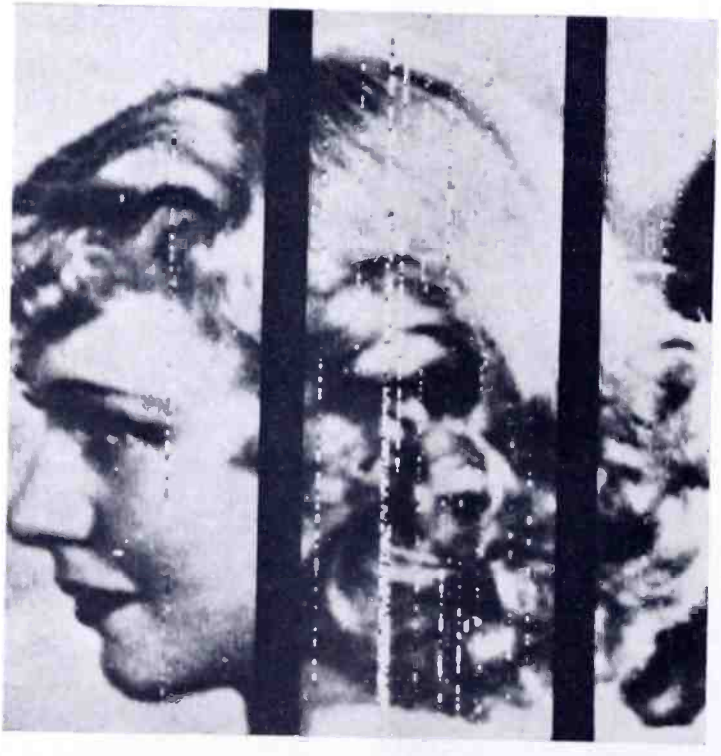

Fig. 5 — Noise improvement obtained by reducing bandwidth. Left and right portions 1.3-kilocycle i-f bandwidth, center portion 4-kilocycle i-f bandwidth.

portion of the picture was recorded using a 1.3-kilocycle bandwidth, the center portion using a 4-kilocycle bandwidth, and the right hand portion using a 1.3-kilocycle bandwidth. This is a small section of the complete picture slightly enlarged. The vertical black stripes were introduced at the receiver to blank out the picture while the bandwidth was being changed. This and the following tests were made over the Bolinas-Riverhead circuit.

4. Interference versus Intermediate-Frequency Bandwidth, RFCS

The improvement in the picture which can be obtained by reducing the bandwidth of the i-f amplifier when interference is present is shown in Figure 6. In this picture, diathermy was present while both

sections were being received. The left hand portion of the picture was recorded using an i-f bandwidth of 1.3 kilocycles and the right hand portion using an i-f bandwidth of 4 kilocycles.

5. One Receiver versus Two Receivers, RFCS

The improvement obtained by using space diversity cannot be evaluated by a single illustration. An examination of over forty pictures, each of which was alternated each minute between one receiver

Fig. 6—Interference reduction obtained by reducing bandwidth. Left portion 1.3-kilocycle i-f bandwidth; right portion, showing diathermy interference, 4-kilocycle i-f bandwidth.

and two receivers, showed noise present in nearly every case when one receiver was used. When two receivers were used, no noise was visible except for some isolated spots on a few pictures. The conclusion was reached that space diversity was definitely worth while.

6. RFCS versus SCFM

At the present time, it is general practice to modulate an SCFM transmitter 60 per cent with the picture tones. A higher percentage

is not used since the circuit may be modulated with voice between pictures. On this basis, the power in one sideband is 10.4 decibels below that in the carrier. The carrier power in a class B telephone transmitter is about 5.7 decibels lower than the same transmitter operated class C telegraph, as would be the case for RFCS. This makes a difference of 16.1 decibels between the RFCS carrier power and the power in one sideband of an SCFM signal from the same transmitter.

At the receiver, both sidebands of the SCFM signal would be utilized; and, if they were always received in phase, a 6-decibel improvement would result. However, propagation over most circuits will change the phase relations so that the average improvement obtained will be more nearly 3 decibels. To offset this, the bandwidth of an RFCS receiver needs to be only 40 per cent of that for an SCFM double-sideband receiver and this narrower bandwidth gives a 4-decibel improvement in signal-to-noise ratio. These two effects approximately cancel each other.

If the SCFM transmitter is modulated 90 per cent instead of 60 per cent, the 16.1-decibel difference between RFCS and SCFM is reduced 3.5 decibels leaving 12.6 decibels as the theoretical advantage of the RFCS system over the SCFM system with 90 per cent modulation.

To compare the two systems, pictures were transmitted alternately by the RFCS and SCFM method. The transmitter at Bolinas had a power input to the final amplifier of 703 watts in the RFCS condition and 462 watts in the SCFM condition with a percentage modulation of 85 per cent. This gave a figure of 10.6 decibels for the ratio of the carrier power in the RFCS condition to the power in one sideband of the SCFM condition. Two-receiver diversity was used for each.

Figures 7 and 8 are consecutive pictures received during a period of high noise caused by a storm in the vicinity. Pictures received preceding and following these showed the same difference. They provide a good illustration of the advantage of RFCS over SCFM. The i-f bandwidths of 9 kilocycles used for SCFM and 4 kilocycles used for RFCS were both wider than necessary by about the same proportion so that Figures 7 and 8 should give a fair comparison of the two systems.

7. *SSB Diversity, SCFM*

For this test, the receiving conditions were alternated between one receiver and a two-receiver diversity. The improvement obtained from diversity was about the same as that described for the RFCS system.

From an examination of the received pictures, it would appear that the separate AFC's on the receivers held closely enough so that it

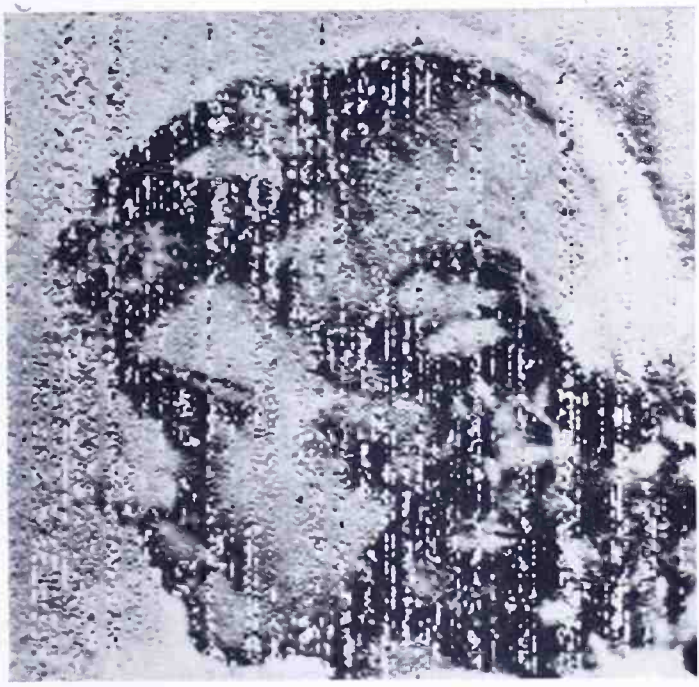

Fig. 7 — SCFM picture received during period of high noise level, 9-kilocycle i-f bandwidth.

would not be necessary to provide a common high-frequency oscillator when the receivers are used in diversity with the RFCS combining equipment.

Results of Operating Experience

The experimental RFCS diversity equipment was installed at the Riverhead receiving station of RCA Communications, Inc. in March,

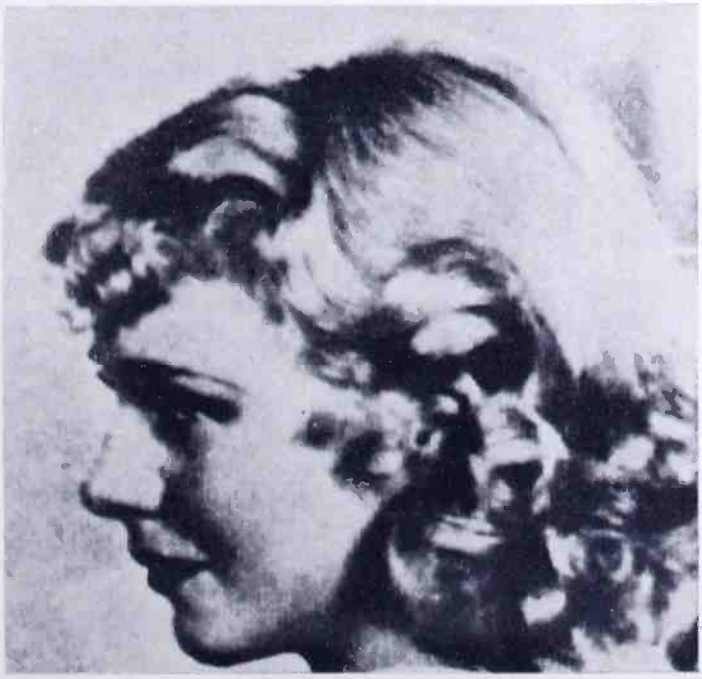

Fig. 8 — RFCS picture received immediately following Figure 7, 4-kilocycle i-f bandwidth.

1950. Since that time, only one radiophoto has been received which was transmitted by the RFCS method owing to the lack of transmitting facilities. However, it has been used extensively for the reception of radiophoto signals transmitted by the SCFM method. The narrow bandwidth of the receiver permitted either sideband to be used as an RFCS signal and a great deal of interference was avoided in this manner. It has also been used for the reception of radiophoto signals transmitted as frequency-modulated tones by SSB transmitters.

The results have shown a marked reduction in interference and noise as a result of the narrow bandwidth. While no tests have been made on the subject, a comparison of the pictures received prior to the installation of the RFCS equipment with those received since indicates that there may be a reduction in stagger with the RFCS equipment.

Acknowledgments

The stability requirements of a system for the transmission and reception of radiophoto signals by the RFCS method were specified by S. H. Simpson, Jr. of RCA Communications, Inc. The idea of reducing switching transients by frequency division was due to H. O. Peterson, of the Riverhead laboratory, under whose general direction the project was carried on. The necessary revisions to the transmitting equipment were designed by H. E. Goldstine, of the Rocky Point laboratory, who also operated the transmitting facilities for the Rocky Point-Riverhead tests. The transmitting station facilities at Bolinas were provided by RCA Communications, Inc., and numerous test schedules were provided with excellent assistance and cooperation by various members of the RCA Communications staff.

RAPID DETERMINATION OF GAS DISCHARGE CONSTANTS FROM PROBE DATA*

By

L. Malter and W. M. Webster

Research Department, RCA Laboratories Division,
Princeton, N. J.

***Summary**—A series of nomograms is presented which make possible the rapid determination of gas discharge constants from double probe data. These constants include plasma density, wall potential, random electron and ion currents. An analysis based upon theory and experiment indicates that the Child-Langmuir space-charge equation is applicable to sheaths with inappreciable error except for the lightest gases and least dense plasmas.*

I. Introduction

LANGMUIR AND MOTT-SMITH[1] have described means for determining the constants of a gas discharge plasma by means of a single probe. More recently Johnson and Malter[2] have shown that by the use of two probes in a floating circuit one can overcome some of the difficulties and disadvantages of single probes.†

In the single-probe method, such quantities as random electron and ion currents, floating potential and plasma potential, as well as electron temperature, are determined quite readily from the probe data. From these quantities one can then compute the plasma density and wall potential directly.

Reference 2 describes the determination of electron temperature directly from double-probe data. However, because of the fact that saturated electron currents cannot be drawn to the probe in the double-probe method, it turns out that there is no simple, direct method for obtaining random currents, plasma density and wall potential in this case. By laborious methods, largely trial and error, these quantities have been obtained in the case of the double-probe method.†† It is the

---

* Decimal Classification: R337.1.

[1] I. Langmuir and H. M. Mott-Smith, "Studies of Electric Discharges in Gases at Low Pressures", *General Electric Review*, Vol. 27, pp. 538, 616, 762, 810, 1924.

[2] E. O. Johnson and L. Malter, "A Floating Double Probe Method for Measurements in Gas Discharges", *The Physical Review*, Vol. 80, No. 1, p. 58, October 1, 1950.

† It is assumed that the reader is familiar with the fundamentals of probe data interpretation.

†† In Reference 2, a sample plasma density determination is carried out. The process there outlined is laborious and quite approximate.

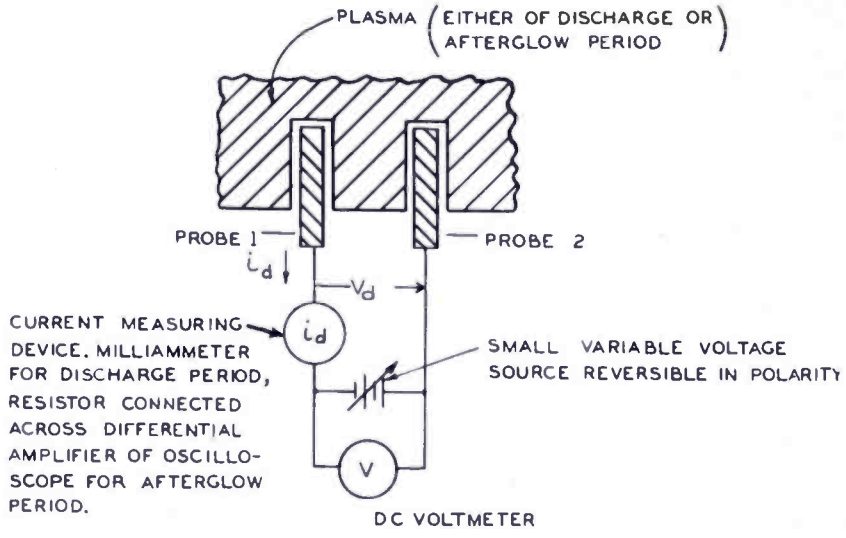

Fig. 1—Double-probe measurement circuit.

prime purpose of this paper to develop a rapid nomographic method for accomplishing this. While the methods here developed find their greatest utility for double probes, they can also be used with single probes. In most cases, however, the Langmuir techniques are better suited for single probes.

II. Review of Double-Probe Properties

The manner of using a double probe is illustrated in Figure 1. The form of current-voltage characteristic is shown in Figure 2. Several methods for obtaining the electron temperature, T_e, from Figure 2 are described in Reference 2. One of them will be outlined here.

The regions of positive ion saturation (EC and FD) are extended back to the current axis. The probe currents at points C and D (where the probes begin to collect electron current) are denoted by i_{p1} and i_{p2} respectively. i_{e2} is then determined from Figure 2. G is computed from

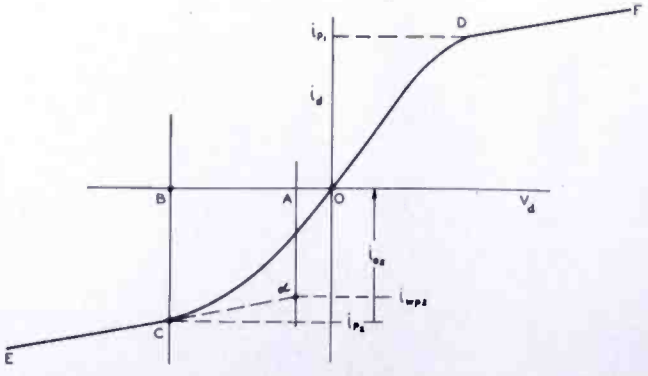

Fig. 2—Typical double-probe voltage-current characteristic.

the expression $G = \dfrac{i_{e2}}{i_{p1} + i_{p2}}$. Figure 3 then yields the quantity $\delta_2 = \dfrac{\Delta V_2}{\Delta V_d}$. Then from point B (directly above C in Figure 2) A is

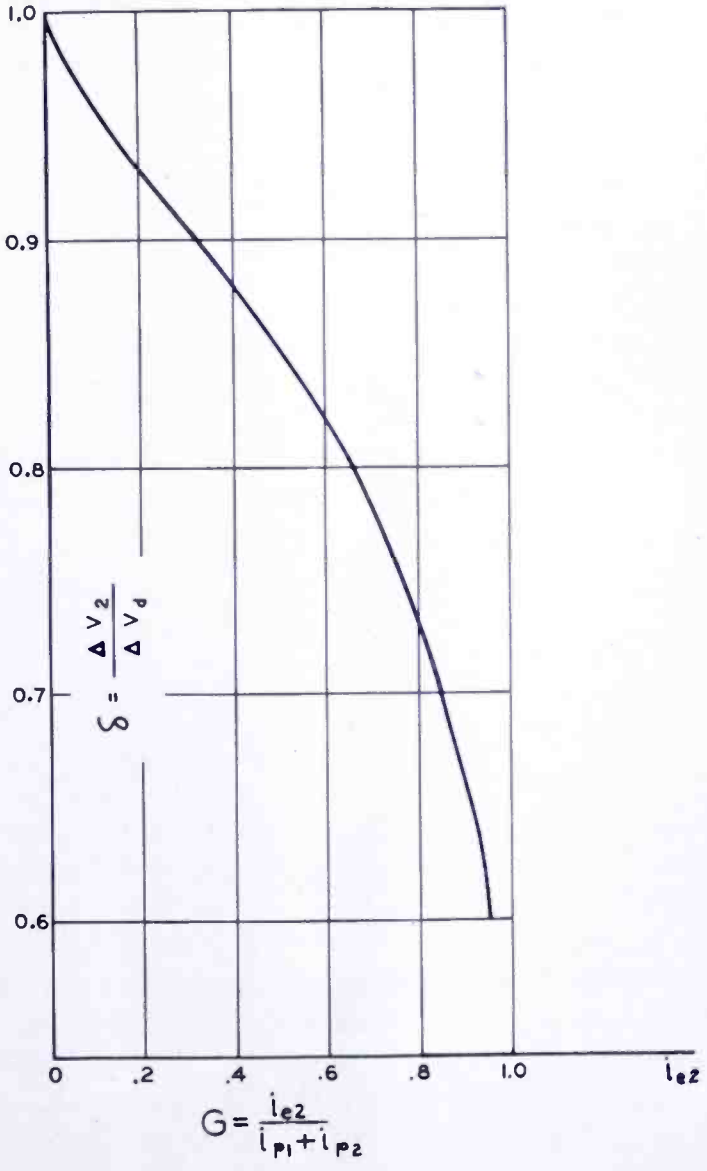

Fig. 3 — Graph for use in determination of probe current when probe is at floating potential.

determined such that $\dfrac{BA}{BO} = \delta_2$. From A drop a perpendicular to EC extended. This determines α. The current (i_{wp2}) corresponding to α is the electron current (and also the positive ion current) to probe No. 2 when it is at floating potential. In the same fashion one can determine the electron and ion current (i_{wp1}) to probe No. 1 when it is at floating

potential. The electron temperature is then obtained from the relation

$$T_e = 11{,}600\, G\,(1-G) \sum i_{wp} \left[\frac{d\,V_d}{d\,i_d}\right]_{V_d=0},$$

where $$\sum i_{wp} = i_{wp1} + i_{wp2},$$

and $\left[\frac{d\,V_d}{d\,i_d}\right]_{V_d=0}$ is the slope of the double-probe characteristic at the point $V_d = 0$.

If the currents to the two probes do not differ by more than about 30 per cent, one can set $G\,(1-G) = 0.25$, and $\delta = 0.85$.

III. Determination of Plasma Density, Sheath Radius, and Wall Potential From Double-Probe Data

Since at no point on the characteristic of Figure 2 is the electron current to the probe saturated, the straightforward single-probe method cannot be employed to determine plasma density. One proceeds in the manner outlined below.

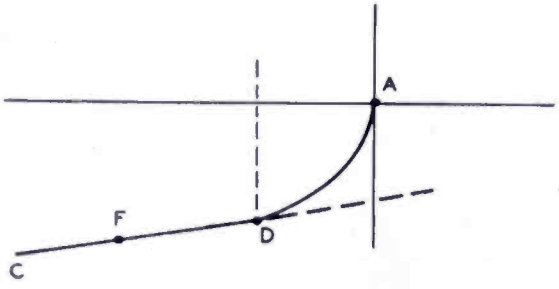

Fig. 4 — Expanded portion of typical double-probe characteristic.

In Figure 4 is shown an expanded presentation of the left-hand portion of Figure 2. It is seen that over a certain region the characteristic is sensibly linear, but then breaks away toward A as high-velocity electrons get to the probe. It is seen further, that CD is not parallel to the voltage axis, indicating that as the probe goes increasingly negative in voltage, its current increases. This arises from the expansion of the sheath surrounding the probe. Since the sheath diameter is not known, it has been customary (in the single-probe method) to extend CD to the point directly below A and compute the random ion current from the extrapolated current value at that point, and from the probe area. This method is reasonably accurate only when the plasma density is so high that the sheath and probe diameters are not appreciably different. For many cases which occur in practice, the

plasma densities are so low that sheath diameter may be considerably larger than that of the probe, even when the probe is at floating potential. It is essential that the sheath diameter be determined in order to permit a determination of the plasma density.

It would appear desirable to attempt the computation for a point on the double-probe characteristic for which saturated positive ion current flows to only one of the probes (such as at point *F* of Figure 4). This is not feasible, however, since the differential probe voltage at such a point is different from the probe-to-plasma potential difference by an amount which is almost equal to wall potential. The latter (which is as yet unknown) may amount to several volts and thus cannot be neglected without introducing serious error. It appears then that the computations must first be carried through for the case where the probes are at floating potential.

If the sheath thickness is known for this case (and as will be seen it can be determined), then from this and the value of the ion current (i_{wp}), the random ion current in the plasma can be computed. From the latter, and from the value of the ion temperature, the plasma density, and wall potential can then be determined.

Determination of positive ion temperature is a difficult matter. Fortunately, from the mechanics of collision processes, it is apparent that under certain conditions the ion temperature must be close to that of the gas. These conditions include one or both of the following:

1. short mean free path.
2. small plasma field.

When these conditions are not satisfied, the ion temperature can greatly exceed that of the gas.[3,4] It may even be the case that a "temperature" cannot be assigned to the positive ions. This paper will be restricted to the case in which equality of ion and gas temperature can be assumed. In the case of decaying plasmas, for which the double probe is particularly suited, the ion temperature can be set equal to that of the gas, regardless of mean free path.

Treatment is restricted to the case of cylindrical probes. Consider the case illustrated in Figure 5 in which the cylindrical cathode (ion source in this case) is external to the collecting anode. The cathode is the boundary between sheath and plasma through which ions diffuse. The anode is the probe. Then, the space-charge-limited ion current per

---

[3] R. L. F. Boyd, "The Collection of Positive Ions by a Probe in an Electrical Discharge", *Proceedings of the Royal Society of London*, Vol. 201, Series A, No. 1066, p. 329, April 26, 1950.

[4] L. Sena, "The Motion of Positive Ions in the Electric Field in a Gas", *Journal of Physics* USSR, Vol. X, No. 2, p. 179, 1946.

unit length to one of the probes may be taken as (see Section V)

$$i_{wp} = 3.43 \times 10^{-7} \frac{V_w^{3/2}}{r_a \beta^2} \left[\frac{1}{M_1} \right]^{1/2} \text{amperes per centimeter,} \quad (1)$$

where V_w is the wall potential (since for the present only the case wherein the probe is at floating potential is being considered),

r_a is the probe radius in centimeters,

M_1 is the ion molecular weight (oxygen = 16),

β^2 is a function of cathode to anode radius given by Langmuir and Blodgett[5].

Since consideration is restricted for the present to the wall potential case,

$$i_{we} = i_{wp}, \quad (2)$$

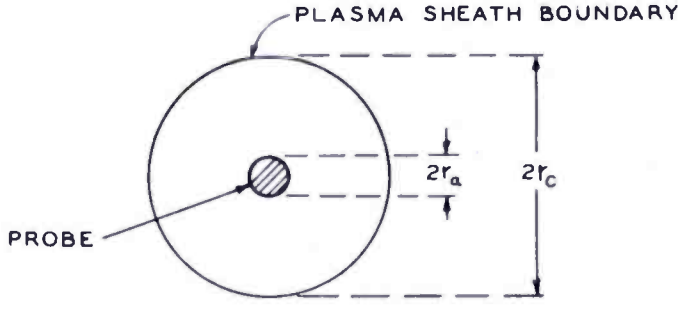

Fig. 5 — Probe-sheath-plasma configuration.

where i_{we} is the electron current to the probe per centimeter length, when the probe is at wall potential.

From kinetic theory,

$$i_{wp} = \frac{n_{op}\, e\, \bar{c}_p}{4} (2\pi r_c), \quad (3)$$

$$i_{we} = j_{eo}\, e^{-\frac{e V_w}{k T_e}} (2\pi r_a), \quad (4)$$

where n_{op} is the plasma density,

$\bar{c}_p$ is the mean ion velocity in plasma,

r_c is the sheath radius,

r_a is the probe radius,

[5] I. Langmuir and Katherine B. Blodgett, "Currents Limited by Space Charge between Coaxial Cylinders", *The Physical Review*, Vol. 22, p. 347, October 1923.

T_e is the electron temperature,

j_{eo} is the random electron current in the plasma in the vicinity of the probe.

$$\bar{c}_p = 1.87 \times 10^{-8} \left[\frac{T_p}{M} \right]^{1/2}, \tag{5}$$

where T_p is the positive ion temperature,

and M is the ion mass, in grams.

Similarly for electrons,

$$j_{eo} = \frac{n_{op}\, e\, \bar{c}_e}{4} = \frac{n_{op}\, e}{4} 1.87 \times 10^{-8} \left[\frac{T_e}{m} \right]^{1/2}, \tag{6}$$

where m is the electron mass, in grams.

Combining (2), (3), (4), (5), and (6) and solving for V_w, gives

$$V_w = \frac{k\, T_e}{e} \ln \frac{r_a}{r_c} \left(\frac{T_e M}{T_p m} \right)^{1/2} = \frac{T_e}{11{,}600} \ln \frac{r_a}{r_c} \left(\frac{T_e M}{T_p m} \right)^{1/2}. \tag{7}$$

Subsitution of (7) in (1) yields

$$i_{wp} = \frac{3.43 \times 10^{-7}\, T_e^{3/2}}{(11{,}600)^{3/2}} \cdot \frac{\left[\ln \frac{r_a}{r_c} \left(\frac{T_e M}{T_p m} \right)^{1/2} \right]^{3/2}}{\beta^2 \quad r_a \quad M_1^{1/2}}. \tag{8}$$

Let $$\frac{\left[\ln \frac{r_a}{r_c} \left(\frac{T_e M}{T_p m} \right)^{1/2} \right]^{3/2}}{\beta^2} = \left(\frac{11{,}600}{T_e} \right)^{3/2} \frac{i_{wp}\, r_a\, M_1^{1/2}}{3.43 \times 10^{-7}} = f. \tag{9}$$

a. Determination of Sheath Radius

In (9) the only unknown quantity is r_c. It is possible to solve for r_c, the sheath thickness, by a tedious series of approximations. To obviate this, a nomogram, as presented in Figure 6 has been prepared, from which the value of r_c can be readily determined.

Draw a line joining i_{wp} and T_e and find its intersection with line A. The quantity A is proportional to $\left(\frac{11{,}600}{T_e} \right)^{3/2} i_{wp}$. Similarly, find

the intersection of line B with the line joining the probe radius, r_a, and the gas. B is proportional to $r_a M_1^{1/2}$. Find the intersection of line f with the line joining the points already located on A and B. This quantity is the f of (9).

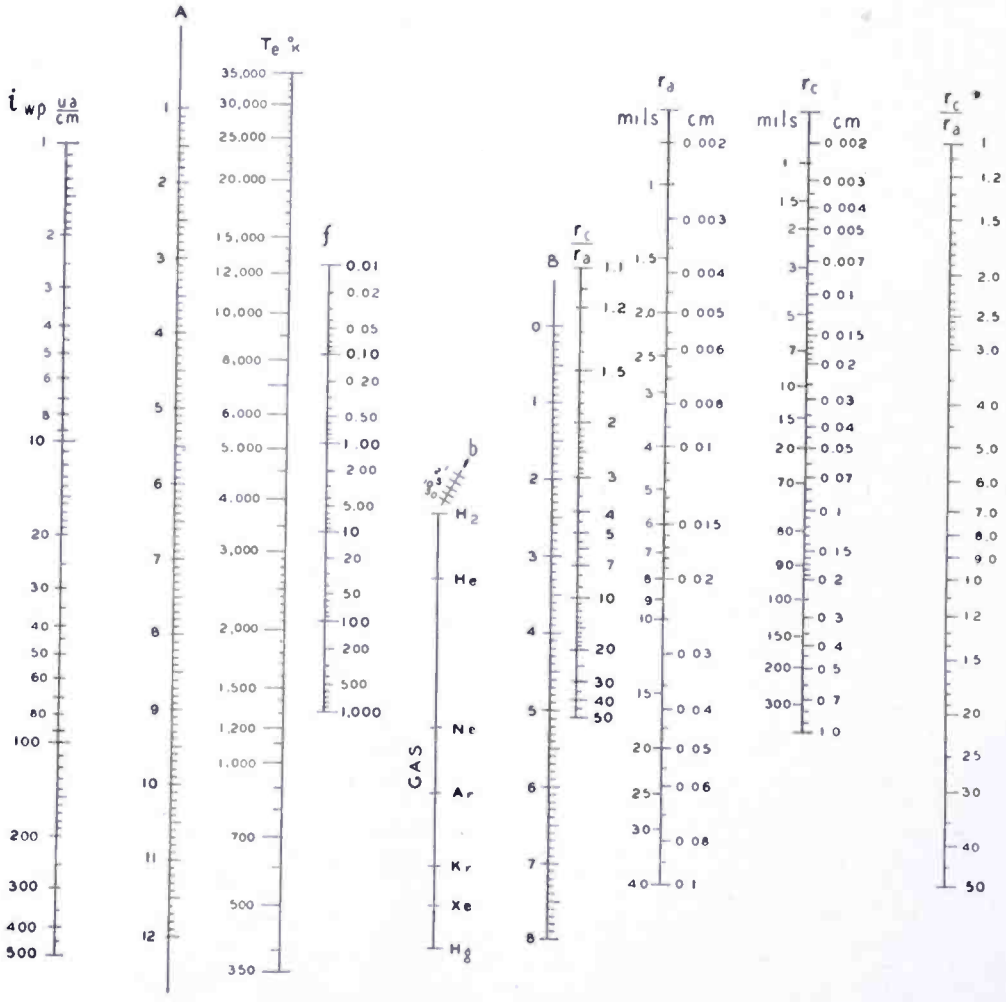

Fig. 6—Nomogram for determination of sheath radius, r_o, from double-probe data when probe is at floating potential.

Instructions: Find intersection on line A of line joining T_e and i_{wp}. Find intersection on B of line joining gas and r_a. Find intersection on f of line joining A and B. Obtain b from Figure 7. Pass line through b from f to r_o/r_a. Transfer r_o/r_a to $(r_o/r_a)^*$. Find intersection on r_o of line joining r_a and $(r_o/r_a)^*$.

From the graph of Figure 7 the quantity b can be obtained from T_e/T_p and the nature of the gas. b is proportional to

$$\left[\frac{T_e}{T_p}\frac{M}{m}\right]^{1/2},$$

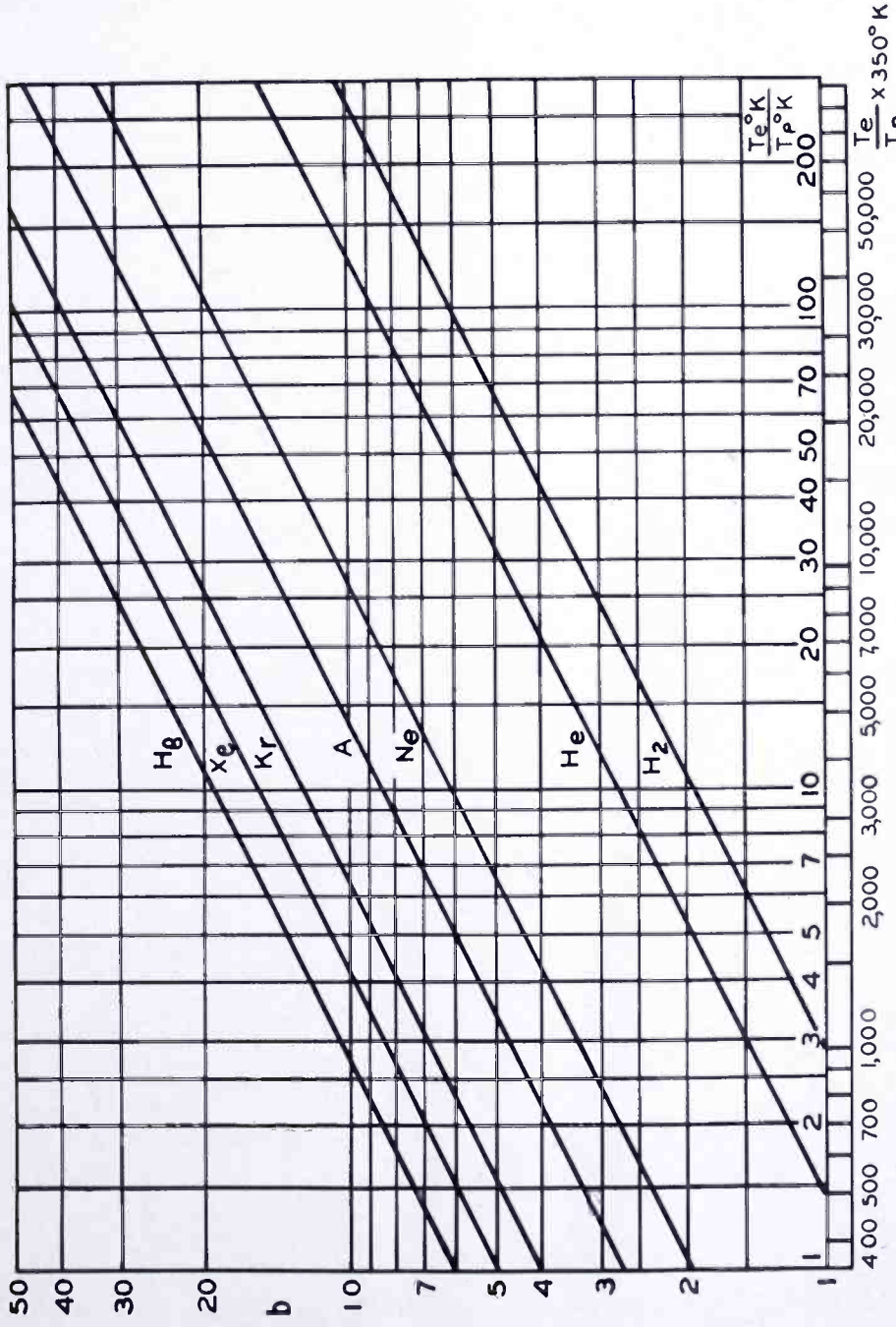

Fig. 7.—Graph of b versus T_e/T_p for various gases.

a quantity contained in the left-hand term of (9). One now has a value for

$$f \propto \frac{\left[\ln \frac{r_a}{r_c}\left[\frac{T_e}{T_p}\frac{M}{m}\right]^{1/2}\right]^{3/2}}{\beta^2},$$

and for

$$b \propto \left[\frac{T_e}{T_p}\frac{M}{m}\right]^{1/2}.$$

A knowledge of f and b should yield a value for r_c/r_a (since β^2 is a function of r_c/r_a). Such is the case. A line drawn from f through b in Figure 6, when extended to the r_c/r_a scale, yields the desired value of r_c/r_a. The value of the sheath radius can now be computed from the known values of r_a and r_c/r_a. To simplify this step, r_c/r_a has been replotted on the logarithmic scale $(r_c/r_a)^*$. A line joining $(r_c/r_a)^*$ and r_a yields the sheath radius r_c on the scale so designated.

b. Determination of Plasma Density

From the value of r_c just obtained and the other known data, the plasma density n_{op} (in the neighborhood of the probe) can now be determined.

By combining (3) and (5),

$$n_{op} = 2.14 \times 10^{26} \frac{i_{wp}}{r_c}\left[\frac{M}{T_p}\right]^{1/2} \text{ ions per cubic centimeter.} \quad (10)$$

In Figure 8, draw a line joining T_p and the gas. This yields on line D a quantity proportional to $\left[\frac{M}{T_p}\right]^{1/2}$. In the same figure join i_{wp} with r_c. On line C this yields a quantity proportional to $\frac{i_{wp}}{r_c}$. The line joining C and D then yields n_{op} on its scale.

c. Determination of Wall Potential

Sufficient information is now available to enable the wall potential V_w to be determined from 7. Again, a nomographic approach yields a rapid solution.

In Figure 9, find the intersection on L with the line joining b and r_c/r_a. Transfer L to L^*. Find the intersection on V_w of the line

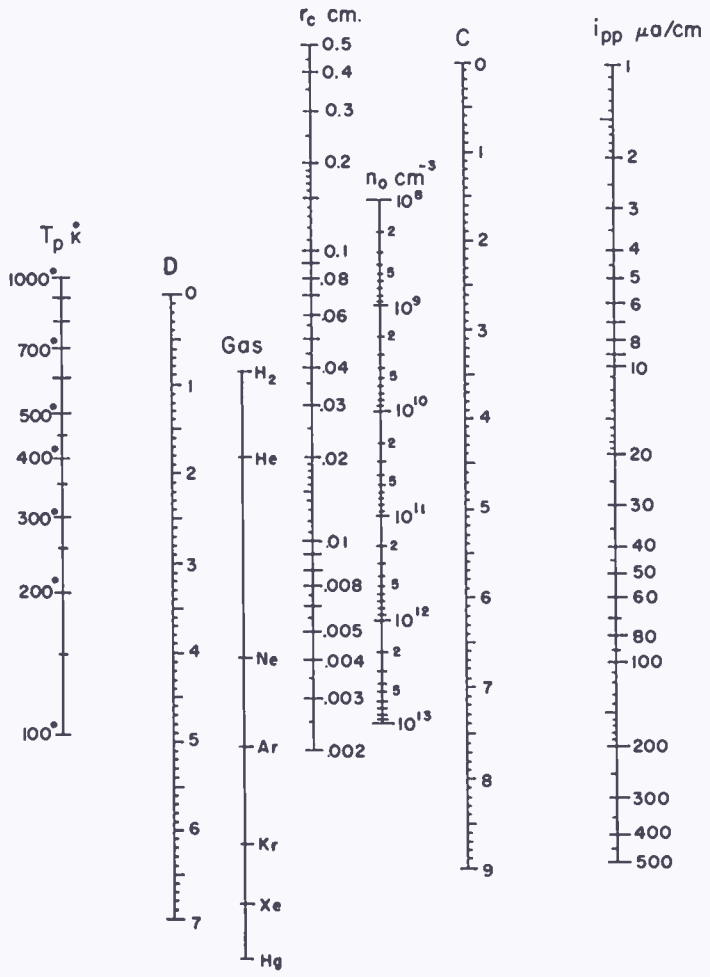

Fig. 8 — Nomogram for determination of plasma density, n_o, from double-probe data.

Instructions: Find intersection on D of line joining T_e and gas. Find intersection on C of line joining i_{pp} and r_c. Find intersection on n_o of line joining C and D.

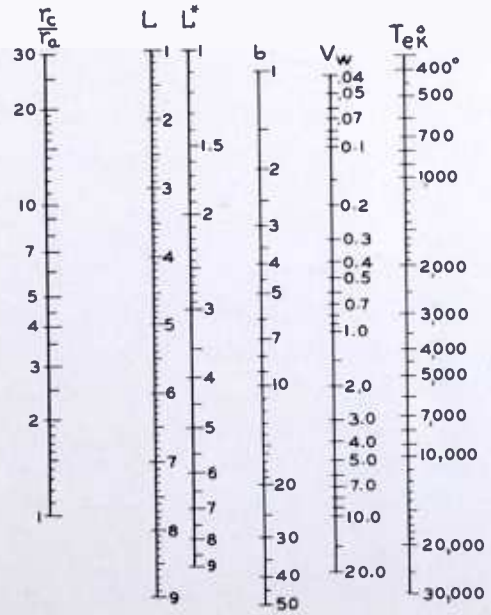

Fig. 9 — Nomogram for determination of wall potential, V_w, from double-probe data.

Instructions: Find intersection on L of line joining b and r_c/r_a. Transfer L to L^*. Find intersection on V_w of line joining L^* and T_e.

joining L^* and T_e. This is the desired value of V_w and constitutes a solution of (7).

d. Determination of Random Electron Current

Equation (6) is a relation between plasma density, n_{op}, random electron current, j_{eo}, and electron temperature, T_e. Figure 10 is a nomogram based on (6) which enables one to go directly from the already determined values of n_{op} and T_e to the random electron current, j_{eo}.

Now that wall potential has been determined it becomes possible to compute plasma density, etc., for points on the double probe characteristic removed from the floating potential case. This discussion will be given following an illustrative series of computations applicable to the floating potential case.

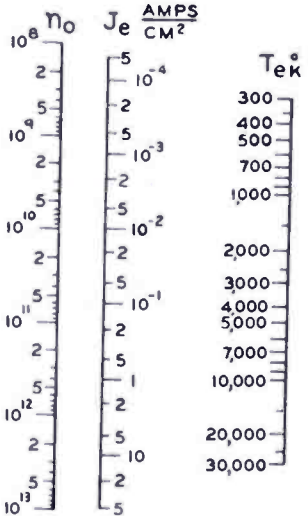

Fig. 10—Nomogram for determination of plasma random electron current, j_{eo}, from plasma density, n_o, and electron temperature.

IV. Application To Actual Case—Double Probes At Floating Potential

For purposes of illustration, the methods of the preceding section are now applied to an actual case.

Measurements were made in a form of discharge in which a temperature value could be assigned to the positive ions. A cylindrical diode with inner tungsten cathode, containing helium at 500 microns was operated at very low anode current. Under these conditions studies show that the potential distribution between cathode and anode is of the form shown in Figure 11.† In this form of discharge the plasma is of low density and has an electron temperature close to that of the cathode. This form of discharge was employed for two reasons:

† This is similar to distribution III shown by M. J. Druyvestyn and F. M. Penning, *Rev. Mod. Phys.*, Vol. 12, p. 148, December 1940 (Figure 61).

1. A temperature value can be assigned to the positive ions.

2. The low plasma density results in large values of r_c/r_a. This is a case in which the determination of plasma density is more difficult than when $r_c/r_a \simeq 1$, and will thus more forcibly illustrate the efficacy of the method here developed. Double probe data were taken and are presented in Figure 12. The probes were cylindrical rods 0.025 centimeter in diameter and 1 centimeter long. As a consequence, the measured probe currents are also the values of probe current per centimeter length. It is seen that the saturated positive ion regions have considerable slope indicating not only an appreciable change in sheath thickness with differential probe voltage, but that the sheath radius must be considerably larger than that of the probe.

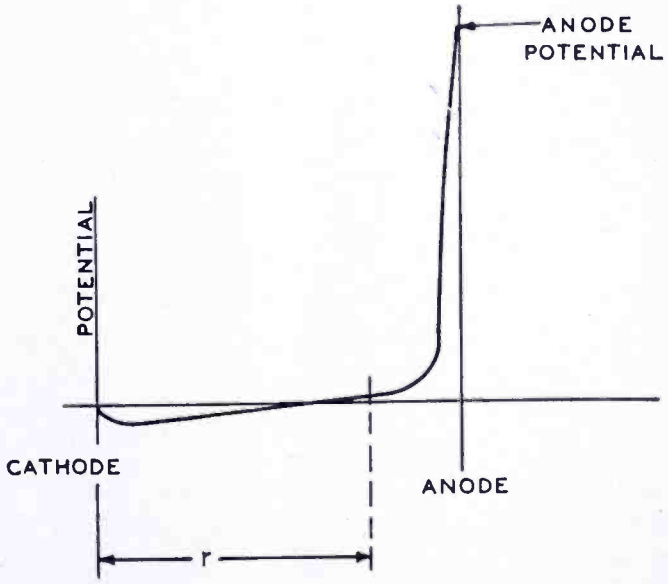

Fig. 11 — Potential distribution through test diode.

The electron temperature was first determined from the data of Figure 12 by the equivalent resistance method described above in section II. It turned out that $T_e = 3400°$ K. It was further assumed that T_p is the same as the gas temperature, in this case 325° K. Thus, $T_e/T_p = 8.0$.

Attention is now fixed upon the point for which I_d in Figure 12 is zero. At this point the probes are at floating potential. The method of section II above is applied to yield the value of positive ion probe current when $I_d = 0$. For the right-hand side of the characteristic it turns out that $i_{wp} = 7.0 \times 10^{-6}$ ampere per centimeter.

The use of Figures 6 and 7 yields $r_c/r_a = 2.46$. Since in this case $r_a = 0.025$ centimeter, $r_c = 0.061$ centimeter. Using this value of r_c, Figure 8 gives $n_{op} = 3.4 \times 10^9$ ions per cubic centimeter. Figure 9 gives the wall potential, $V_w = 1.4$ volts. Finally from Figure 10, the

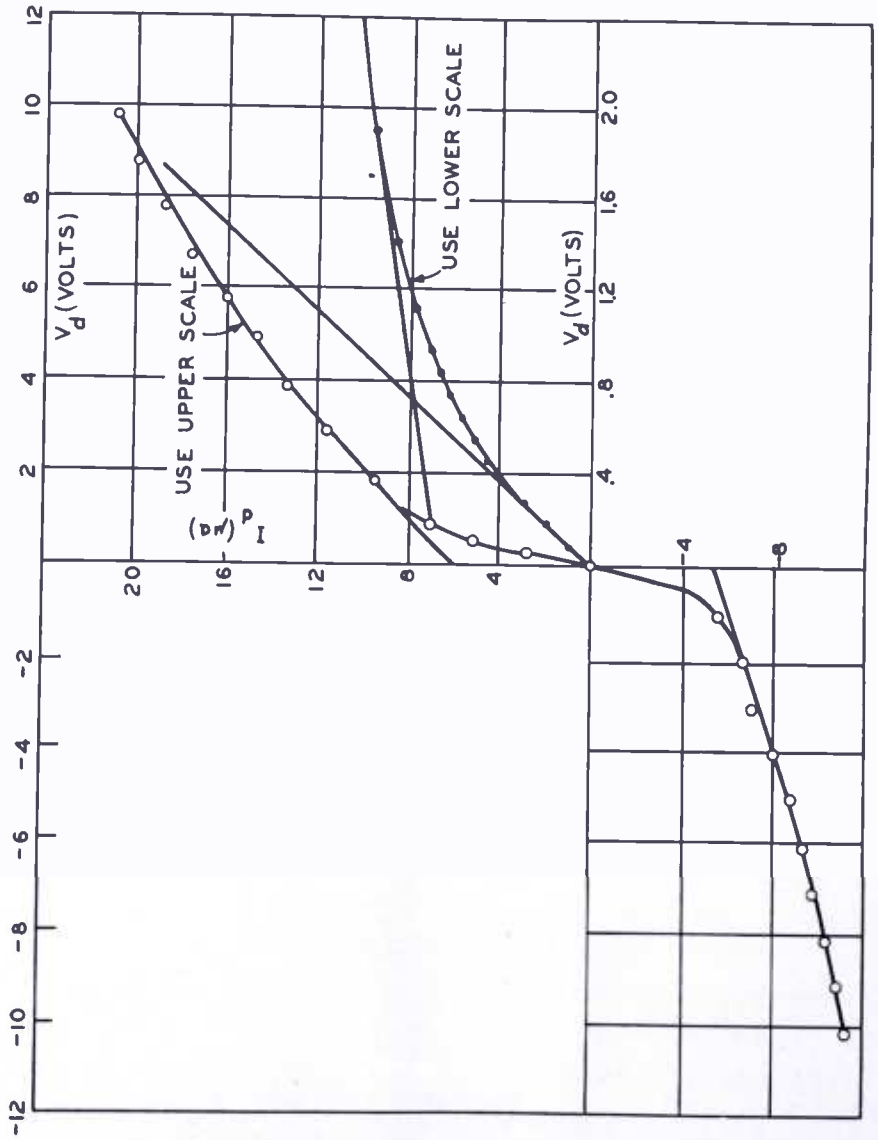

Fig. 12—Double-probe characteristic obtained with test diode.

random electron current in the plasma, $j_{eo} = 5.1 \times 10^{-4}$ ampere per square centimeter.

V. Considerations Regarding Sheath Thickness

Equation (1) is a solution of Poisson's Equation for the case of an infinitely copious cylindrical source emitting only ions with zero velocity towards an inner (or outer) cylindrical collector. The idealized plasma-sheath boundary does not satisfy the above in at least three respects:

1. The source is not infinitely copious but is limited by the random currents in the plasma.
2. The ions are "emitted" with appreciable velocities.
3. Electrons as well as positive ions are "emitted" by the plasma.

The effects of points 1 and 2 above are treated in Appendix 1 (for the plane case). The plasma-sheath solution turns out to be one in which the sheath thickness adjusts itself so that (1) is still satisfied. If the velocity of the ions is zero, the solution is identical with (1). An application of this more exact solution to the problem at hand, with subsequent corrections, indicates that except for the lightest of gases and rarest of plasmas, corrections to Equation (1) are not significant. For the case just treated, the correction is about 10 per cent for sheath thickness and for plasma density. Further experiments, to be described below, indicate that even this estimated correction is excessive.

Attempts to take into account the fact that the plasma also "emits" electrons have not been rewarding. Certain inferences can be drawn from a treatment of Langmuir.[6] He has considered the case of the plasma-sheath combination for zero emission velocity of ions. If one neglects his solution near the origin, which appears to be physically unacceptable, based very likely on his assumption that the gradient at the origin is zero, one obtains corrections for sheath thickness of about the same magnitude as those for the above computed case. These are not sufficiently significant in most cases to justify their consideration.

As will be seen in the next section, experiment bears this out.

VI. Plasma Parameter Determination When Probes Are Not At Floating Potential

Computations will now be carried out for a point at which one of

[6] Irving Langmuir, "The Interaction of Electron and Positive Ion Space Charges in Cathode Sheaths", *The Physical Review*, Vol. 33, No. 6, p. 954, June 1929.

the probes is far removed from plasma potential. The potential configuration for such a case is shown in Figure 13. It is seen that

$$V_{pp} = V_d + V_w - v, \tag{11}$$

where V_{pp} = difference of potential between plasma and probe No. 2,

V_d = differential probe voltage,

v = the change in the potential of probe No. 1 required to permit its electron current to change by an amount equal to the change in the ion current to probe No. 2 as the differential probe voltage changes from zero to V_d. This change in ion current is given by $i_{pp} - i_{wp}$, where i_{pp} is the positive ion current to probe No. 2 when

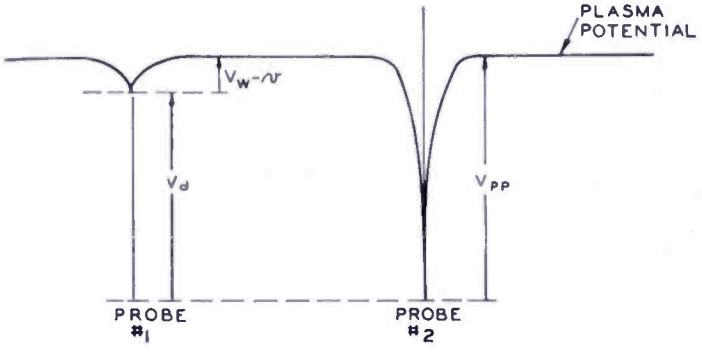

Fig. 13 — Potential distribution through double probes when one of probes is collecting saturated positive ion current only.

$V_d \neq 0$. Then from the Boltzmann relation

$$v = \frac{kT_e}{e} \ln \frac{i_{pp}}{i_{wp}}. \tag{12}$$

In many cases v will be negligibly small. Equation (1) can be rewritten

$$i_{pp} = \frac{3.43 \times 10^{-7} V_{pp}^{3/2}}{r_a \beta^2 M_1^{1/2}}. \tag{13}$$

V_{pp} is given by (11); V_d is determined by the method of Section IV; v is determined from (13). From Equation (13) one can determine $r_c/r_a = f(\beta^2)$. To make unnecessary the solution of (13), a nomogram (Figure 14) has been prepared which yields r_c/r_a from V_{pp}, i_{pp}, the nature of the gas, and the probe geometry. Then from Figures 6, 7, and 8 one obtains the plasma density, n_{op}.

The above will now be applied to the illustrative case of Section IV. At $V_d = 2$ volts, $i_{pp} = 10$ microamperes. Since $i_{wp} = 7$ microamperes,

(13) yields $v = 0.1$ volt. Then, since $V_w = 1.4$ volts (see section IV), $V_{pp} = (2 + 1.4 - 0.1)$ volts $= 3.3$ volts. Using the values of V_{pp} and i_{pp} in Figure 14, $r_c/r_a = 3.40$, $n_{op} = 3.5 \times 10^9$ ions per cubic centimeter.

Similar computations were carried out at other values of V_d. The

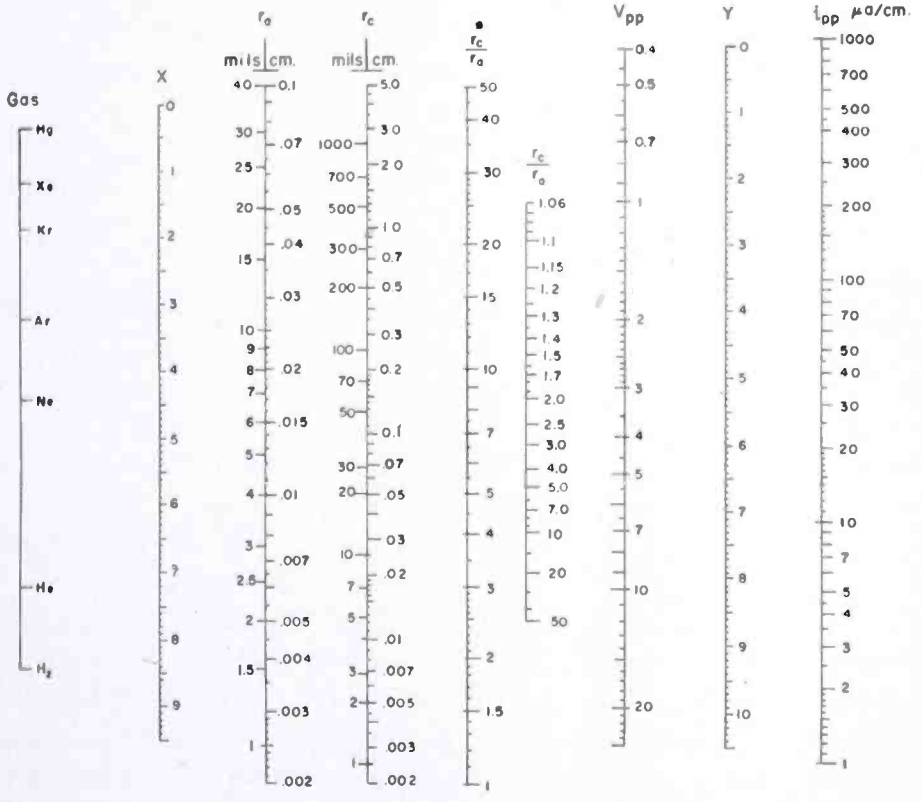

Fig. 14—Nomogram for determination of sheath radius, r_c, from probe data when probe is not at floating potential.

Instructions: (V_{pp} is probe to plasma potential). Find intersection on X of line joining gas and r_a. Find intersection on Y of line joining V_{pp} and i_{pp}. Find intersection on r_c/r_a of line joining X and Y. Transfer r_c/r_a to $(r_c/r_a)^*$. Find intersection on r_c of line joining $(r_c/r_a)^*$ and r_a.

results, together with those for the floating potential case, are given in Table I.

Table I

V_d	i_d	V_{pp}	n_{op}	r_c/r_a	β^2	r_c (cm.)
0	7.0×10^{-6}	1.4	3.4×10^9	2.4		
2	10.0×10^{-6}	3.3	3.5×10^9	3.40	4.12	0.0524
4	13.4×10^{-6}	5.2	3.9×10^9	4.02	6.16	0.0782
6	16.3×10^{-6}	7.2	4.3×10^9	4.57	8.15	0.114
8	17.9×10^{-6}	9.1	3.9×10^9	5.18	10.58	0.130
10	20.9×10^{-6}	11.1	4.1×10^9	5.53	12.2	0.140

From section V it would appear that the determined values for n_{op} should increase with increasing values of V_d. Actually, for V_d equal to 4 volts, or greater, the values of n_{op} have a range of only ± 5 per cent. Even if the value of $V_d = 0$ is included (for which the determination of i_d involves an extrapolation), the range is less than ± 12 per cent. It appears reasonable to believe that if the values of r_c/r_a were appreciably in error over the range of 0 to 10 volts for V_d, the range of n_{op} would be considerable. Thus, experiment too suggests that the accuracy of the determinations of plasma density based upon the simple space-charge equation (1) is adequate for the type of experiment involved.

VII. Single Probe Considerations

As a rule, plasma density can best be determined in the single-probe method by the measurement of saturated electron probe current. Under certain conditions, e.g., if drawing saturated plasma current to the probe disturbs the discharge, it may be desirable to make the density determination from positive ion probe currents. This is possible only when temperature values can be assigned to the ions. Such can be done for many types of discharge, particularly of the hot-cathode type where pressures are not too low or plasma gradients high.

T_e is determined from the lower portions of the ascending probe characteristic where electron flow to the probe starts. (In this region the electron probe currents will not unduly disturb the discharge.) If the positive ion probe current, i_{pp}, is measured for the case wherein the probe is highly negative with respect to the plasma, then for the plasma to probe potential one can use, as a first approximation, the difference between the potential at which the probe draws positive ion current, i_{pp}, and the potential at which it draws zero current. This potential difference is designated V_{po}. If a better approximation is desired, an approximate value for wall potential, $V_w{}^*$, can be obtained from Equation (7) by setting $r_c/r_a = 1$. Since the conditions of the experiment require that $V_w \ll V_{po}$, it follows that the error introduced by neglecting the fact that $r_c/r_a \neq 1$, will be small.

Setting $V_{pp} = V_{po} + V_w{}^*$, the plasma parameters can then be determined from Figures 14, 6, 7 and 8 as indicated in section VI. If greater precision is required, one can then use the value of r_c/r_a obtained to recompute $V_w{}^*$ and V_{pp} and then proceed as before. The process can be repeated if necessary.

VIII. Conclusion

Direct and simple methods have previously been described for obtaining electron temperature by means of double probes. Determination

of other gas discharge parameters such as plasma density, random currents in the plasma, and wall potential, from double probe data requires tedious trial and error solution of transcendental equations. Methods are described whereby these quantities can be determined very rapidly by means of a family of nomograms.

It is shown how the nomograms may also be applied to single probe data, thus permitting the use of single probes in a manner less disturbing to a discharge than the methods conventionally employed.

NOTE: A limited number of large scale reproductions of the nomograms shown in Figures 6, 8, 9, 10 and 14 are available and may be obtained from the authors.

APPENDIX†

SPACE-CHARGE EQUATION FOR FINITE CURRENT SOURCE AND FINITE EMISSION VELOCITIES

Consider a planar source of positive ions of current density j_p. Let the ions be emitted with a uniform velocity $v_o = \sqrt{2\frac{e}{m}V_o}$ toward a parallel plane anode at potential V_b at a distance b from the ion source. This can be considered as simulating a positive ion sheath in which the velocity v_o with which the ions enter the sheath is given by their mean Maxwellian velocity in the plasma.

Poisson's Equation for this case is

$$\frac{d^2V}{dx^2} = \frac{4\pi e\, j_p}{\left[2\frac{e}{m}(V+V_o)\right]^{1/2}}, \tag{14}$$

where V is the potential at point x in the sheath. The solution of (14), subject to the conditions $V=0$ at $x=0$; $\frac{dV}{dx}=0$ at $x=0$; $V=V_b$ at $x=b$, has the form

$$b = \frac{V_b^{3/4}}{\left[9\pi\, j_p\left(\frac{m}{2e}\right)^{1/2}\right]^{1/2}}\left[\frac{1.5}{\mu_b^{3/2}}\int_o^{\mu_b}\frac{\mu d\mu}{[\mu - n(1+\mu)]^{1/2}}\right], \tag{15}$$

where $\mu = \left[\frac{V}{V_o}\right]^{1/2}$, and $\mu_b = \left[\frac{V_b}{V_o}\right]^{1/2}$.

† This analysis is due to E. O. Johnson of this laboratory.

If the ions enter the sheath with zero velocity, then $\mu = \infty$ and the quantity in the bracket of (15) is equal to unity. Then

$$[b]_{V_0=0} = b_0 = \frac{V_b^{3/4}}{\left[9\pi j_p \left(\frac{m}{2e}\right)^{1/2}\right]^{1/2}}, \tag{16}$$

where b_0 is the conventional expression for the spacing between cathode and anode for the case of zero emission velocities. Thus

$$\frac{b}{b_0} = \frac{1.5}{\mu_b} \int_0^{\mu_b} \frac{\mu d\mu}{[\mu - \ln(1+\mu)]^{1/2}}, \tag{17}$$

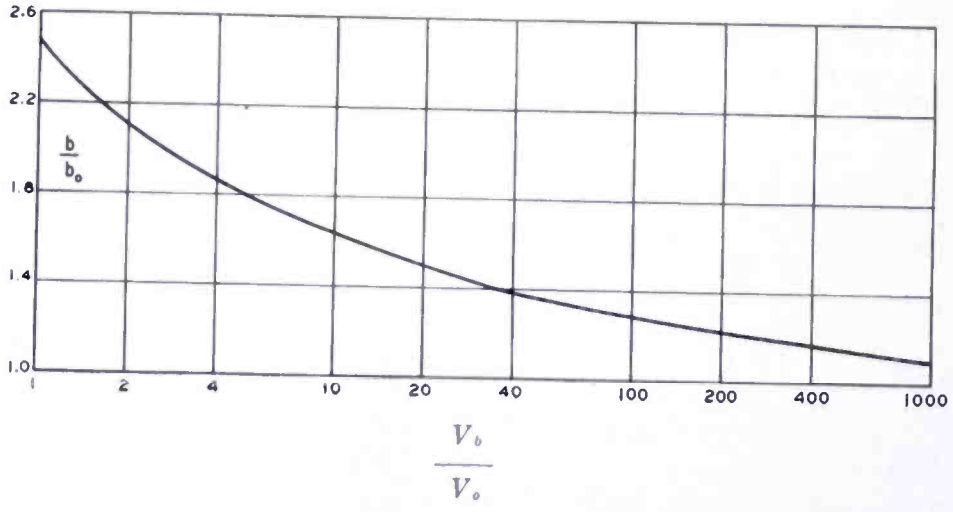

Fig. 15—Corrections to sheath thickness resulting from initial velocity of ions (plane case).

is a measure of the effect of the initial velocity of the ions upon the sheath thickness. Figure 15 is a plot of b/b_0 as a function of $\frac{1}{\mu_b^2} = \frac{V_0}{V_b}$. If the ion temperature is 350° K, then $V_0 \simeq 0.03$ volt. If $V_b = 10$ volts, then $\frac{V_0}{V_b} \simeq 300$. In that case $b/b_0 \simeq 1.2$. For cylindrical probes the sheath expansion due to initial velocity of the ions will be less than in the case of a plane probe. This results from the concentration of field at the cylindrical probe.

A NEW TELEVISION STUDIO AUDIO CONSOLE*

By

Robert W. Byloff

Engineering Department, National Broadcasting Company, Inc.,
New York, N. Y.

Summary—A new audio console, equally useful in television and radio studios, has been built. It combines a large number of operating facilities, exceptional flexibility, and compactness. Specific attention was given to the layout of controls to achieve operational convenience. Among the features are a twelve position mixer split three ways, a built-in sound effects filter, microphone equalization, lighted controls, sound effects switching, and video monitoring. This article describes the mechanical features of the console as well as the reasoning underlying its design. A description of the circuit configuration and of an unusual mixing circuit is included. Performance data of the system is also given.

Introduction

As the size and complexity of television studio productions have grown, it has become obvious that a studio audio system specifically designed for television was needed. Such a system had to incorporate not only the special facilities demanded by television but, at the same time, in the interests of standardization, it was necessary that it be equally usable for radio production. This last requirement was given added importance when it became the practice to use the same program simultaneously for television and sound radio.

An investigation of the requirements of such a studio audio system disclosed that it must be more flexible and larger than one to be used for sound broadcasting alone. Specifically, the investigation showed that the system must include more fader positions, more facilities for combining or mastering these faders, a simple way of handling program sources (nemos) outside the studio, special equalization to compensate for unavoidably poor microphone placement, a switching system for special effects filters, special control lighting and indexing, automatic gain control, and provision for built-in video monitoring.

A system, designed from these requirements and described herein, has actually been built and is installed in several new television studios. Among these are the world's largest dramatic studio and the world's largest television theater.

---

* Decimal Classification: R610.

Mechanical Features

The principles used in the mechanical design of the console were as follows:

1. The console to be as small as possible in all dimensions to allow its use in the normally crowded spaces allotted to television control rooms, and to allow good visibility over the console.
2. All controls to be within easy reach.
3. Space to be provided for a script or cue sheet.
4. Primary operating controls to be on the front panel and properly indexed, and secondary and preset controls to be on the side panels.
5. Space to be provided for five video monitors in the console, since video monitoring for the audio operator is essential in keeping the microphone boom out of the picture.
6. The video monitor portion to be attachable as a separate item to allow use of the console in radio studios or any locations not requiring picture monitoring.
7. The console equipment to be accessible for maintenance from the front of the console to the extent necessary to provide maximum flexibility of console location in the control booth.
8. All equipment, not requiring manipulation by the operator, to be mounted elsewhere to save operating space and to permit easy maintenance.

Figure 1 is a view of the console. The unit as shown is 66 inches long, 36 inches deep, and 41 inches high. Without the video monitoring portion, the depth is reduced to 23 inches and the height toward the front to 36 inches. The distance from the center of one side panel to the other is 45 inches, which permits easy reach to either side. The desk top is wide enough to allow legal size sheets of paper, which is normal script size, to be placed on it without overhang. The sloping portions of the top allow the panels to be set down and thus reduce overall height. This feature also allows the operator's hands to reach the top controls on the front panel more comfortably. On the right side of the desk top is a sliding panel which covers a well in which the microphone preamplifier inputs appear on drop cords. These drop cords (similar to telephone switchboard cords) are used for microphone selection, and can be patched into the microphone receptacle jacks in the jackfield directly above the well.

The front panel, sloped at 20 degrees from vertical for maximum operating ease, has in its top row of controls 12 microphone faders. The center group of controls in the lower row are the red, white, and green submaster faders, a studio master fader and a remote master fader. These submaster faders are color coded to provide a convenient

visual tie-in with fader assignments as described below. The controls on the ends of the panel are for studio playback and reverberation. All faders on the front panel have dials, which are illuminated when they are in use. Each dial is calibrated and, in addition, contains an illuminated pointer enabling the operator to tell at a glance the position of the fader. Above each microphone fader is a translucent window which lights up red, white, or green depending on whether the fader is assigned to be mastered by the red, white, or green submaster. The window is dark when the fader is unassigned. The surface of the window is roughened to allow the operator to pencil and erase any

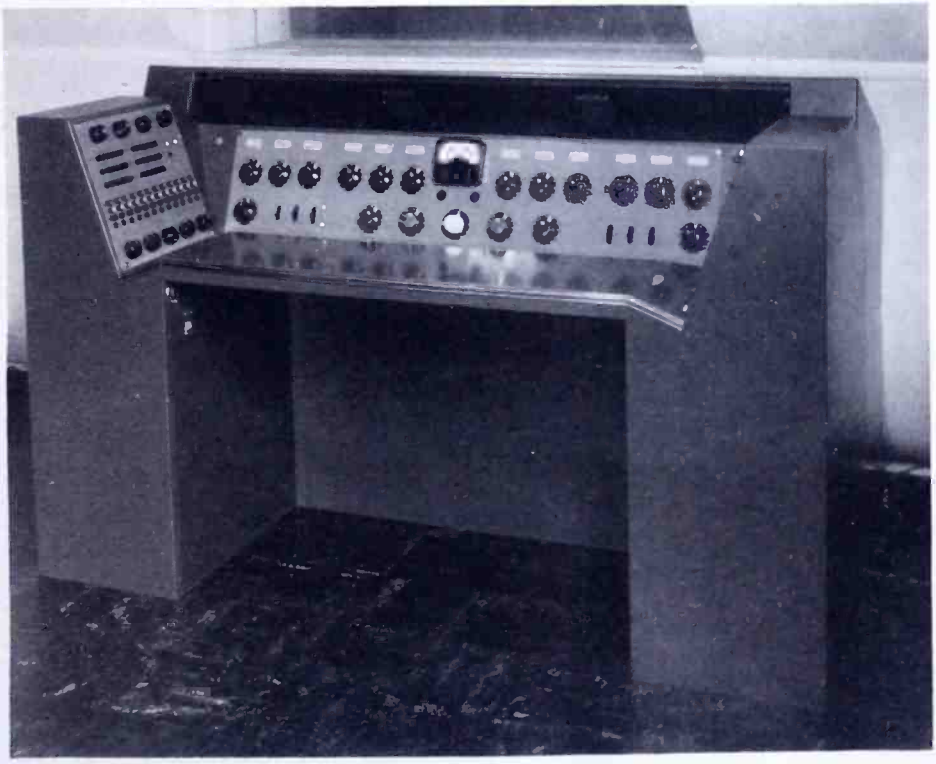

Fig. 1—The studio console shown in position with video monitor housing attached.

supplementary information he wishes on it. He may, for example, write "orchestra" or "cast" or "boom" on these windows, and the light behind the window makes his writing show up in the darkened control room. Thus these windows indicate to the operator whether or not the fader is connected, the submaster to which it is connected, and any other information about that channel he may wish to indicate. Lever keys on the front panel select remote programs, sound preview remote programs, control sound effects filter, and do auxiliary switching. An illuminated volume indicator in the center of the panel shows the volume level on the output of the system.

The right side panel contains a jackfield for patching up effects, equalizers, microphones, and other program sources, and for emergencies. This panel also contains equalizer controls for microphone equalization, and a control for the selection of limiting or compression in the program amplifier.

The left side panel at the top contains four microphone faders in a separate four position auxiliary mixer which is used for audience reaction and is normally preset. Controls for monitoring and sound effects filter frequency response and gain are contained at the bottom of the panel. In the center of the panel are push buttons, for assigning faders to submasters. There are four buttons for each fader: a red, a white, a green, and a black one for "off". Pressing the red button for fader 1, for example, connects it to the red submaster and lights up the indicator window above fader 1 in red. Another set of push buttons on this panel is used for effects switching as described below.

Fig. 2—Racks containing all necessary amplifiers, power supplies, and relays for the audio system.

The housing attached to the back of the console allows five 10-inch video monitors, set on dollies with their kinescope faces up, to be placed in the console. These kinescopes are viewed by reflection from a front surfaced mirror set in the housing. These monitors enable the audio operator on a television program to observe the outputs of all of the cameras and also the program leaving the studio. This is particularly important to him from the standpoint of keeping the mike out of the picture. The housing is completely independent of the rest of the console and may be removed if not required.

The three panels inside the kneehole of the console are removable for maintenance of the equipment. The front panel is hinged and drops forward; the side panels are removable with thumb screws.

Figure 2 shows the rack equipment required for the console. The jackfield is used primarily for maintenance checking. The racks contain preamplifiers, boosters, power supplies, relays, and monitoring amplifiers for the system.

Electrical Features

Figure 3 shows a simplified block diagram of the over-all system. No attempt has been made in this drawing to show specific circuit components, which are known to anyone familiar with audio practices.

Twenty-four microphone outlets are available at the console, and may be connected to the twelve preamplifier inputs by drop cords. These sources are then normalled through preamplifiers to the twelve regular faders. A push button control system as described previously at the fader outputs enables each fader to be connected to any of three mixers. The reason for having three mixers is to permit mastering in three groups. This grouping reduces the need for individual fader manipulation and confines much of the operator's attention to three controls. The outputs of these mixers, following amplification are connected to the three submaster faders. The outputs of the submasters are then mixed and routed to the studio master fader. The studio master fader output is mixed with a nemo (or remote) master output which in turn goes to the studio amplifier to bring the program level to studio bus level, or to line level if the output is to feed telephone lines. The studio amplifier is a special automatic gain control amplifier with selection of either limiting or compression characteristics. The characteristic to be used is selected by the audio operator by means of a key at the console. One of the advantages of an amplifier of this type in the system is that it permits greater latitude in gain settings and thus assists the operator in that respect on a program.

The input of the nemo master fader comes from selector relays, which choose one of two remote program inputs which are sent to the studio by the transmission section of the studio plant. Selection of the proper nemo program is made either by the audio engineer with a key at his position or, if he desires, it may be accomplished by the picture switcher. When this set-up is used, audio and video switching to remote programs is done together automatically. Having the nemo master fader and studio master in parallel enables the audio operator to fade out his studio program and fade in the remote program with these two knobs alone. This feature is desirable particularly for commercial film insertions in a studio program.

Bridges are taken off the remote lines as they enter the studio system and are brought to a key for selection. The selected program is

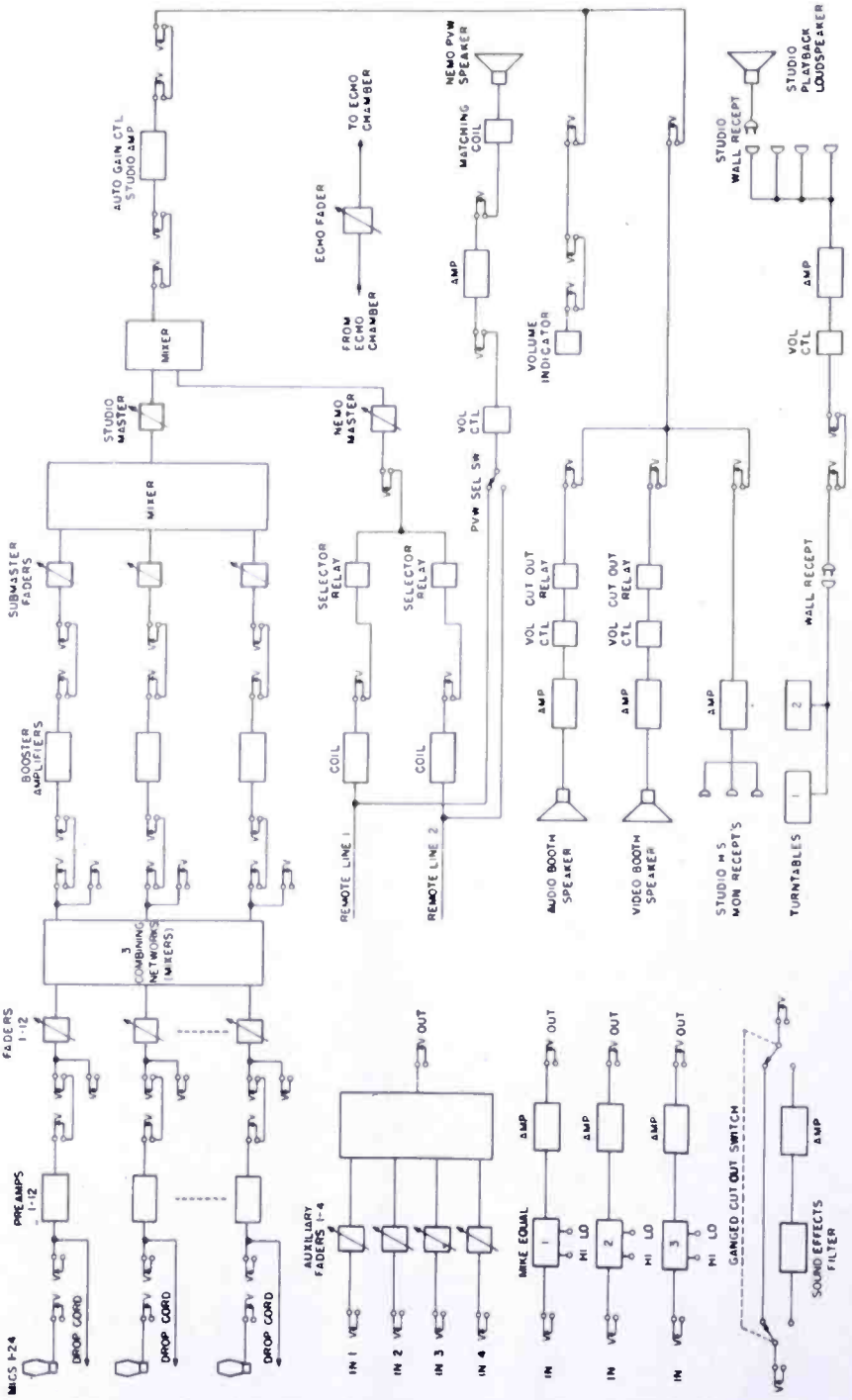

Fig. 3—Block diagram of studio audio system.

then amplified and sent to a small loudspeaker so that the audio man may listen to the remote program on a preview speaker before he puts it on the air.

Two turntables are usually provided in television studios for bridge music, themes, and actions where a voice intending to portray the thoughts of the actor is heard. These bits must be played back to the studio so that the actors may better know what is happening. In the console the turntable outputs are normalled to the input of a studio loudspeaker volume control which goes to a loudspeaker amplifier, the output of which is sent to outlets in the studio. A portable loudspeaker may be placed near the scene of the action and plugged into the nearest outlet. This placement enables low volume level on the loudspeaker and avoids excessive echo in the studio. Actual program from the turntables is connected to a program fader for transmission and control.

The auxiliary four-position mixer has four input jacks going to four faders. These fader outputs are combined and appear on a jack which may be used to patch this system to any console input. This mixer allows applause control of four microphones using only one regular fader position.

Monitoring feeds from the studio bus or line go to the console volume indicator, to the video and audio booth speaker amplifiers, and to a headset monitoring amplifier. The booth speaker amplifiers have cutoff relays on their inputs to avoid feedbacks when the studio address system in the control booth is used. The headset monitor amplifier output is fed to studio receptacles for the use of sound effects technicians, orchestra leaders, and stage managers.

All equalizers and sound effects filters in the system are arranged for zero insertion loss by providing amplification in these circuits to compensate for filter losses. The three microphone equalizers have low- and high-frequency control and are on jacks, so that they may be connected to any microphone channel desired. The sound effects filter has a by-pass switch around it, so that it may be inserted on cue, and a gain control to compensate for different settings of the filter.

The effects switching system is shown in Figure 4. This is a relay switching system with three inputs and three outputs. If three microphone channels are connected through this system, they may each be connected, through operation of appropriate relays, to any effect required such as a sound effects filter, an echo chamber, or simply a volume control. This switching then allows an echo chamber, for example, to be inserted in different microphone channels during a program without repatching. In television audio work this facility is important because a special filter or echo microphone cannot be assigned for use by the actors as the program demands, and so these effects

must be available on several microphones. The system is also useful in telephone conversation effects where both ends of the conversation are shown with first one party on filter, and in the next instant, the other party on filter. Control of these relays is provided at the console. This control may be done either by the engineer at the console with simple on-off buttons or he may elect to tie the system to camera switching. If so, the filter switching is caused by the switching of cameras. A tally panel in the console shows the audio operator which camera is on the air.

In addition to the above facilities, the system contains contrast controls on the console for the video monitors, rack to console tie trunks, jack multiple strips, auxiliary isolation coils, talkback facilities to the studio address speaker and to the headphones of the boom operator, telephone facilities to other studios and to master control, and telephone facilities to other audio operators in the same studio. Multiple jacks on microphone channels are provided for connecting to an auxiliary public

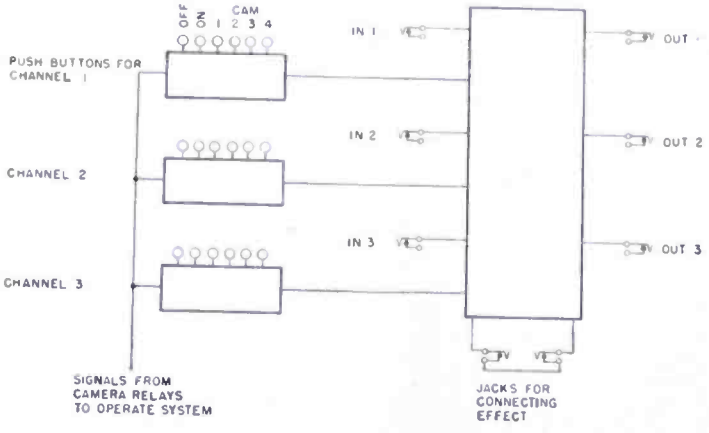

Fig. 4 — Block diagram of effects switching system.

address system if the console is used in an audience studio. This provision allows for individual microphone public address, which has been found to be essential for television studio public address systems.

An unusual feature of the console is the microphone channel mixer. In the past when a split mixer was provided, it was necessary to have switching keys of complex configuration for connecting the microphone channel to one or the other mixer. This complexity was required because the mixer was a matched impedance system and whenever a fader was removed, a resistor of the same impedance had to be substituted for the fader in order to keep the same loss through the mixer. If the mixer must be split three ways, the complexity of the switching key becomes so great as to be impractical. Therefore, a bridging mixer was employed. In this system, the series resistors going to the faders are large enough to keep the mixer from knowing whether a fader is connected or not. Terminating resistors are provided at each of the twelve

inputs to terminate the faders properly. Some compromise must be made in this system to prevent excessive loss of level. The compromise agreed on was to allow a 2-decibel variation in mixer loss between the extremes of having one or twelve faders connected to the same mixer. With this compromise it was possible to design a mixing system with approximately 7 decibels more loss than in a conventional matched impedence mixer. This loss is easily made up in modern high-gain amplifiers. The mixing system employed is shown in Figure 5.

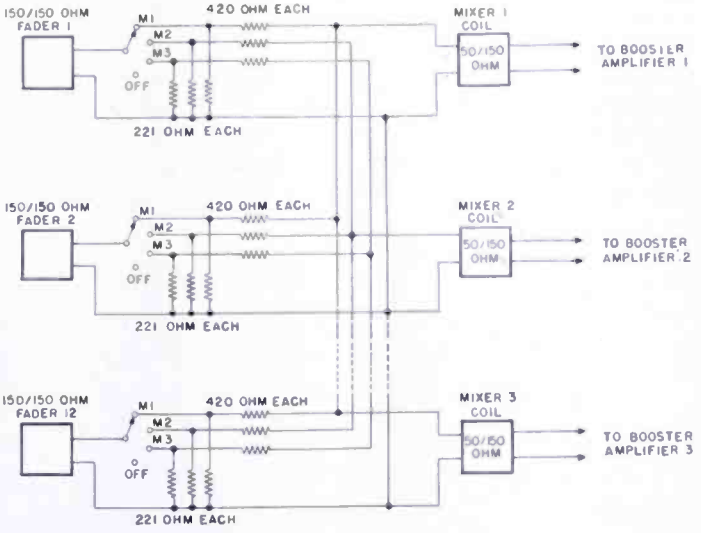

Fig. 5 — Schematic drawing of bridging mixers employed in audio console.

Performance Data

The performance of the overall system is of considerable interest. The frequency response is essentially flat from 30 to 15,000 cycles per second. Distortion at 10 decibels higher than normal level through the system is less than 0.5 per cent and the signal-to-noise ratio is 77 decibels below the level at which the distortion measurements were made. These performance figures far exceed the FCC requirements for sound or television broadcasting.

Acknowledgments

The author wishes to express thanks to C. A. Rackey, D. H. Castle, G. M. Hastings, and F. R. Rojas of the National Broadcasting Company for their encouragement and helpful suggestions during the design of this apparatus, and to M. E. Gunn of the RCA Victor Division for his invaluable contributions to this project.

A STORAGE OSCILLOSCOPE*

By

L. E. Flory, J. E. Dilley, W. S. Pike and R. W. Smith

Research Department, RCA Laboratories Division,
Princeton, N. J.

Summary—With the continued increase in operational speed of electronic devices, visual observation of the consequent short duration and often non-repetitive phenomena produced has become increasingly difficult. Long persistence phosphors or photography may be used, but they have obvious disadvantages. This paper describes a storage oscilloscope built around a Graphechon electronic storage tube which may be used for viewing such transients. Such a device is shown to offer certain advantages in convenience, speed, flexibility and viewing time over more conventional methods.

Introduction

With the continued increase in the speed of operation of electronic devices, the problem of observation of phenomena of extremely short duration has become increasingly difficult. This is especially true of events which occur at a very low repetition rate or perhaps singly as do many transient phenomena. For example, in microwave radar applications, pulses of .1 microsecond or shorter often must be studied, frequently at very low duty cycles. Also, disturbances generated by various nuclear disintegration processes may occur at a random rate or only once and frequently last no longer than 10^{-9} second. Since the information is to be received in an extremely short time and studied for a relatively long period, it is obvious that some storage system is required and preferably one more flexible than photography.

Two methods for the observation of nonrecurrent phenomena are generally used. For direct observation, a long-persistence phosphor may be used or the trace on a phosphor may be photographed for later study. Both methods have many disadvantages. The long-persistence phosphor has a long persistence in a relative sense only, the decay being quite rapid, especially during the first part of the curve. Photography has the obvious disadvantage of inconvenience and delay, particularly important where circuit adjustment depends upon continuous observation of successive traces.

A number of electronic storage devices have been developed which

* Decimal Classification: R371.5.

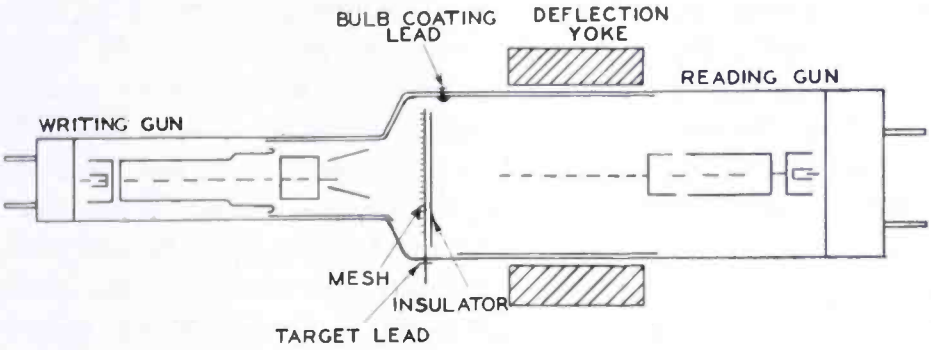

Fig. 1—Development model Graphechon tube.

can accept electrical information, retain it for a period and then reproduce it once or many times as desired. One such tube described recently is the Graphechon.[1] In this tube, a surface capable of accepting and retaining a charge pattern is scanned by an electron beam, for instance in a television raster. As the beam scans the surface, a secondary emission picture of the entire scanned area is produced in much the same manner that the signal is generated in a television pickup tube. By this means, any charge distribution over the surface can be reproduced on a television monitor. If the wave form to be observed is written as a charge trace on the storage surface, it will then be reproduced for viewing.

Figure 1 shows a schematic diagram of a development model of the Graphechon storage tube, and a photograph of the tube is shown in Figure 2. The target or storage element consists of a fine mesh screen supporting a very thin layer of aluminum on which in turn is deposited a thin layer of insulating material. An electron beam which is called the reading beam, scans over the insulating surface and establishes a condition of potential equilibrium. Once this equilibrium is established, further scanning with no signal applied produces no signal output. If now a second beam from the opposite side of the target and of

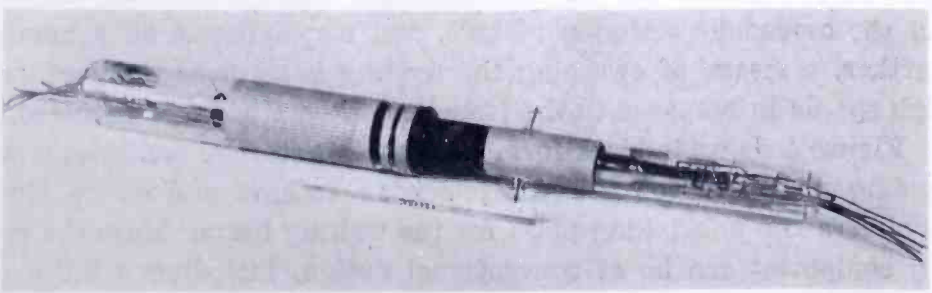

Fig. 2—Developmental Graphechon used in the storage oscilloscope.

[1] L. Pensak, "The Graphechon — A Picture Storage Tube", *RCA Review*, Vol. IX, No. 1, p. 59, March 1949.

sufficient energy to penetrate the aluminum and insulating film is caused to strike the target and scan some pattern over the surface, it will upset this equilibrium condition by depositing or removing charge from the insulator. This beam is called the writing beam. This condition must then be corrected by the reading beam and the process of restoring equilibrium generates the reading signal. If the amount of charge removed or deposited by the writing beam in one scan is large compared to the amount which can be restored by the reading beam in one scan, then many scans of the reading beam will be necessary to restore the original conditions, and thus many reproductions of the written signal will be obtained. This process provides the mechanism of storage utilized in the instrument to be described.

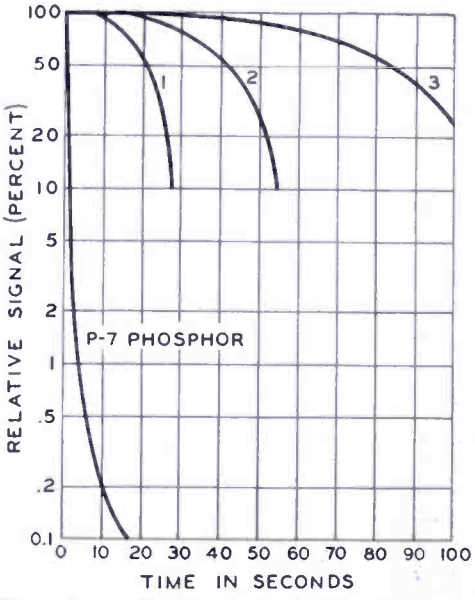

Fig. 3 — Discharge characteristic of typical Graphechon read at 30 frames per second for different values of reading-beam current.

Figure 3 shows the discharge characteristic of a typical Graphechon storage tube for different values of reading current. The curves shown were taken at television scanning rates of thirty frames per second. From these curves, it can be seen that the viewing time can be adjusted by varying the amount of reading-beam current. For purposes of comparison, the decay curve for the most common of the long-persistence phosphors, the P-7, is also shown. Useful viewing times up to a minute can be obtained as shown by these curves.

In order to utilize a tube of this type as an oscilloscope, it is necessary to provide means for scanning the storage surface, amplifying the secondary emission picture, and displaying it on a monitor. Further, a means of sweeping the writing beam over the surface at high speeds in response to the transient to be studied is required.

Figure 4 shows in block form the complete storage oscilloscope with reading means in conventional television fashion and sweep circuit amplifiers and unblanking pulse for the writing beam. Since the reading equipment can be of conventional design, including a video amplifier, deflecting circuits and monitor tube with necessary power supplies, it is not necessary to go into detail on this part of the equipment. One point which might be mentioned is that of modulating the

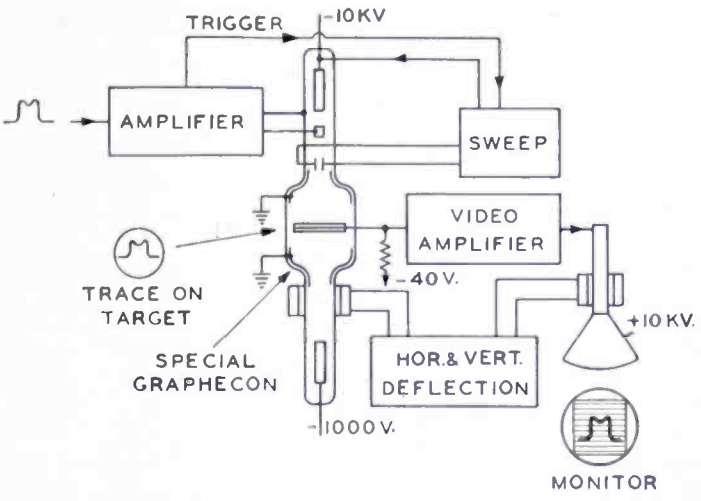

Fig. 4 — Block diagram of storage oscilloscope.

reading beam class C with a frequency of the order of 25 megacycles, permitting the use of standard television intermediate-frequency amplifiers for the video, and at the same time reducing the trouble which would have been encountered with hum, microphonics, etc. in an amplifier designed to pass low frequencies. This type of operation also serves to separate writing signals from reading signals.

Since the main use of the storage oscilloscope is for the observation of high speed transients, it follows that a high speed triggered sweep is necessary. Shown in Figure 5 is the simplified schematic of the sweep circuit used in the present instrument. The incoming trigger pulse is amplified and used to trigger a biased-off blocking oscillator which generates a very sharp pulse. This pulse is in turn, used to trigger a single-shot cathode coupled multivibrator which generates a pulse whose width depends upon the time constant of the cathode coupling circuit. Different lengths of sweep can thus be obtained by changing the time constant in this circuit. This pulse is then applied to a saw-tooth generating tube which generates in its plate circuit a linearly varying current signal during the charging of the plate capacitor. The size of

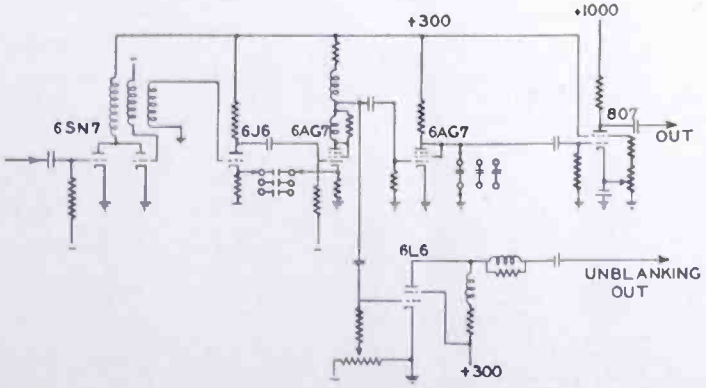

Fig. 5—Basic sweep circuit used in the oscilloscope.

this capacitor is matched to the time constant of the multivibrator in order that the same amplitude of linear deflection will be obtained at all speeds. The output of this tube is used to drive an 807 output tube. In order to keep the plate dissipation of the output tube at a reasonable value, the tube is operated in a partially biased-off condition, since the grid signal is always in a positive direction, and since for most applications the duty cycle is extremely low. About 700 volts of deflection are generated with a steady plate current of 20 milliamperes. The shortest sweep time is about 0.15 microsecond. For shorter sweep times a line-type pulser may be used.

A pulse taken from the multivibrator is also used to generate an unblanking pulse which is applied to the grid of the writing gun and serves to turn on the writing beam only during the sweep time. Since this pulse comes from the same source as the sweep signal, it automatically comes out the proper length.

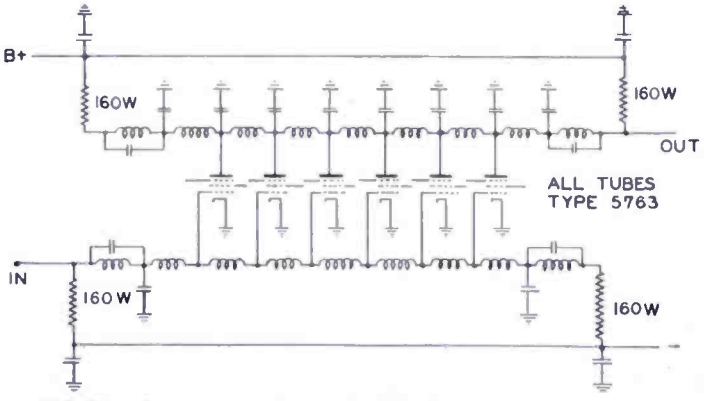

Fig. 6 — Distributed type amplifier.

While the operation of the instrument is such that it is difficult to assign a value to deflection sensitivity in the usual sense, as will be apparent as the operation of the instrument is further described, 50 to 100 volts of signal are necessary to obtain usable deflections. For a great many applications therefore, some amplification is necessary. Since the objective of the development was aimed toward a resolving time of 10^{-8} second or better, it is obvious that conventional video amplifiers would not be satisfactory. There has recently been considerable work done on a type of amplifier known as a distributed amplifier or travelling wave amplifier.[2] A schematic of such an amplifier is shown in Figure 6.

In this amplifier, the input signal travels down the transmission line in the plate and grid at the same rate so that plate signals from successive tubes add to produce a larger signal across the output termination. By this means, the tubes are essentially in parallel as far

[2] E. L. Ginzton, W. R. Hewlett, J. H. Jasberg and J. D. Noe, "Distributed Amplification", *Proc. I.R.E.*, Vol. 36, No. 8, p. 956, August, 1948.

as signal is concerned but the capacities of the tubes are isolated by the sections of the line. Approximately one half the sum of the plate currents of the tubes is effective, the other half being lost in the termination at the opposite end of the plate line. Useful gains with bandwidths up to 200 megacycles have been obtained in this manner. The tubes shown in this amplifier are 5763's which have a mutual conductance of 7000 micromhos and a plate current of 50 milliamperes or more each at 100 volts plate voltage. This permits an output of about 50 volts peak-to-peak across the lines which are about 160 ohms impedance. Two such amplifiers are used in push-pull and may be driven by a third similar stage through a phase inverter. This arrangement is shown in Figure 7. If it is desired to trip the sweep directly from the signal to be observed, a delay line may be placed between the sweep sync input and the input of the deflection amplifiers to permit the sweep to start ahead of the signal deflection.

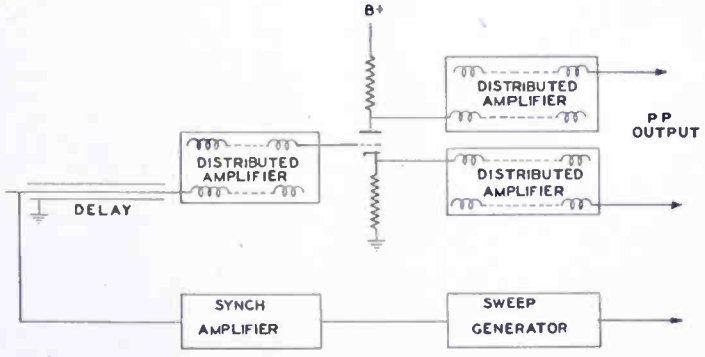

Fig. 7 — Push-pull distributed amplifier.

The over-all voltage gain of the arrangement shown in Figure 7 is about 15. Additional amplifier stages may of course be added as desired, depending upon the application. Front and back views of the complete instrument are shown in Figures 8 and 9.

The method of reproducing the traces by television scanning techniques permits flexibilities not otherwise possible. For instance, by scanning a small area on the storage target while maintaining full deflection on the monitor, it is possible to realize a scanning magnification. It is for this reason that conventional sensitivity figures of volts per inch deflection are meaningless. A more accurate realization of the sensitivity may be gained in terms of volts per line width of the trace. Stated in this manner, about 10 volts signal per line width of deflection is required.

To carry the scanning magnification principle further, it is obviously possible to enlarge the trace by television projection to a theatre size screen. The amount of additional information which can be obtained by such magnification is of course limited by the resolution of

the scanning beams. Aside from this, however, the enlarged picture is of advantage where a large number of people wish to view the display, as in classroom instruction. In this regard, it is also possible to take advantage of television transmission techniques for transferring the display information to one or more remote locations where it may be viewed for instruction purposes on standard television receivers. Since the output signal can be complete with sync pulses, it may be transmitted over the usual coaxial cable and introduced into the video section of a receiver with no modification.

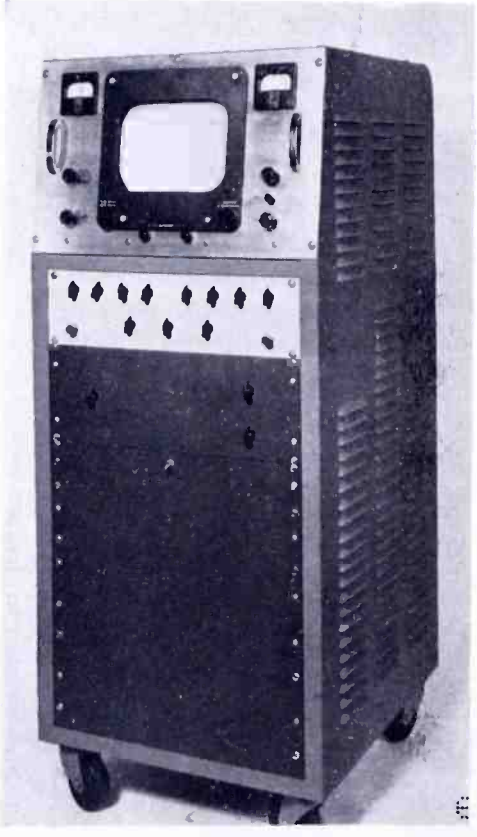

Fig. 8 — Front view of completed storage oscilloscope.

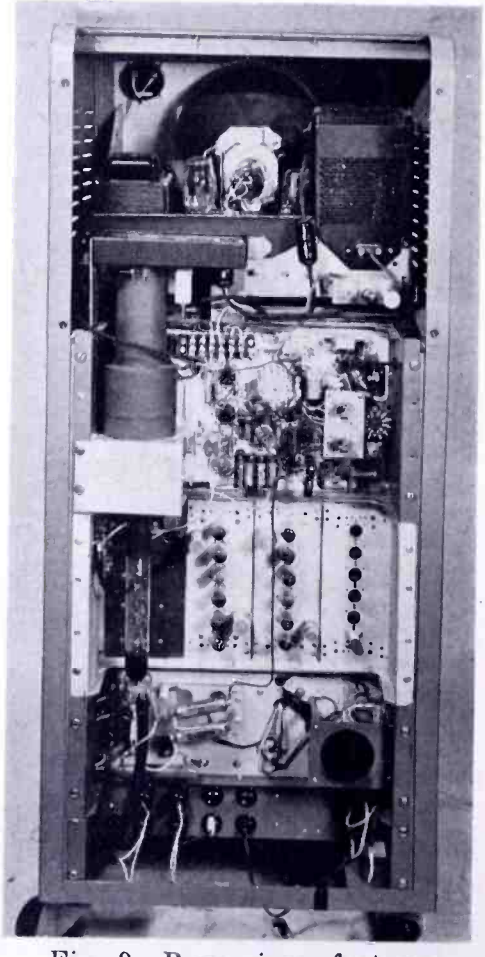

Fig. 9—Rear view of storage oscilloscope.

The extreme speed of response of the storage tube, combined with the flexibility of the monitoring method, permits the observation of phenomena which would otherwise be difficult. Figure 10 shows a .05-microsecond pulse recorded in a single sweep and photographed from the monitor screen. The trace in this case was visible for about a minute. The rise time is 10^{-8} second.

In cases where a photographic record of a trace is desired, the

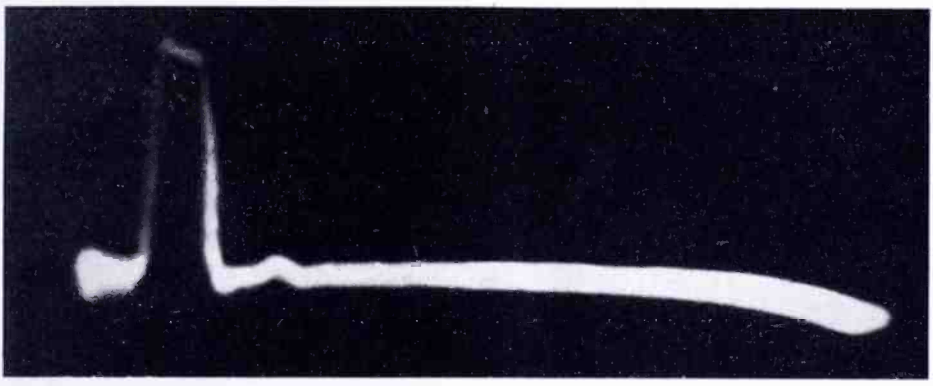

Fig. 10—.05-microsecond pulse recorded in a single sweep. Rise time 10^{-8} second.

feature of being able to view the trace before photographing is of great assistance. It enables the operator to make sure that a satisfactory trace has been obtained before a photograph is actually taken. The long viewing time permits the use of ordinary snap shot techniques with only minor precautions in eliminating stray light.

Figure 11 shows a portion of the build-up of a pulsed 50-megacycle oscillator. The sweep time was of the order of 0.5 microsecond. The separate loops of the 50-megacycle signal are plainly visible at the start of the build-up. Again this trace was recorded in one single sweep of the writing beam.

One of the more interesting applications of the instrument, as was mentioned earlier, is in the observation of nuclear phenomena. Figure 12 shows three traces taken of the output of a scintillation type counter. The traces are one microsecond in length and were recorded in succession on the storage tube and photographed simultaneously. This is an illustration of an additional flexibility of the instrument, in that

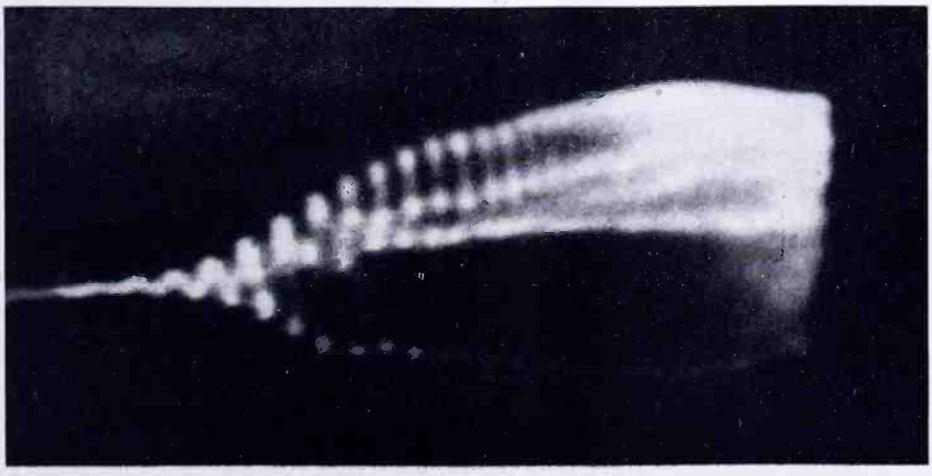

Fig. 11—Build-up of pulsed 50-megacycle oscillator.

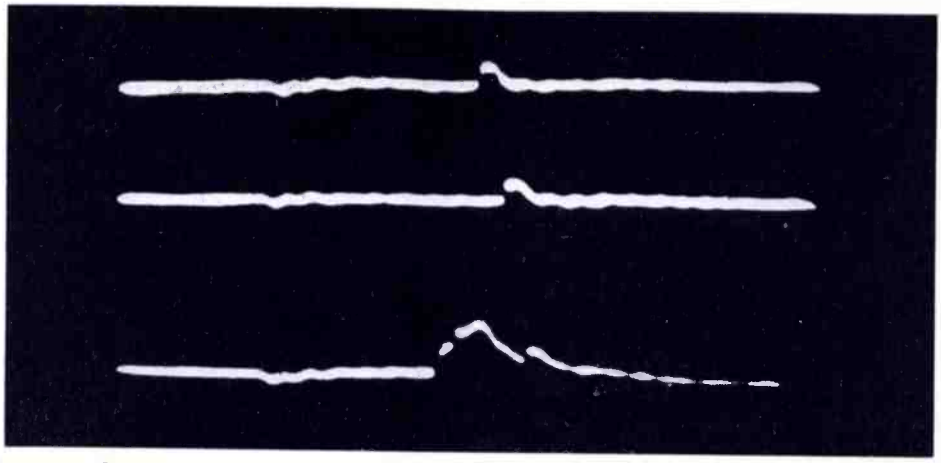

Fig. 12—Output of scintillation counter viewed on storage oscilloscope. All traces are 1.0 microsecond long.

several traces may be recorded in sequence on the target simply by shifting the position of the beam between traces. All the traces may then be viewed together for comparison or photography. The last trace is of particular interest, since it represents a burst of particles resulting in a jagged pulse. The rise times in the sharp changes in amplitude are of the order of 10^{-8} second.

A further application to nuclear processes is shown in Figure 13. The upper trace was made with a sweep time of about .15 microsecond and represents again the output of a scintillation counter in response to a single electron at its input. The rise time shown here is of the order of 10^{-9} second. The second trace is a similar reaction with a sweep of one microsecond.

While the high speed operation of the device has been emphasized because of its more spectacular nature, it should also be recognized

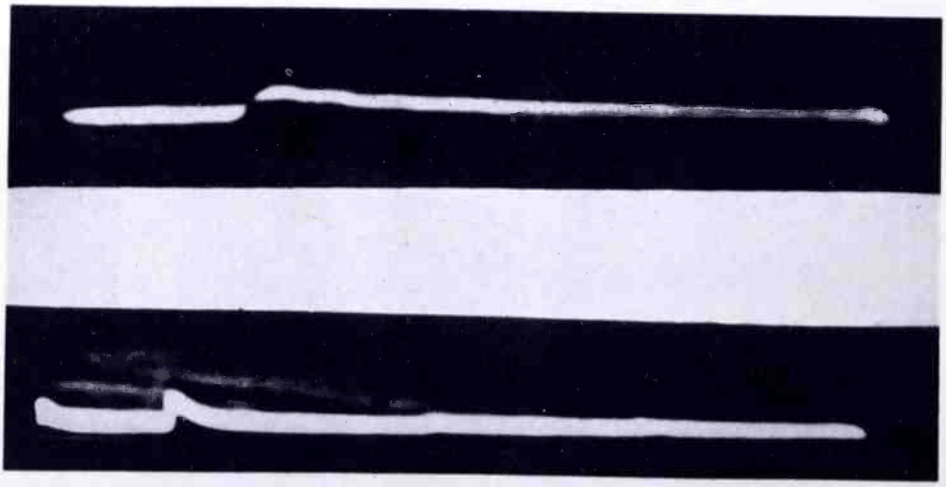

Fig. 13—Output of scintillation counter in response to a single electron at the input. Upper trace sweep time 0.15 microsecond. Lower trace, a similar reaction with sweep time 1.0 microsecond.

that there are many transient phenomena occurring at much slower speeds than those illustrated here, but which still require storage for their satisfactory observation. For example, the study of spark discharges in automobile ignition systems, the transients occurring when a circuit breaker opens, or any of hundreds of phenomena now observable only by photography, might be more conveniently observed by electronic storage.

Also, it should be emphasized that this instrument is not necessarily limited to the observation of single traces, but may be used to great advantage in the study of low speed repetitive waves where even though repetitive, the duty cycle may be so low as to make observation difficult, as anyone who has tried to observe pulses shorter than .1 microsecond at a sixty-cycle repetition rate can testify.

The instrument described is an experimental model built to study the possibilities of such a device. It is still in a state of development and its possibilities have not been fully explored. The purpose of this paper is to present the principle of electronic storage in oscillography as a new tool in the hopes that it may prove a useful device to facilitate the study of transient phenomena.

ACKNOWLEDGMENT

Acknowledgment is made to V. K. Zworykin, Director of Electronic Research of this laboratory, under whose direction this work was done, and to G. A. Morton and members of his group who generously provided materials, equipment and assistance in recording the scintillation counter pulses.

GRAPHECHON WRITING CHARACTERISTICS*

By

A. H. Benner and L. M. Seeberger

Engineering Products Department, RCA Victor Division, Camden, N. J.

Summary—The results of experimental investigations of small-area writing on a Graphechon are presented. The study was conducted to ascertain the practical limits of small-area writing, and to provide evidence for the further understanding of phenomena occurring on the target. Sample calculations are presented to illustrate how the performance of Graphechon systems may be predicted.

Introduction

THE Graphechon tube is a storage device used primarily as a scan converter. An outgrowth of the Teleran system requirements, the Graphechon finds its widest application in converting a radar plan position indicator (PPI) presentation into a television type of scan for transmission and subsequent display at high intensity.

Experience has shown the need for more precise information on the writing behavior of the Graphechon storage tube. The construction and fundamental theory of operation have been discussed elsewhere.[1,2] Also a great deal of experimental data has already been taken with the tube under conditions of "saturated" writing. (By "saturated" writing is meant a signal of such an amplitude that an increase in the writing level will cause no further increase in the storage time as observed in the reading circuit.) Qualitative predictions of the Graphechon's performance in the region of "unsaturated" writing could be made, but exact knowledge of the output to be expected from the tube at the lower limit of writing energy had not yet been obtained. It is, therefore, the purpose of this paper to describe the writing characteristics of the Graphechon in detail, especially in regard to small areas.

Measurements were made to establish the relationship between spot size and beam current, as it was known that the upper limit of video drive was set by resolution requirements. It was considered

---

* Decimal Classification: R583.15.

[1] L. Pensak, "Picture Storage Tube", *Electronics*, Vol. 22, pp. 84-88, July 1949.

[2] L. Pensak, "The Graphechon — A Picture Storage Tube", *RCA Review*, Vol. X, No. 1, pp. 59-73, March 1949.

desirable to use the surface potential of the target insulator (reading side) as a measure of the degree of target discharge. However, early experiments soon indicated that such measurements would be very difficult to make, if not altogether impossible, with a conventional Graphechon. Consequently, an indirect approach to the determination of the degree of discharge was adopted.

To make the information as fundamental as possible, and independent of the geometry of the writing-scanning process, it was decided to bombard the target with an undeflected beam of known amplitude, size, and time duration, and to deflect the reading beam in a standard television scan. The status of the charge so produced on the insulator's surface was determined by recording such measurable items as initial amplitude of the video signal in the reading circuit, and the length of time necessary for the charge pattern to be completely removed by the reading beam (storage time). Useful data was also obtained by noting the behavior of the amplitude of the reading signal, caused by a given amount of writing excitation, as a function of time.

From this data one may calculate the expected performance of any Graphechon system. Once the time-rate of the writing scan is known, the desired storage time, or reading signal-to-noise ratio, may be determined in terms of the remaining parameters which are held constant.

Presentation of Results

In this section of the paper, measurements of the Graphechon target circuit voltages resulting from one or more writing pulses are presented.

Residual Writing Beam. Early in the experiment, it was discovered that with the undeflected writing beam biased to or beyond cutoff without excitation, in which case no actual writing beam was expected to be present, a spot on the target was discharged to saturation after a period of a few seconds. This condition was especially noticeable when the reading beam was removed for a period of about ten seconds and then restored to normal. The static-target and writing-collector currents were obtained for several tubes near the region of cutoff as the writing-grid bias was varied. Two classes of tubes were examined; the normal-thickness (½ micron) insulating film tube, and a thin (⅙ micron) insulating film tube. Unless otherwise specified, the discussions and figures refer to the normal-target tube.

A plot of writing-collector and target current from an undeflected beam with the reading gun biased below cutoff, is shown in Figure 1.

The relative amplitude of the amount of target discharge produced by the writing beam, as seen by momentarily activating the reading beam, is also shown in Figure 1. This latter curve shows that even if the undeflected writing beam is biased to twice the cutoff value the target

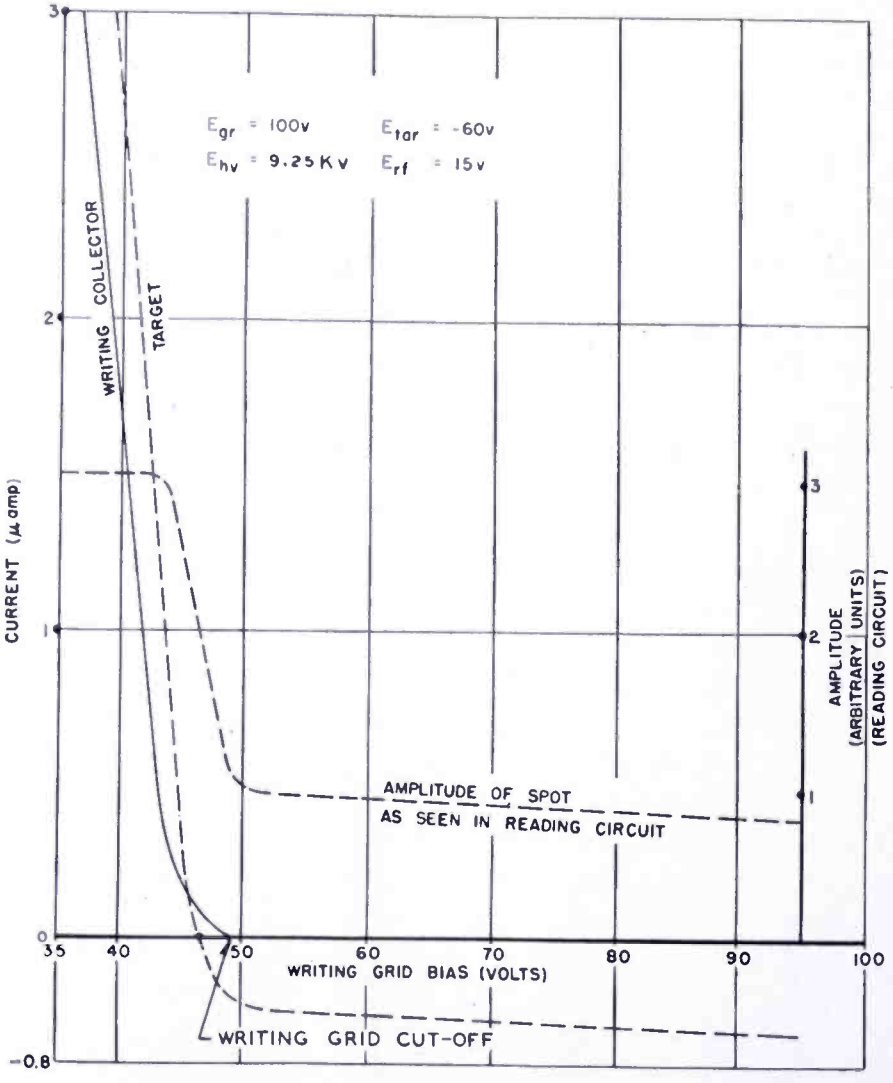

Fig. 1—Static target and writing collector current versus writing-grid bias with the reading beam biased far below cutoff for an undeflected writing beam, and the amplitude of the written spot, as seen by activating the reading beam, versus the writing-grid bias. (*See appendix for legend of symbols for all figures.*)
For the amplitude reading, the reading-grid bias is changed from —100 volts to —30 volts. The amplitude shown by the curve is attained in a writing time of about 5 seconds.

is still, to a large degree, discharged in a short period of time (about 5 seconds). The current curves of Figure 1 were obtained in the presumed absence of the reading beam; if this beam is activated to its normal value, the target current is shifted by a constant value of 3.0

microamperes in the negative current direction. Hence, below writing-gun cutoff it appears that most of the target current comes from the reading gun, even though the reading gun is also biased below cutoff. The reading and writing beams cause opposite current flow in the target because the writing beam is operated beyond the second cross-over in the secondary emission curve and the reading beam is operated between the first and second crossovers. The existence of a target current below writing cutoff may be the result of grid emission. That is, the electron beam from the cathode of either gun or from both guns may be completely blocked by its respective control grid, but the grid itself may be emitting electrons. A second possible source of this spurious current might be photoemission. Illumination from external or internal sources such as the filaments may be sufficient to release electrons from gun elements or getter materials. Whatever the source of this residual current, it has a detrimental effect as it results in a rise in the noise level in general application, and masks further application of writing current in the desired experiments. To overcome this difficulty in the experiments, a system of deflecting the writing beam was devised and is described in the Appendix.

Writing-Beam Current. The total writing-beam current as a function of writing-grid drive was determined by operating the target at a high enough positive potential to assure that the target collected all released secondary electrons. A known capacitance was inserted in the target circuit and the writing beam was activated by the writing-grid voltage, e_{gw}. The rate of change of voltage across the capacitance was noted and the current found from $i = C\ \triangle v/\triangle t$. The results of these measurements are illustrated in Figure 2. This curve is helpful in explaining some later results where multiple-pulse signals are applied to the target, because of its nonlinear character.

Storage Time. One of the most important characteristics of the Graphechon is its storage time. The storage time of a tube with normal target was studied as a function of three different variables: writing-grid drive, duration of writing excitation, and number of pulses applied. The first of these is shown in Figure 3. These curves show the behavior of storage time as a function of writing-grid drive for a single pulse of four different pulse durations. It is evident that a condition of storage saturation is reached in all cases, but below 30 volts, the storage time drops off rapidly. A different family of curves is shown in Figure 4. Here the duration of writing excitation is varied from 0.5 microsecond to 45 microseconds at three different amplitude levels. For each amplitude a saturation condition is reached, but below a

duration of about 15 microseconds the storage time diminishes rapidly. If the reading-current bias in cases portrayed by either Figures 3 or 4 is increased, the storage time is also increased. A cross plot between these two curves shows that the data is consistent, though not equal in absolute value. A third type of storage curve is shown

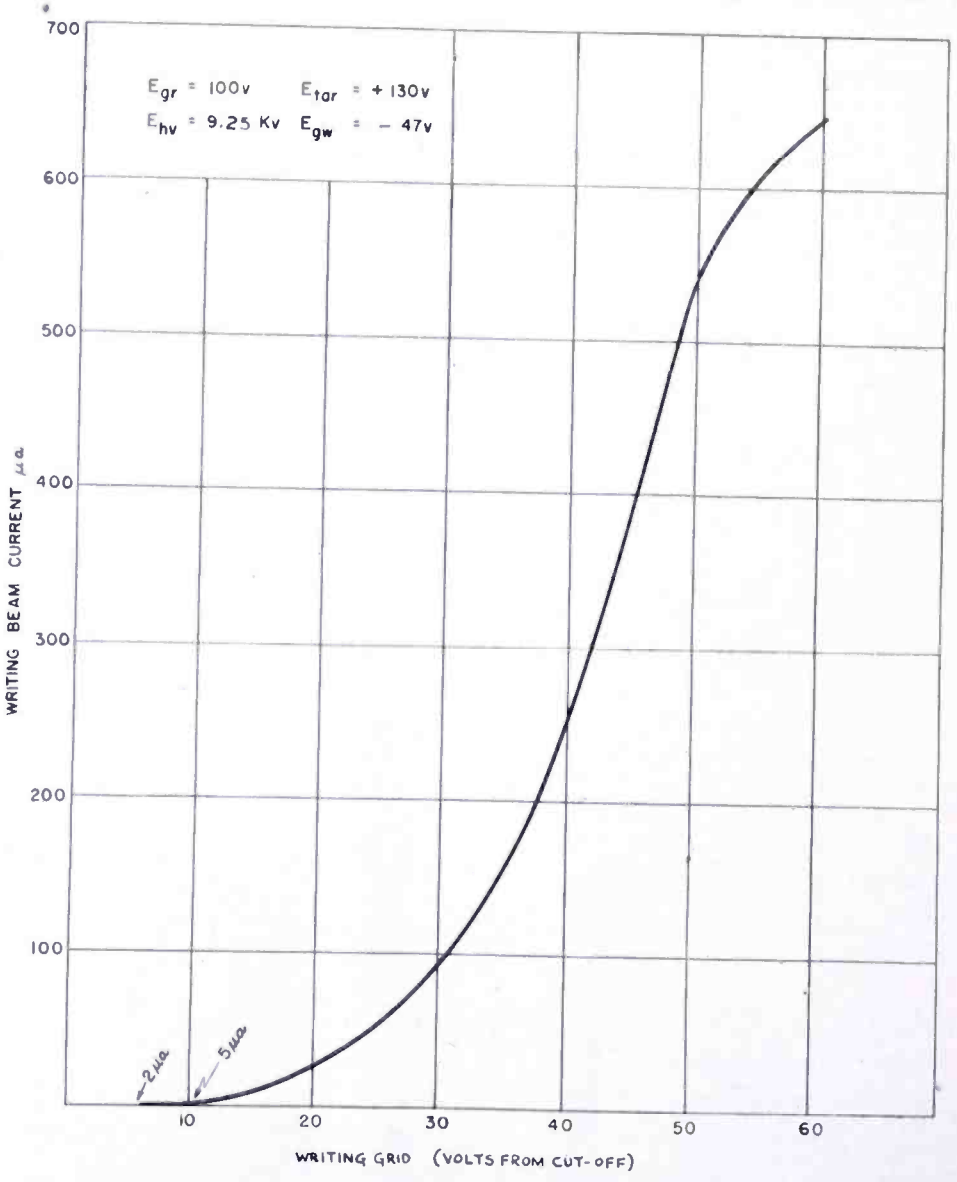

Fig. 2—Writing-beam current from a single spot written dynamically in volts from writing-grid cutoff.

in Figure 5. In this case a varying number of 1.0-microsecond pulses of three different amplitudes is written on the target sequentially; then the reading gun is activated and the storage time noted. It is at once evident that n pulses of amplitude a do not have the same storage time as $n/2$ pulses of amplitude $2a$. This is explainable with

reference to Figure 2. From this figure it can be seen that because of the high degree of nonlinearity, the total charge deposited on the target for the conditions stated above may differ considerably, and, hence, the storage times differ.

In an effort to understand more clearly the operation of the tube, all of the data from Figures 3, 4 and 5 was examined as a function of total beam charge and also of beam-charge density. The total beam charge was considered as equal to the beam current, as determined

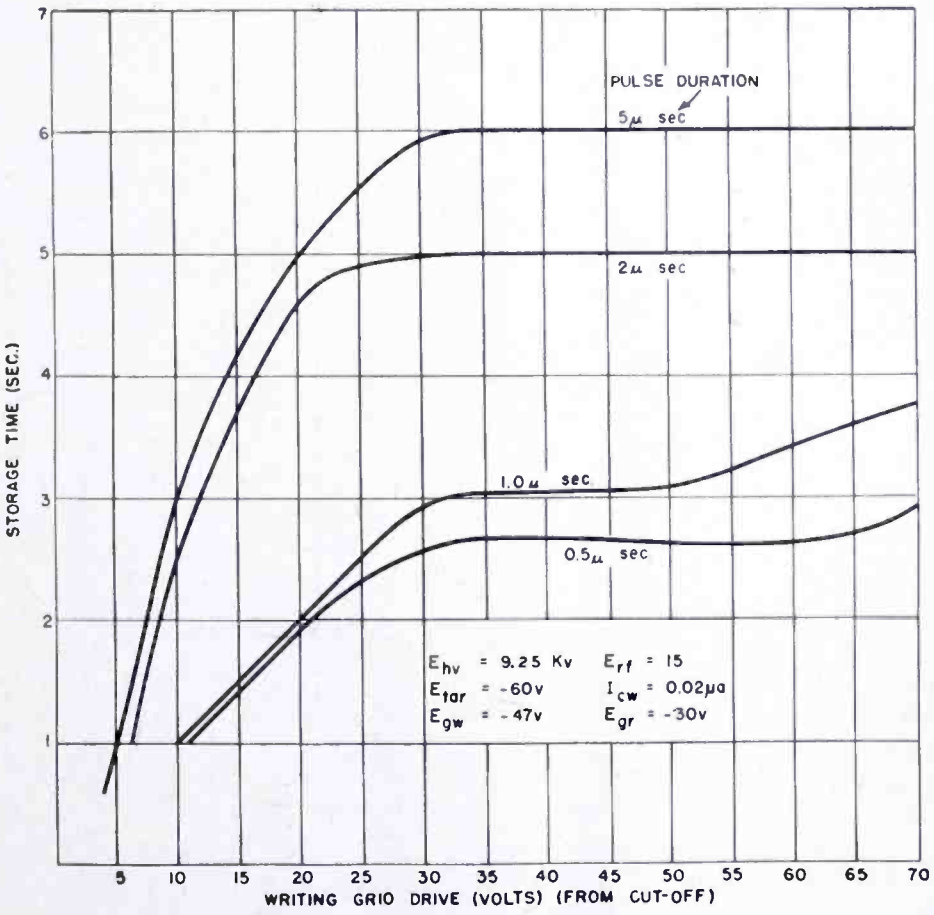

Fig. 3—Storage time versus writing-grid drive (peak pulse amplitude above cutoff). Each curve represents a single pulse of duration as labeled. The storage time is measured from the commencement of reading until the signal disappears into the noise.

from Figure 2, multiplied by the duration of the writing-grid excitation. The beam-charge density was taken as the beam charge divided by the spot area. There existed no logical relationship between either of these two quantities and storage time. This tends to indicate that the storage time is not alone a function of beam charge or charge density but is influenced to a considerable extent by other parameters, in particular, the secondary emission behavior.

Several curves with abscissas the same as in Figures 3, 4 and 5 were obtained with the amplitude of the read signal as the ordinate. In Figures 6, 7 and 8, comparisons of the curves can be made in a slightly limited manner. Because of the time lapse between experiments and the inability to reset controls precisely, reference among the curves was established by referring to a given noise level. Thus, the absolute value of the ordinate among the three curves is subject to error in the ability to reset to the noise level.

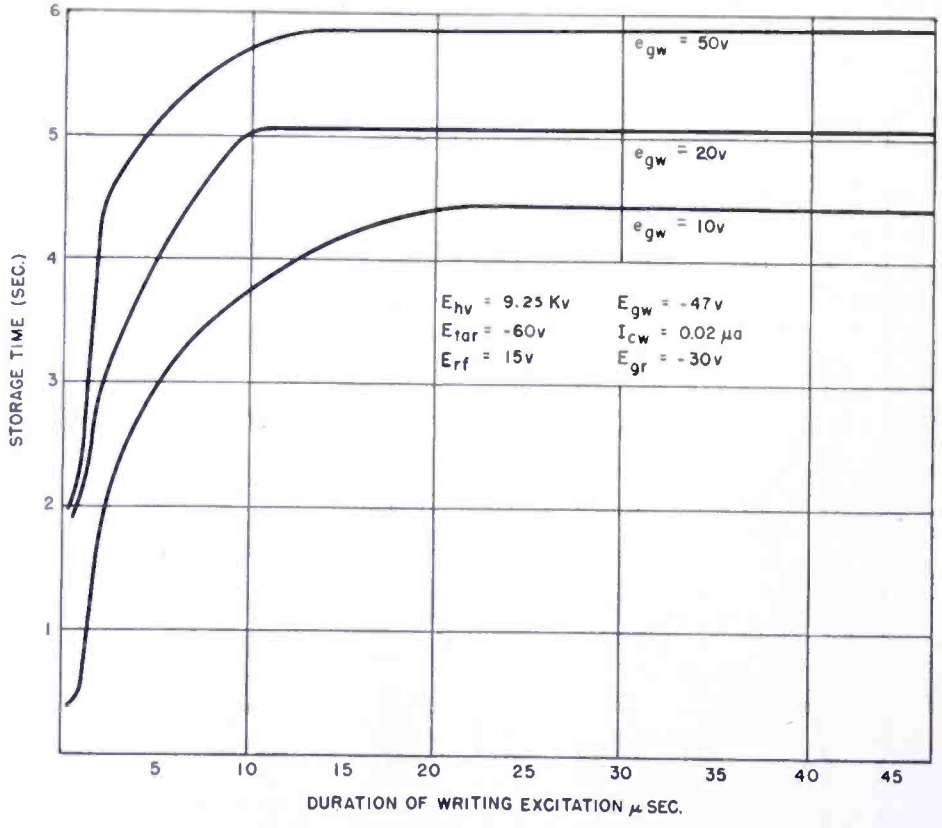

Fig. 4—Storage time versus duration of writing excitation. Each curve represents a single pulse of amplitude above cutoff as labeled.

Figure 6 gives the relative amplitude of the output signal from the spot on the target in arbitrary units at the instant the reading process begins. Figure 7 shows the variation of amplitude with duration of writing excitation and, Figure 8, the amplitude as a function of multiple pulse input.

Beam Size. A final set of curves for the normal-target tube must be presented prior to explaining any unusual characteristics of the previous figures. This last set shows the behavior of the spot size or resolution with writing-grid excitation. These curves are presented in Figures 9 and 10. From a study of these, it is apparent that the

resolution becomes increasingly poor with increased amplitude of writing excitation, while a condition of saturation is reached as the duration of writing excitation is increased. This is a logical consequence of a broadened beam at larger writing excitation, while the length of time the beam is on does not influence the beam width. In this test the target was circumscribed by the reading raster, so that the time of traverse across the target diameter was approximately 53

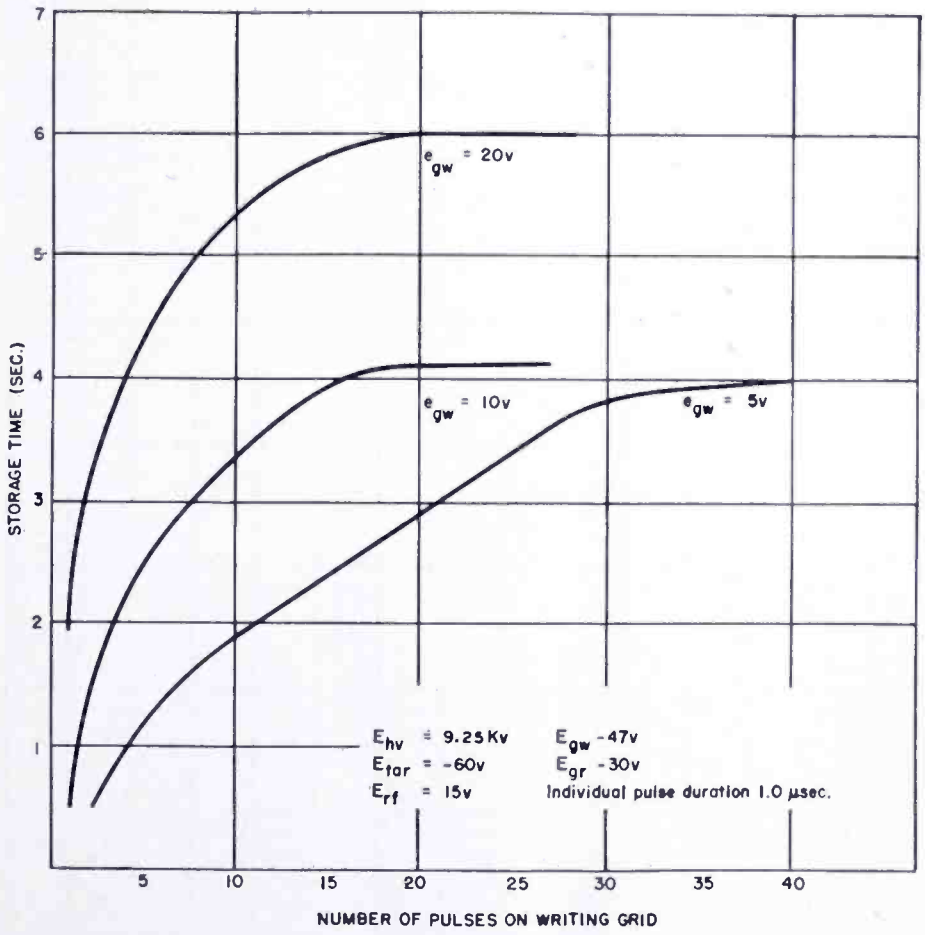

Fig. 5—Storage time versus number of pulses on writing grid. Then pulses are written in a time of about $n \times 0.5$ seconds. The amplitude of the writing excitation for each pulse is as labeled on each curve in peak volts above writing-grid cutoff.

microseconds. The spot size was measured at one-half amplitude immediately on reading.

The resolution in lines as used for one ordinate scale requires a note of explanation. In the definition of resolution, some distinction should be made of the degree of contrast. In the limiting resolution the contrast is a very small value. The conversion from spot size to number of lines of limiting resolution in Figures 9 and 10 is based

on the following assumptions. First, it is assumed for simplicity that overlapping charges from two adjacent spots add linearly. Furthermore, it is assumed that there is approximately zero contrast between two spots which are adjacent at their normal half-amplitude points, by virtue of the charge additions and their initial shapes. This condition is assumed in computing the limiting resolution. For example, in Figure 9, a spot 0.3 microsecond wide, the smallest discernible spot

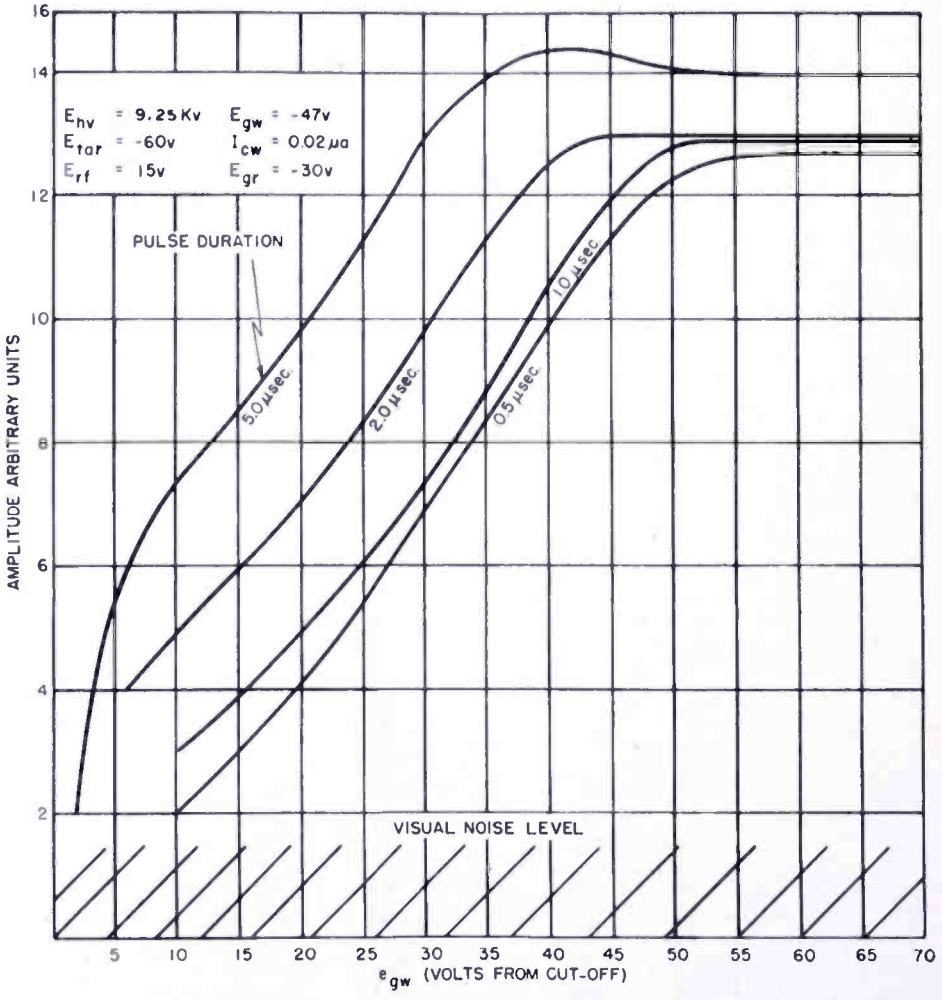

Fig. 6—Output signal amplitude versus writing excitation.

in a 53-microsecond scan, indicates a resolution equivalent to 177 black lines or a total of 354 black and white lines. It should be noted that this resolution was computed on the basis of zero writing speed; that is, no account was taken of the spot broadening due to the movement of the writing beam.

Rising-Amplitude Effect. A phenomenon which has been previously noted and which was observed carefully in these tests was the rising-

amplitude (video) effect. This effect is characterized by a signal from the Graphechon whose amplitude, as reading progresses, increases above its initial value to a maximum and then decays to zero.

L. Pensak† has explained this action in the following manner: Under writing action the target surface is driven negative only behind the holes in the mesh, where, shadowed by the mesh wires, the

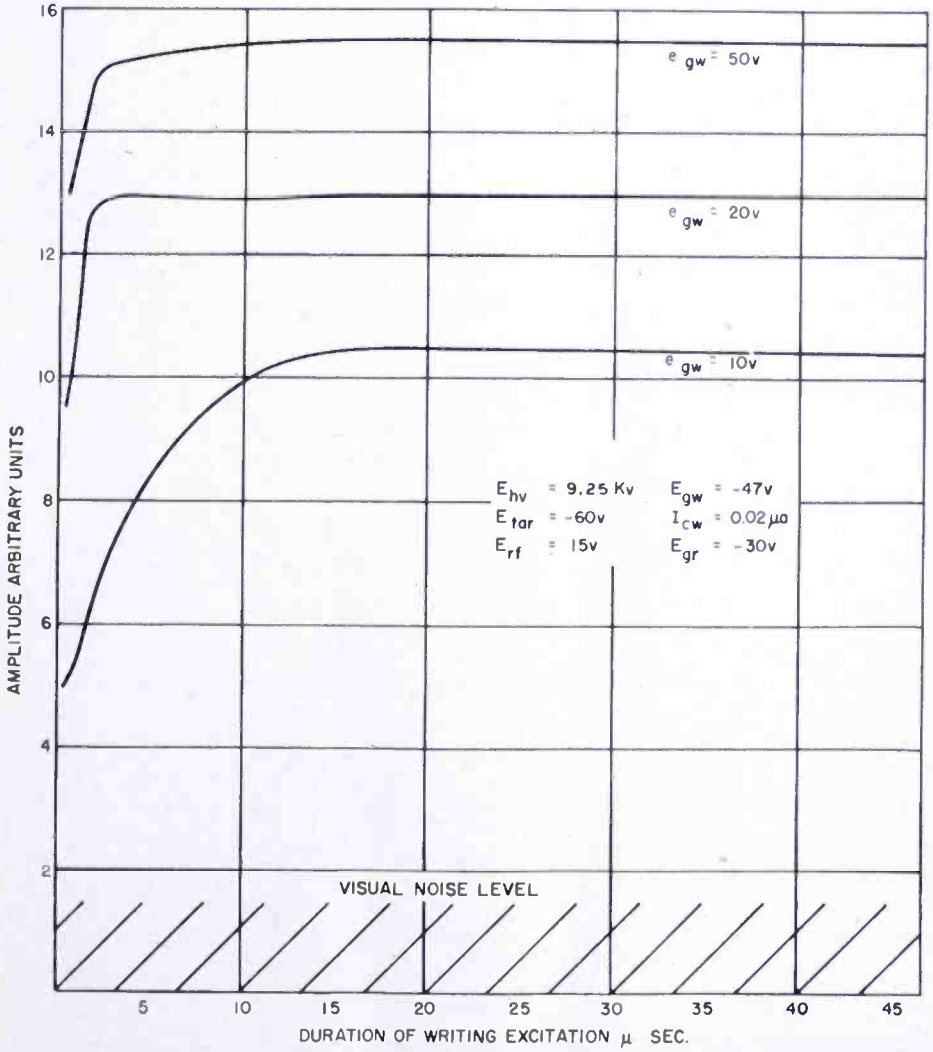

Fig. 7—Output signal amplitude versus duration of writing excitation.

target is less negative. On reading, the secondaries released from the bombarded areas do not all travel to the collector, but some fall into the shadowed areas. As this process continues, the bombarded areas approach the potential of the shadowed areas and full secondary emission may occur. This results in an increased current flow and,

† RCA Laboratories Division.

hence, an increase in the video amplitude. The decay then proceeds in the conventional manner.

In the experiments covered by this report, the video amplitude was noted at initiation of reading and at its maximum. The rising characteristic did not occur for low writing excitation of short duration, although no lower limit of either parameter may be cited alone. In terms of total writing beam charge, a reasonably well defined lower limit of about 900×10^{-12} coulomb may be given, below which the

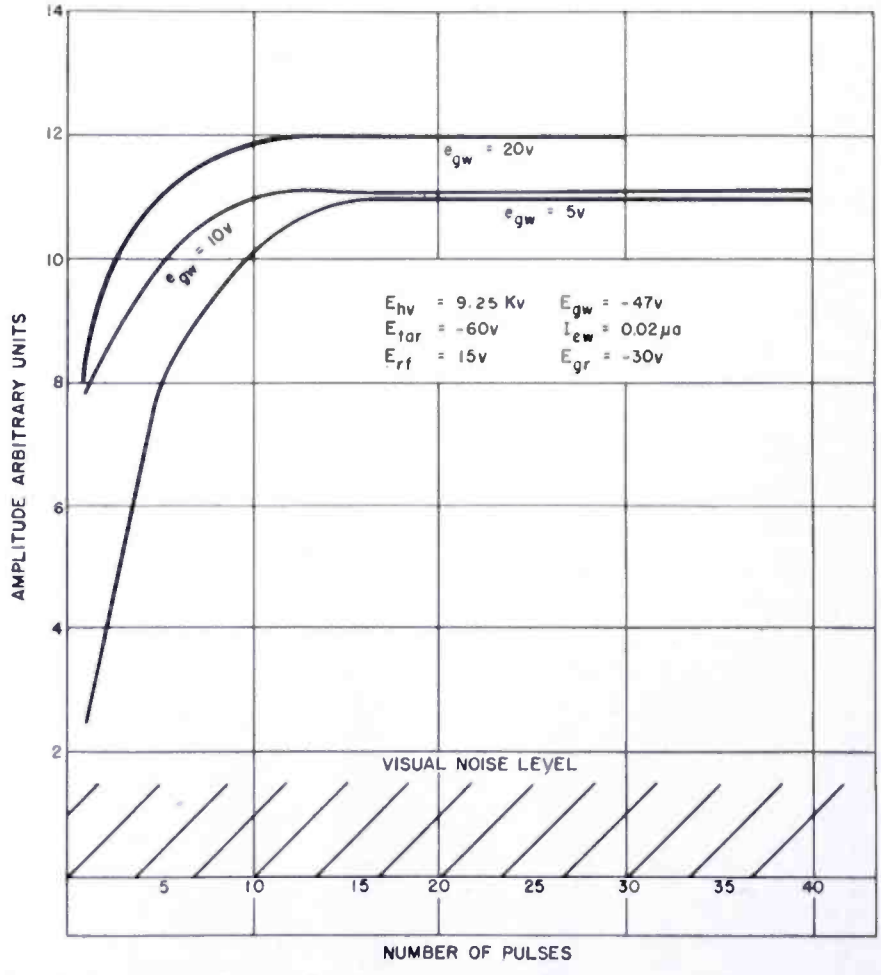

Fig. 8—Output signal amplitude versus number of one-microsecond pulses on writing grid.

rising characteristic was not observed under conditions as cited for Figure 3.

The following theory may also be offered to explain why, in the saturation region, the curves in Figure 7 are separated in amplitude while those in Figure 6 are not. Referring to the spot size diagrams, where Figure 9 has the same abscissa as Figure 6, and 10 as 7, it is seen that spot size, as shown in the family of curves with writing

excitation as the independent variable, is very similar over the saturation range. However, Figure 10 demonstrates that the spot size is considerably different for the curves of the family. This, then, would lead one to believe that in the larger spot sizes associated with higher

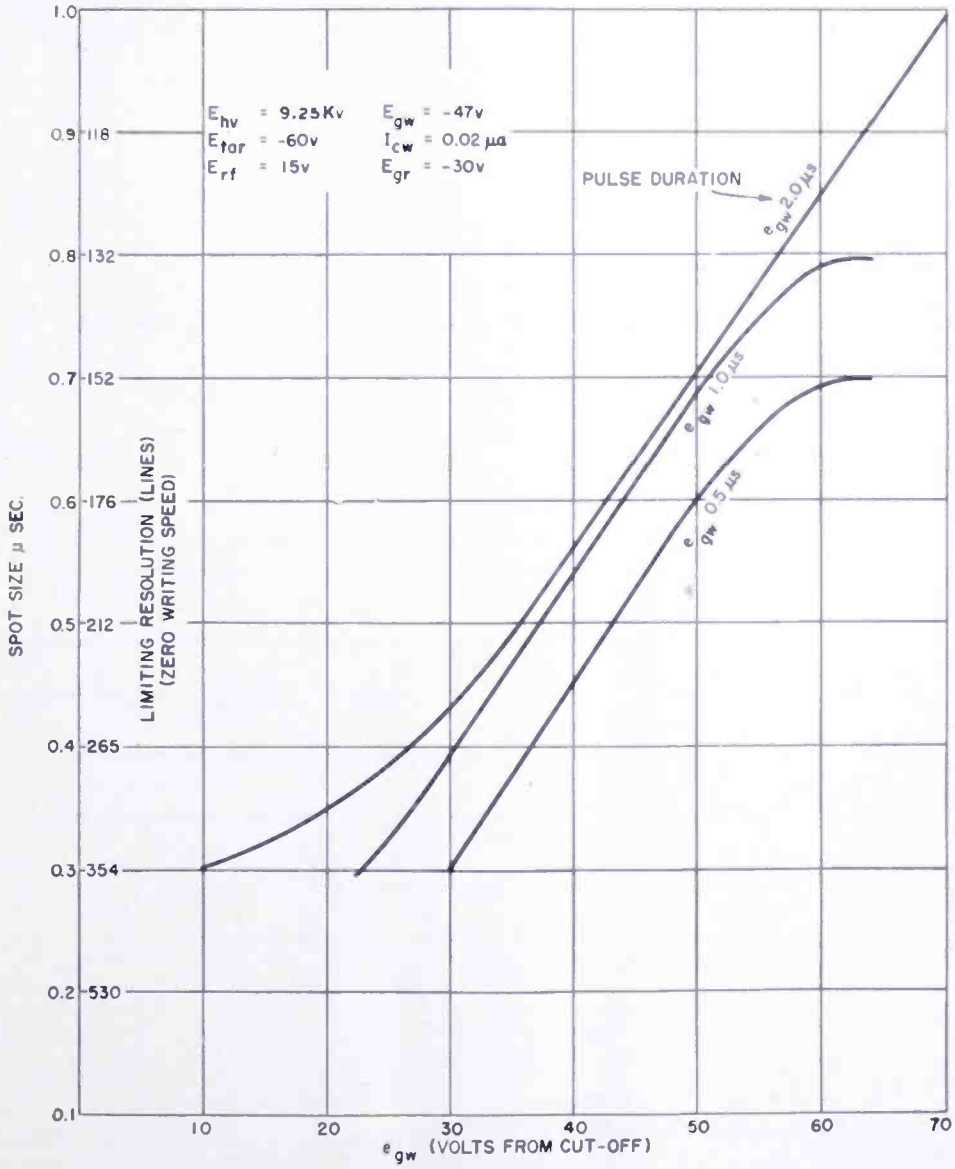

Fig. 9—Spot size on the target as a function of the writing-grid excitation. On this test the target was circumscribed by the reading raster, so that the time of traverse across the target diameter was approximately 53 microseconds. The spot size was measured at one-half amplitude immediately on reading.

levels of amplitude saturation, the spot is large enough to repel some secondary electrons which tend to fall back to the target, thus, raising the amplitude over a small spot where redistribution of the secondaries is possible.

The improvement of resolution with viewing time, noticed in previous operations, was not perceived to a large degree in these tests. In the small amount of quantitative data taken on this subject, no improvement greater than 15 per cent was recognized. It is, however, easy to explain why the resolution should improve. The charge distribution laid down on the target by the writing beam is spread into a

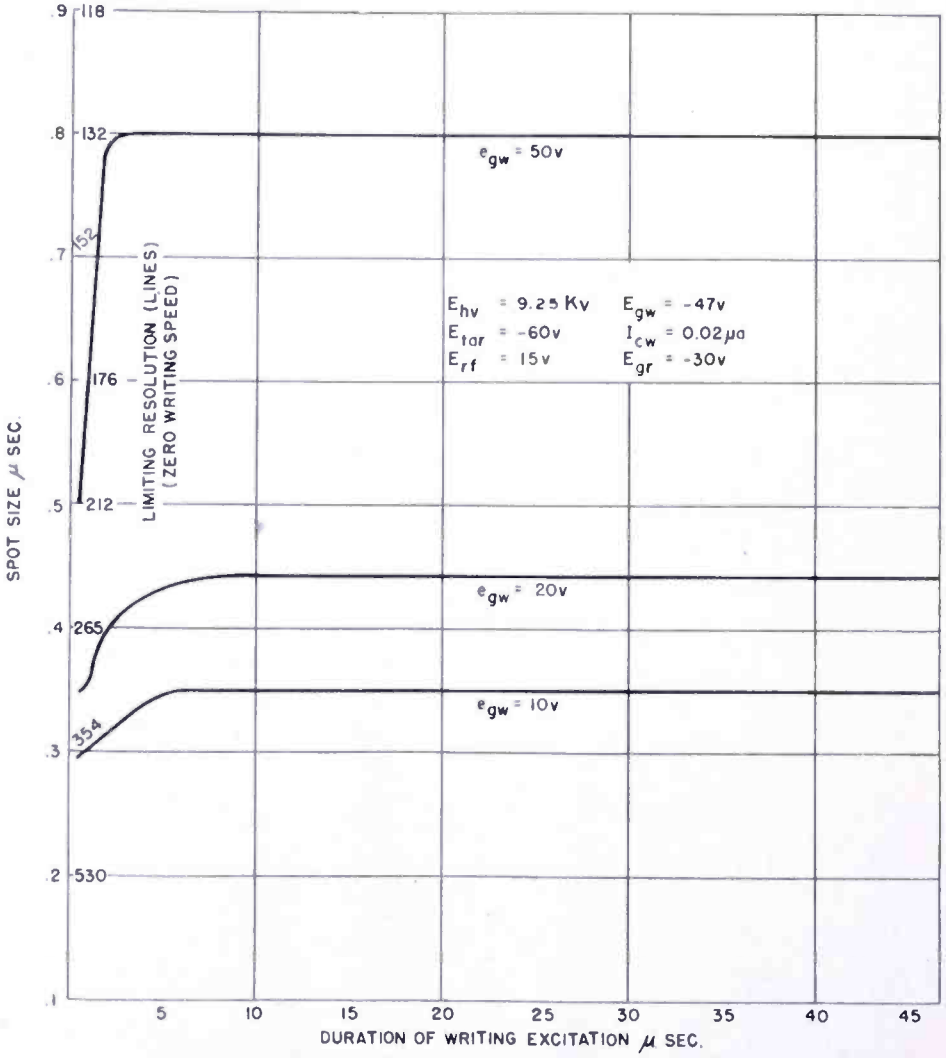

Fig. 10—Spot size on the target as a function of the duration of the writing excitation.

near normal shape. This means that maximum charge occurs at the center of the spot and that the charge decreases to the edges. It has been shown previously in Figure 4 that the storage time is shorter for smaller beam charge, hence, the spot narrows as it decays.

Signal-to-Noise Ratio. Another interesting observation to be noted is the signal-to-noise ratio which may be quickly seen from Figures 6, 7 or 8. This noise, of course, originates primarily in the input

circuit of the reading intermediate-frequency strip, and it is probably less than that which would be introduced by the radar itself.

In a radar with the fictitious parameters noted below, the storage time and signal-to-internal-noise ratio may be determined from the curves. Let the radar have a one-microsecond pulse length, 15 revolu-

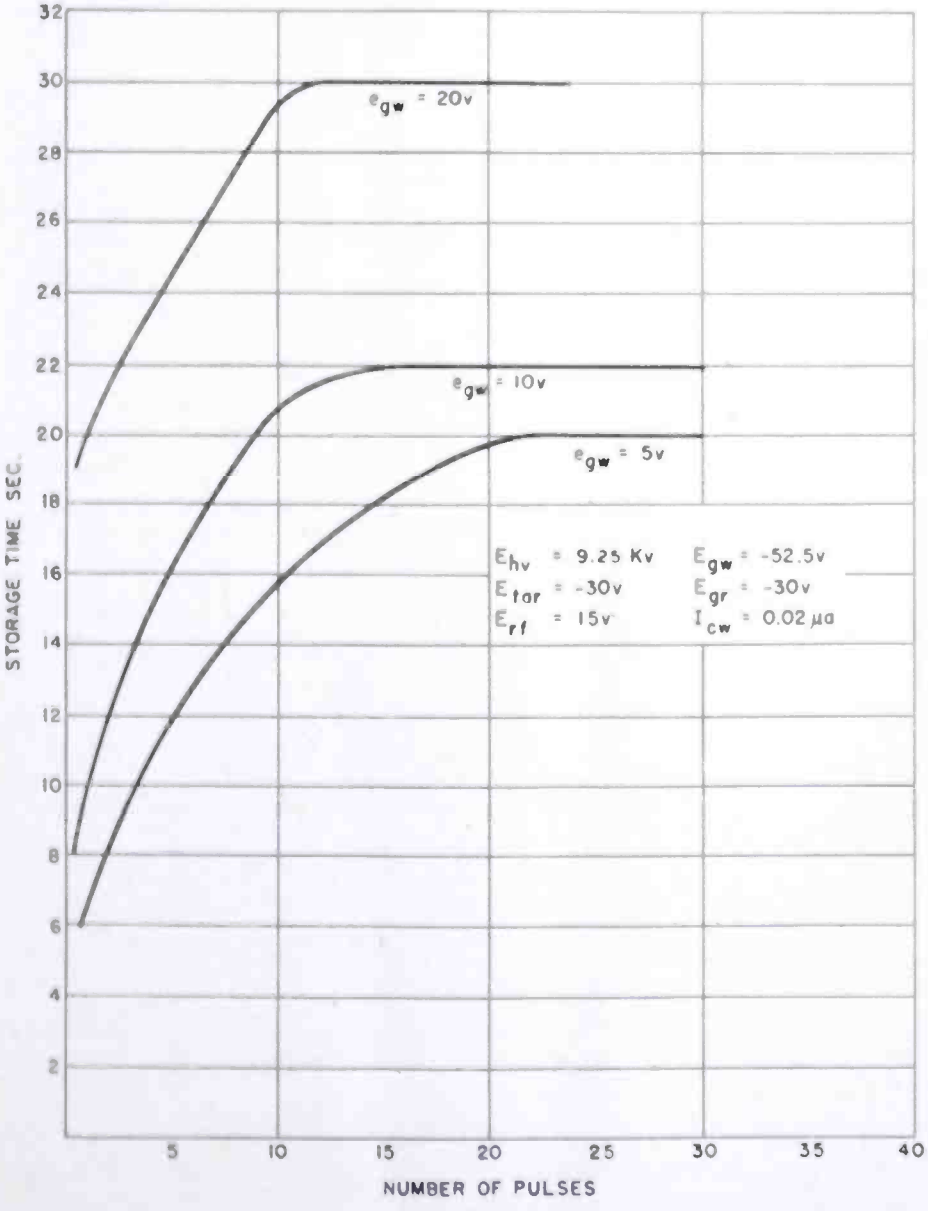

Fig. 11—Storage time versus number of pulses on thin-target tube.

tions per minute scan rotation rate, and an expected 20 pulses per hit. From Figure 9, if about 354-line limiting resolution is required, the writing excitation must be limited to about 20 volts; so from Figures 8 and 5 the signal-to-noise ratio is 8 and the storage time is 6 seconds.

Two Graphechons with thin targets were also examined. The storage time and amplitude versus number of pulses were determined for these tubes. Both tubes behaved similarly, and the results of one are shown in Figures 11 and 12. Comparing these curves with those of a normal-target tube in Figures 5 and 8, it can be seen that the storage time for the thin-target tube is approximately five times that of the normal tube even with a lower target voltage on the latter.

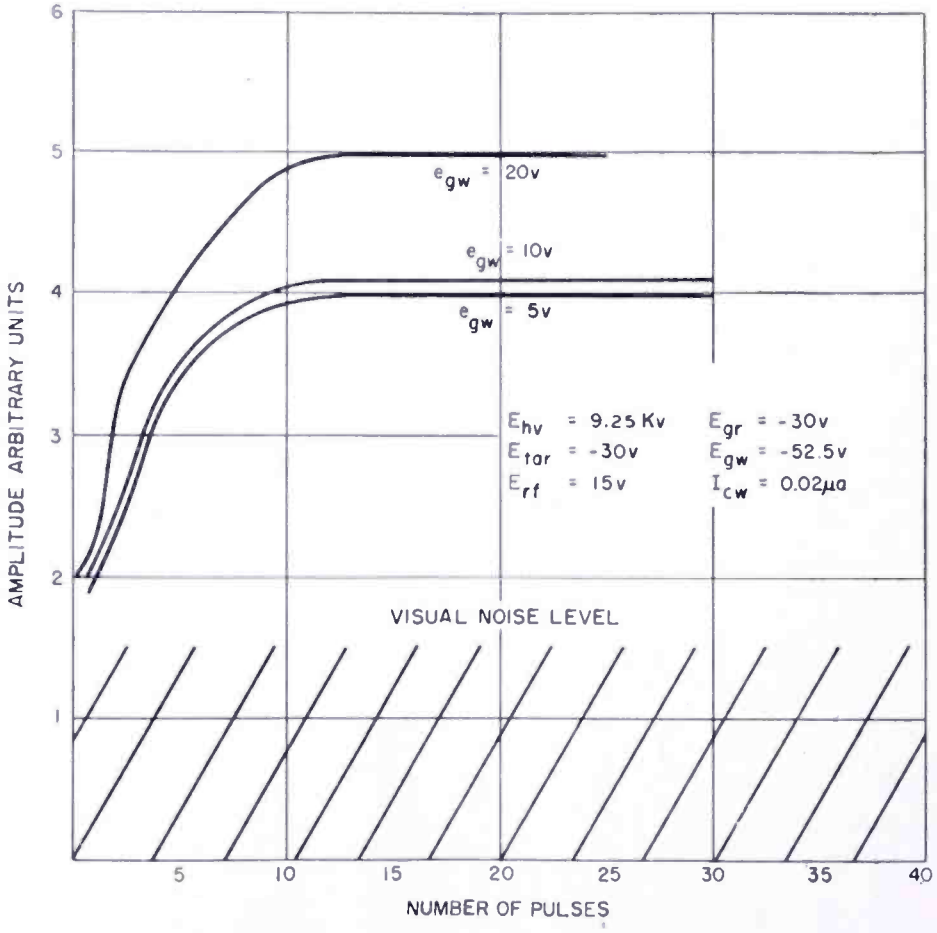

Fig. 12—Output amplitude in arbitrary units versus the number of pulses for the thin-target tube.

However, comparison of the amplitude curves reveals that the signal-to-noise ratio of the thin-target tube is in general about 3 times as bad as that of the normal-target tube.

During the course of the experiment, it was noticed that when the rising amplitude characteristic was absent, the amplitude of the signal decayed continuously with increasing time. This result was contrary to previous observations and, therefore, was examined further. Figure 13 shows such decay characteristics for the normal-target tube, and

Figure 14 gives the same information for the thin-target tube. In the former, it is apparent that the amplitude starts to drop immediately on reading and does not exhibit a concave downward curve as was previously expected for the single-pulse situation. Where 10

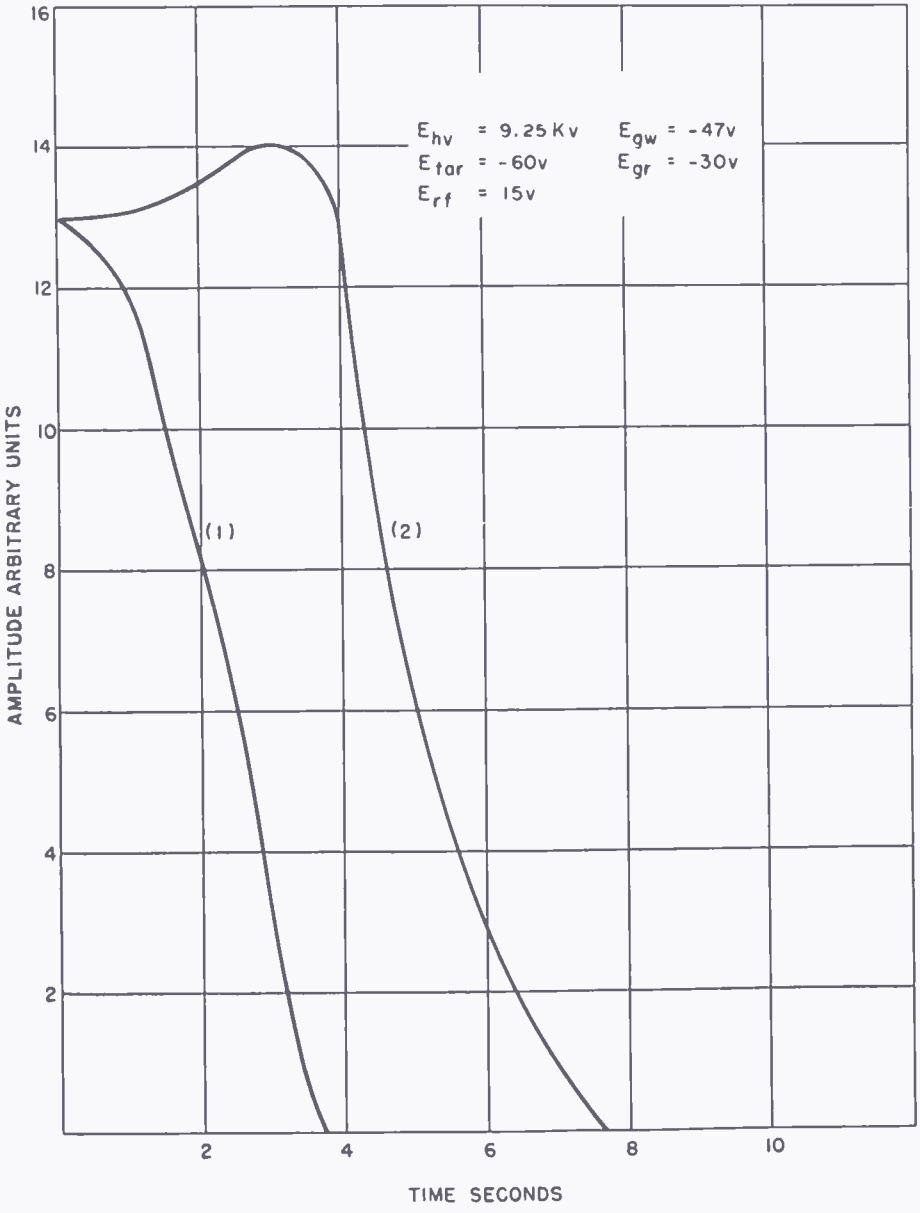

Fig. 13—Decay characteristics of the normal-target Graphechon (amplitude versus time). Curve (1): 1 — 1-microsecond 70-volt pulse; curve (2): 10 — 1-microsecond 70-volt sequentially applied pulses.

pulses are applied in rapid succession, the amplitude does display a partially concave downward configuration. This, however, is not a true amplitude memory, but is actually due to the rising amplitude characteristic which has been discussed above.

The thin-target Graphechon decay characteristic shows neither amplitude plateau nor rising amplitude effect for either condition of operation. It also has an abnormally long tail. This long decay characteristic of this thin-target tube is believed to be due to the phenomenon of trapped electrons in the center of the target insulator. During bombardment some electrons may be trapped in potential wells in the interior of the target. These electrons migrate toward the surface of the target, but at a rate which is too slow to allow them to appear on the surface of a normal target tube in a normal reading

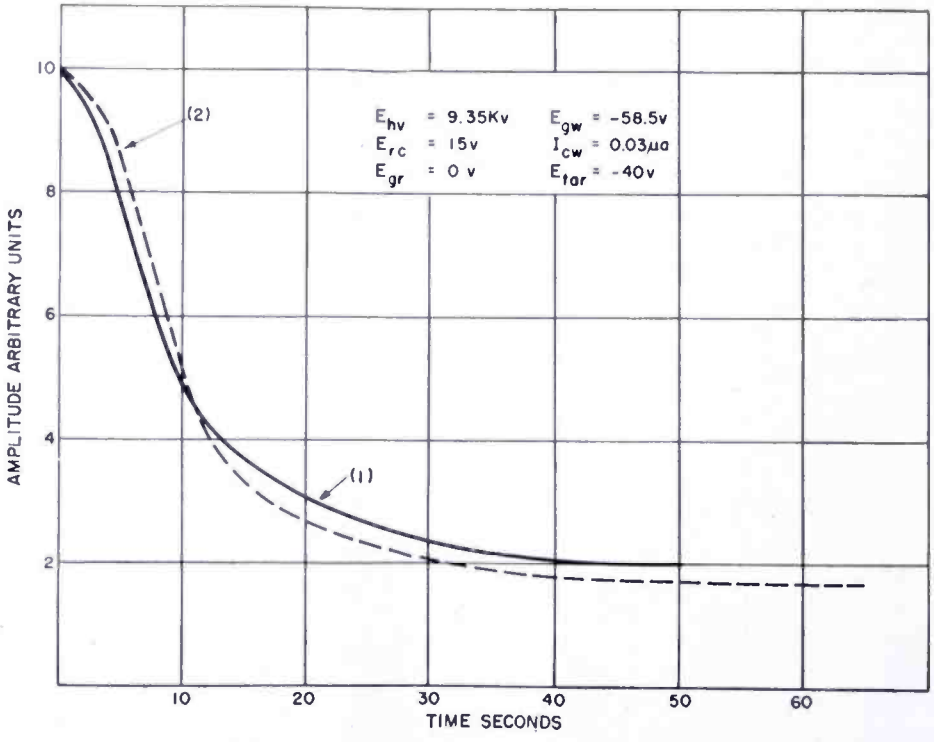

Fig. 14—Decay characteristics of thin-target Graphechon (amplitude versus time). Curve (1): 1 — 1-microsecond 70-volt pulse; curve (2): 10 — 1-microsecond 70-volt sequentially applied pulses.

time. They may arrive at the surface hours later, and in fact, such an effect has been noticed. In the thin-target tube, however, the path over which the electrons must migrate is shorter and the potential gradient is larger, hence, these electrons may arrive at the target during the latter part of the decay process and account for the long tail of Figure 14.

Conclusions

Increase of Signal-to-Noise Ratio by Integration of Signals of High Pulse Repetition Frequency. Several of the curves which have been

presented reveal interesting information dealing with possible enhancement of the detectibility of signals through integration. In most prior practice, it was necessary to operate with strong signals that "saturate" the target in both storage time and amplitude in a single application. A study of Figure 8 shows that small pulses add linearly up to about 10 pulses. If a number of echoes are returned on one azimuth scan of a radar at such a rate that they are written on the same spot of the Graphechon, the well known signal-to-noise advantage by integration may be obtained. It is valid to use the data of Figure 8 where the pulses were written on the target in rapid succession in the absence of the reading beam, or if the pulse repetition frequency of the radar is high compared to the reading field rate. For example, if the reading beam scans at a standard RMA television rate, any small area is partially scanned by the reading beam every 1/30 of a second. If, however, the radar has a pulse repetition frequency of 2000 and has 10 echoes from a target on one azimuth scan, the time needed for this integration is only 10/2000th or 1/200th of a second and, therefore, will probably not be partially erased by the reading beam during the writing period.

Demonstration of Usefulness of Curves. To demonstrate the usefulness of the curves presented in this paper, consider the following example: It is desired to determine the storage time, necessary signal amplitude and signal-to-noise ratio (considering noise from Graphechon circuits only) of a single 0.5-microsecond pulse with the stipulation that resolution is equal to or greater than 100 lines at 50 per cent contrast. From Figure 9, 100-line resolution is approximately equivalent to a spot size of 0.53 microsecond on a 53-microsecond base and a 50 per cent contrast, so the signal amplitude must be equal to or less than 45 volts above writing-grid cutoff. From Figure 6, this yields a signal-to-noise ratio of 7.3 or less; and from Figure 3, the storage time is approximately 2.7 seconds or less. Other cases using specific radar parameters may be examined in a similar manner.

ACKNOWLEDGMENT

The data contained in this paper was obtained with the aid of J. H. Sweer of the Advanced Development Section. In addition to contributing to the general plan of the investigation, Mr. Sweer suggested the deflection-shift method so successfully employed in the data runs. The authors wish, also, to acknowledge the cooperation and contributions of L. Pensak of the RCA Laboratories Division.

APPENDIX

Experimental Techniques

The equipment used in the data runs consisted primarily of the Graphechon test set with modifications that were necessary to produce the single, undeflected writing spot. Figure 15 is a block diagram of the apparatus as set up in the laboratory and Figure 16 is a detailed block diagram of the Graphechon test set.

Initial experiments were made by removing the output tubes from the writing deflection circuits of the Graphechon test set to produce

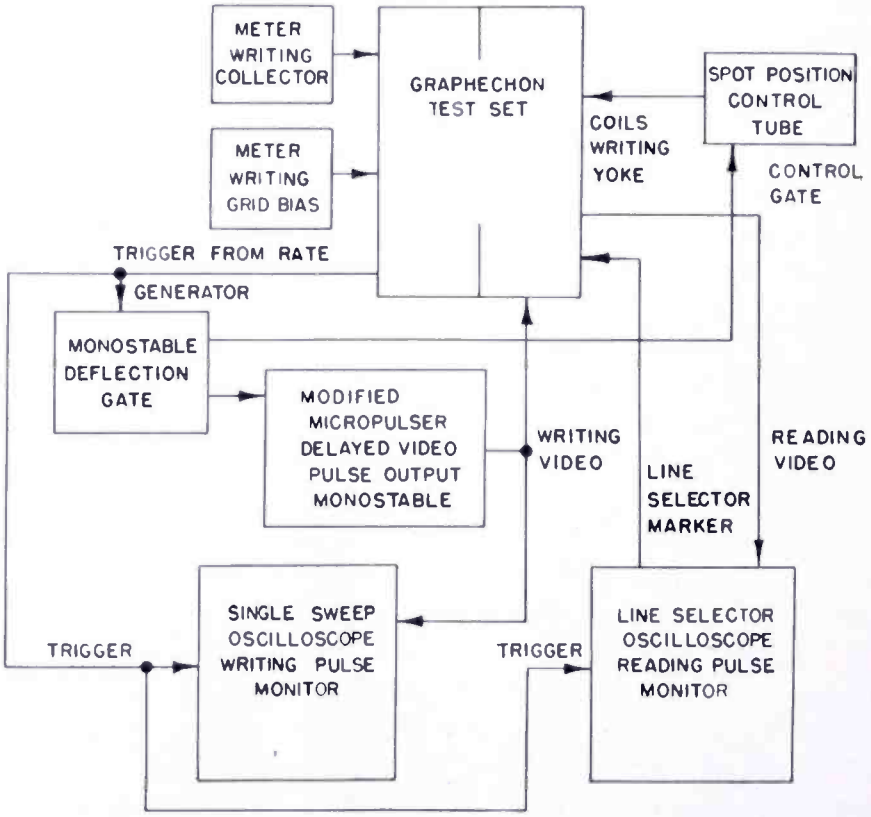

Fig. 15—Block diagram of laboratory apparatus.

a single undeflected spot on the target. The writing deflection coil and centering circuits were undisturbed and provided a means for locating the spot on some clear portion of the target. Experiments performed with this writing method were not satisfactory because of the residual gun current remaining after cutoff. It was observed that the static writing collector current would drop to a very low value (about .002 microampere) at cutoff and then remain constant as the grid bias was increased to large negative values. This residual current, thought to be caused by control-grid emission (considerable

variation was seen from tube to tube), was well focussed at the target and, in the absence of the reading beam, was sufficient to cause complete target discharge in 10 to 15 seconds. This condition made it impossible to obtain consistent results as the time interval between interruption of the reading beam and the application of the writing pulse was a variable over which little control was had. It was, therefore, necessary to change the technique to one where the residual gun current could not influence the data.

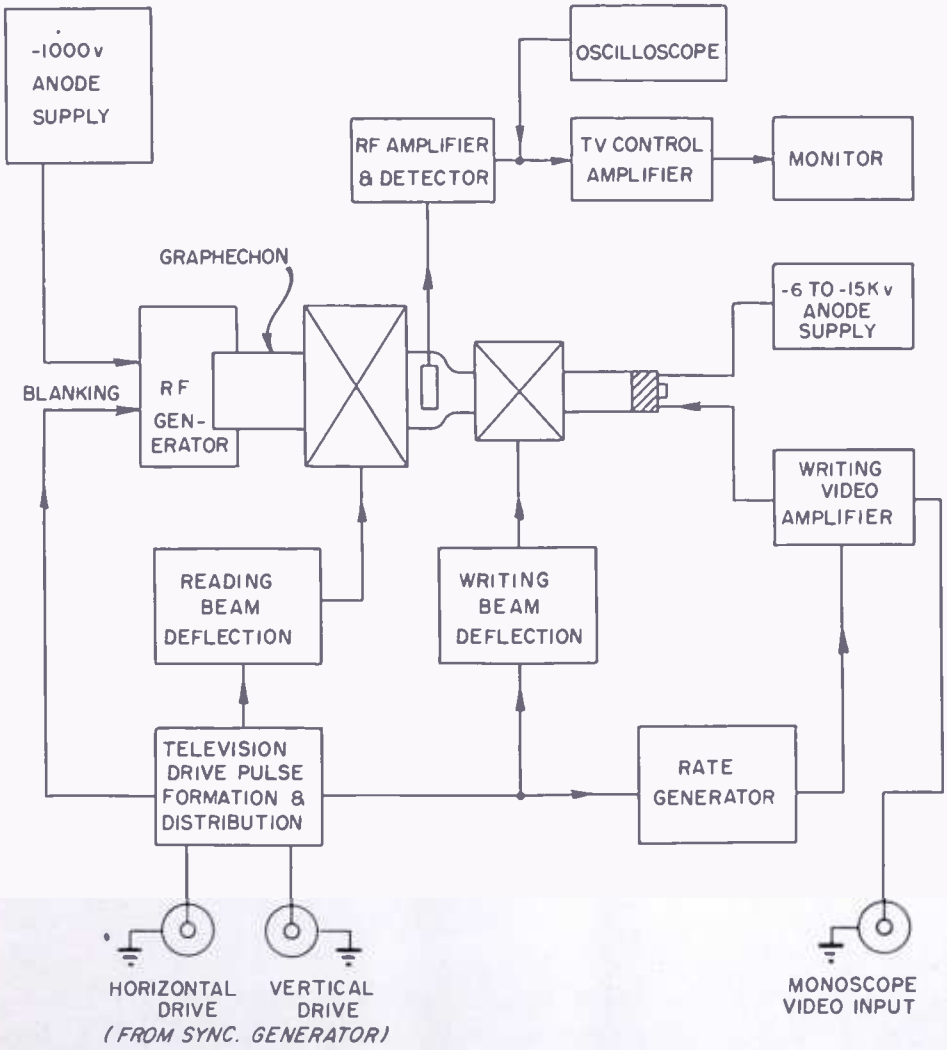

Fig. 16—Block diagram of the Graphechon test set.

The spot-deflection method was developed to overcome the effects of residual gun-current and still provide data from a single stationary spot. The writing spot is deflected to the edge of the target where it remains until data is desired. An initiating trigger pulse trips the monostable deflection gate which permits the spot to move into posi-

tion on the target. A few microseconds after the trigger, the spot comes to rest at its new position on the target at which time the video pulser causes the beam to write a known amount of charge on the target. A short time later, the beam returns to its resting position as the monostable deflection gate completes its cycle. The system is now ready for the next initiating pulse which may come at any time set by the operator. The spot deflection method does not allow the beam to remain at the measuring position on the target long enough for the residual gun current to appreciably affect the results.

Legend of Symbols

E_{rf} — The zero-to-peak value of the radio-frequency modulation as measured between the control grid and cathode of the reading gun.

E_{gr} — The d-c voltage present between the control grid and cathode (a negative voltage) of the reading gun.

E_{kw} — Negative potential on cathode of writing gun.

E_{tar} — The target voltage with respect to the collector.

E_{gw} — The d-c voltage between the control grid and cathode of the writing gun.

I_{cw} — Writing collector current.

e_{gw} — The peak amplitude of the video modulation present between the control grid and cathode of the writing gun.

METHODS TO EXTEND THE FREQUENCY RANGE OF UNTUNED DIODE NOISE GENERATORS*

By

Harwick Johnson

Research Department, RCA Laboratories Division,
Princeton, N. J.

Summary—*The use of a peaking inductance to compensate for the effects of diode capacitance at high frequencies is shown to substantially double the usable frequency range of untuned broad-band diode noise generators. A similar extension of frequency range is possible through the use of a symmetrical diode arrangement. This latter circuit is of particular interest for balanced line very-high-frequency operation since it may be constructed without the need of specialized alignment equipment. The two methods may be combined to secure the advantages of each, giving an extended usable frequency range about four times that of a single-tube generator.*

Introduction

UNTUNED broad-band noise generators, which consist of a temperature-limited diode shunted by a terminating resistance, possess an upper usable frequency limit determined by the diode self-capacitance, which alters the source impedance of the generator at high frequencies. Diode noise sources have been used above this limit, in the past, by resonating the diode capacitance with an inductance. This leads to a narrow band generator requiring a tuning adjustment if a reasonable frequency range is to be covered by the generator. Two methods of substantially extending the frequency range of untuned generators will be discussed here. The first of these methods involves the introduction of an inductance in series with the terminating resistance after the manner of the peaking inductance in video circuits. It should be pointed out, however, that, although the physical arrangement is similar to that of a compensating inductance in video circuits, the usual video circuit equations do not apply to the noise generator case. The calculation for the performance of the noise generator is somewhat more involved. The second method to be discussed below involves a symmetrical arrangement of two diodes and offers important practical advantages for balanced line generators. The two methods may be combined without loss of the advantages of either one.

* Decimal Classification: R355.913.21.

Generator with Compensating Inductance

Consider the equivalent circuit of Figure 1, which shows a noise generator connected to a receiver through a transmission line of characteristic impedance Z_o. The performance of the noise generator may be evaluated by computing the ratio of the direct-current (dc) diode current of the generator of Figure 1 to the dc diode current in an ideal generator, where $L_p = L_l = C = 0$, to produce a given receiver response. Since the generated noise power is proportional to the dc diode current, this is a power ratio which may be expressed in decibels to give the error in the measurement of receiver noise factor. The general relation[1] expressing this ratio involves, in addition to the source impedance of the generator, the length of transmission line connecting the noise generator to the receiver and the absolute magnitude of the reflection coefficient of the receiver input.

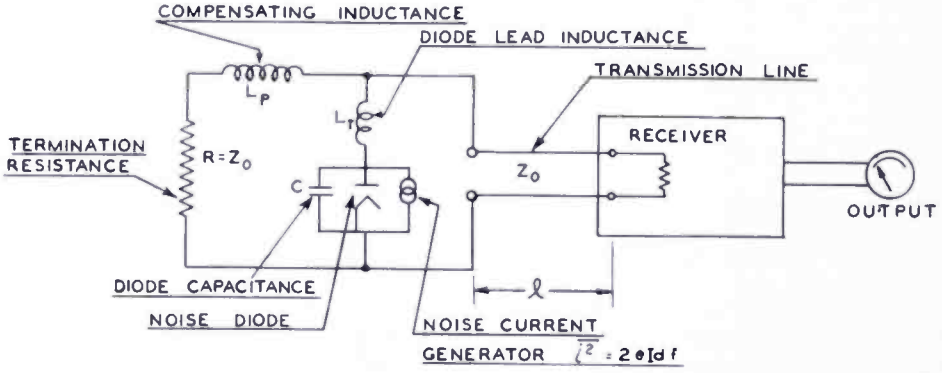

Fig. 1—Equivalent circuit of a diode noise generator.

For the present evaluation, it will suffice to compute the maximum and minimum values of this ratio (maximum errors). That is, as the source impedance of the generator is varied, the line length will be adjusted so that this ratio is either a maximum or minimum. If the absolute value of the reflection coefficient of the receiver input is taken as unity, the extreme values to these maxima and minima will be obtained. Under these conditions, the maximum and minimum values of the power ratio may be expressed as

$$M = \frac{1}{4}\{[(G+1)^2 + B^2]^{\frac{1}{2}} \pm [(G-1)^2 + B^2]^{\frac{1}{2}}\}^2, \qquad (1)$$

where G is the normalized source conductance of the generator and B is the normalized source susceptance of the generator. These admit-

[1] I. J. Melman, "Noise Generators and Measuring Technics", *Tele.-Tech.*, Vol. 9, p. 36, July 1950.

tances are normalized with respect to the characteristic admittance ($Y_o = 1/Z_o$) of the transmission line connecting the noise generator to the receiver.

If the normalized conductance and susceptance of the generator of Figure 1 are computed and inserted in Equation (1), it is found, after some manipulation, that the power ratio is given by

$$M = \frac{1}{4}\left\{(1-b^2x^2)\left[\left\{\left(\frac{1}{1+a^2x^2}+1\right)^2+x^2\left(\frac{1}{1-b^2x^2}-\frac{a}{1+a^2x^2}\right)^2\right\}^{\frac{1}{2}}\right.\right.$$

$$\left.\left.\pm\left\{\left(\frac{1}{1+a^2x^2}-1\right)^2+x^2\left(\frac{1}{1-b^2x^2}-\frac{a}{1-a^2x^2}\right)^2\right\}^{\frac{1}{2}}\right]\right\}^2,$$

where $x = \omega CZ_o$, $a = L_p/CZ_o^2$ and $b = L_t/CZ_o^2$.

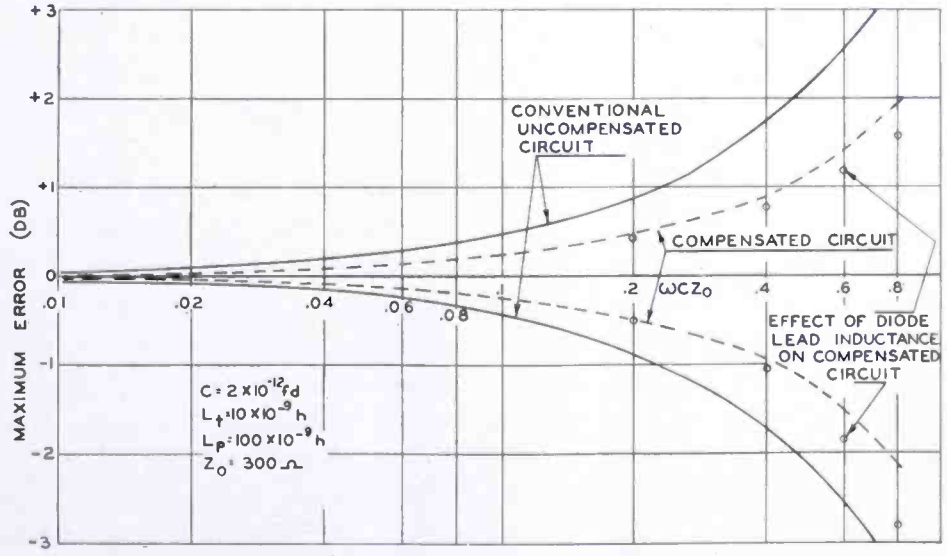

Fig. 2—Typical calculated curves showing maximum errors for conventional and compensated noise generators.

This power ratio (in decibels) is plotted in Figure 2 as a function of ωCZ_o. For a typical selection of parameters corresponding to diodes of glass envelope construction, it was assumed that the diode capacitance, $C = 2 \times 10^{-12}$ farad, the diode lead inductance, $L_t = 10^{-8}$ henry, and the characteristic impedance of the line, $Z_o = 300$ ohms. The parameter a was taken as 0.5 (this value is commonly used in the design of video peaking circuits) for which the compensating inductance, in this case, is 10^{-7} henry. The solid curves showing the greatest positive and negative errors are for the circuit without the compensating inductance ($L_p = 0$). This is the conventional broad-band noise

generator circuit. The tube lead inductance, L_t, has a negligible effect upon the computations for this case so that the solid curves apply whether or not the tube lead inductance is included in the calculation. It perhaps should be pointed out that these curves give the maximum positive and negative errors and that the error in an actual measurement may lie anywhere between these limits depending upon the length of transmission line and the reflection coefficient of the receiver.

The dotted curves show how the above errors are reduced and/or the frequency range extended by the use of a compensating inductance, L_p, in series with the terminating resistance. It is seen that, for a given maximum error of ± 1 decibel, the frequency range is about twice that of the uncompensated circuit. The dotted curves do not include the effect of the tube lead inductance, L_t. The circles lying near the dotted curves show the effect of including the tube lead inductance in the calculations for the compensated circuit. It is noted that the effect of the tube-lead inductance is appreciable but not sufficiently significant to alter the general conclusion that, through the use of a compensating inductance in series with the terminating resistance, the usable frequency of untuned diode noise generators may be substantially doubled.

The curves of Figure 2 are intended only to represent the results of a typical calculation and do not exploit all the special cases which may find application. For example, the approximate symmetry of the curves of Figure 2 for the particular parameters selected suggest that, if a reflectionless "line stretcher" were inserted between the diode generator and the receiver, and two noise readings made with the line stretcher adjusted to give maximum and minimum readings, these readings could be averaged to secure a measurement of greater accuracy. This situation holds only for a certain selection of the parameters. For other selections, the error curves are not symmetrical about the zero error axis. The general tendency, as the parameter a is increased, is for the curves to approach the zero line in a non-symmetrical manner and to diverge more rapidly at the higher frequencies. This manner of selection of parameters may be useful to obtain a reduced spread between the positive and negative errors and to obtain increased accuracies. However, due to the rapid divergence of the negative error curve, the frequency range (for allowable errors of, say, ± 1 decibel) is not significantly different from that illustrated by the parameter selection of Figure 2.

Symmetrical Diode Generator

The second method of extending the frequency range of untuned

diode generators involves simply a symmetrical arrangement of two diodes in order to reduce the total effective capacitance. This method is of considerable interest because of the many practical constructional advantages it affords in the construction of very-high-frequency balanced-line generators.

The basic circuit of this symmetrical[2] arrangement is shown in Figure 3. Since the two diode capacitances are effectively connected in series across the line, the effective diode capacitance is half that of a single diode. In terms of the curves of Figure 2 (the solid curves for the uncompensated case), the parameter $x = \omega C Z_o$ is reduced by one-half or, stated in another way, the frequency, ω, may be doubled for the same maximum error. It is evident that compensating inductances may also be used with this symmetrical arrangement to extend further the usable frequency range.

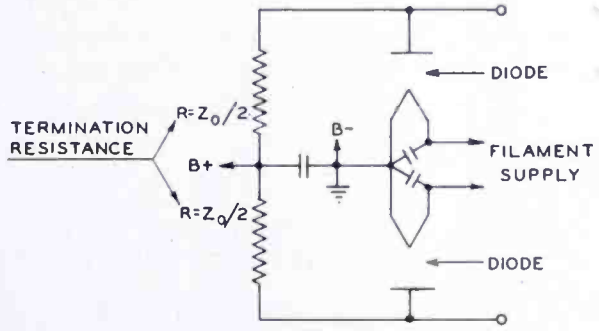

Fig. 3—Symmetrical diode noise generator circuit for balanced-line operation.

The circuit of Figure 3 is of equal interest because of its suitability for balanced-line operation without the many complications ordinarily encountered in attempting to use a single diode for balanced line operation. Single diodes used in this application at very high frequencies (30-300 megacycles) have been complicated by two factors. First, it has been necessary to resonate the diode capacitance, which otherwise shunts a portion of the noise current produced by the diode. Second, the circuit problem presented by the necessity of supplying heating current to the filament, which is connected to one side of the line, requires the use of chokes. A choke used for this purpose adds very substantially to the effective reactance and is more important in limiting the bandwidth than the diode capacitance. Hence, the frequency

[2] The arrangement of Figure 3 might have been denoted as a "push-pull" arrangement by analogy to familiar amplifier circuitry. However, the term symmetrical is preferred here in order to avoid confusion (by implication) concerning the manner in which the noise currents produced by the two diodes are added. The noise currents must be added in quadrature.

coverage without switching is small. Furthermore, the alignment and adjustment of the tuned circuits ordinarily used requires equipment and skill in its use which may not be readily available.

It has been shown above that the circuit of Figure 3 minimizes the first consideration, and the advantages of this circuit with respect to the second consideration will now be pointed out. It is seen in Figure 3 that, by supplying the anode potential at the mid-tap of the terminating resistance, all of the dc supply connections are at ground potential. This eliminates the need for critically tuned chokes in the supply leads. For other reasons, it may be advisable to insert chokes in the supply leads but these chokes, in contrast to the tuned case, are not critical and special equipment for their adjustment is not necessary.

The familiar formula, $F = 20\ IR$, for the measurement of receiver noise factor by doubling the receiver noise power output by means of the noise source, must be revised for the present arrangement. By the use of Thevenins' Theorem, the equivalent noise generator for the circuit of Figure 3 will be found by calculating the short-circuit noise current due to the two diodes. It is readily shown that the total mean-squared short-circuit noise current is

$$\overline{i^2} = \tfrac{1}{2}\, e\, (I_{d1} + I_{d2})\, df = \tfrac{1}{2}\, e\, I_d\, df,$$

where I_{d1} is the dc current of one diode, I_{d2} is that of the second diode and I_d is the sum of the two dc currents. The current division between the two diodes is of no consequence and only the total current need be metered. This equivalent noise generator produces a mean-squared current equal to one-fourth of that produced by a single diode in a conventional arrangement (e.g., Figure 1) carrying the dc current I_d. Then, the formula for the measurement of receiver noise factor by doubling the noise power output of the receiver becomes $F = 5\ IR$. For $R = 300$ ohms, $F = 1.5\ I_{ma}$, where the current is in milliamperes.

It is seen that the symmetrical diode arrangement has achieved untuned wide-band balanced-line very-high-frequency operation (of extended frequency range compared with untuned single-diode circuits) and has eliminated the switches and critically tuned circuits (as well as the specialized alignment equipment necessary for their adjustment) ordinarily found in balanced-line very-high-frequency generators. This has been achieved at the cost of an additional diode, an increase in the dc power requirement, and a loss in the available noise power per unit current.

An experimental noise generator employing a symmetrical diode arrangement was constructed for use in noise measurements on very-

high-frequency television receivers. Type 5722 noise diodes were used (without sockets) and the components were arranged with a minimum of lead length. It should be pointed out that the burden of success in the construction of an untuned generator for high-frequency use lies in the care with which the circuits are assembled to avoid stray capacitances and inductances. While no precise absolute determination of the accuracy of this experimental unit was made, measurements made on average television receivers were compared with measurements made using a tuned-circuit type noise generator.

Up to frequencies of 186 megacycles, the readings of the two units differed by less than 1 decibel; the differences averaging around 0.5 decibel. Above 186 megacycles, increased differences of 1 to 2 decibels were found. Since the overall accuracy of these measurements was probably not greater than 0.5 decibel, the performance was considered satisfactory for many applications where precise determinations are unnecessary. It thus appears that the symmetrical diode arrangement offers a simple means of construction of a very-high-frequency balanced-line noise generator which may be particularly attractive to the experimenter to whom the specialized alignment equipment necessary for tuned type generators is unavailable. It should also be pointed out that these experimental results may be improved through the addition of a compensating inductance as described above.

Conclusions

It has been shown that the useful frequency range of untuned diode noise generators may be substantially doubled through the use of a peaking inductance in series with the terminating resistor to compensate for the deleterious effects of the diode capacitance at high frequencies. A symmetrical diode arrangement of extended frequency range has also been described which is of particular interest in the construction of untuned balanced-line generators for very-high-frequency use. This arrangement is of particular interest for such applications because it may be assembled without the need for specialized tuning and alignment equipment. These two methods may be combined to obtain the advantages of each.

HIGH-SPEED TEN-VOLT EFFECT*†

By

R. M. Matheson and L. S. Nergaard

Research Department, RCA Laboratories Division,
Princeton, N. J.

Summary—In 1935, H. Nelson observed that tubes with oxide-coated cathodes operating under space-charge-limited conditions show a small deviation from the Child-Langmuir law for anode voltages exceeding ten volts. Recent measurements confirm his observations. The effect is stable, and is independent of frequency for all frequencies for which the electron transit time may be neglected. Measurements made on triodes, rotating-anode diodes, and diodes with cathode probes indicate that the effect is not caused directly by the cathode. Observations on diodes in which the anode temperature could be varied associate the effect with the anode. It is shown that an increase of space charge by secondary and reflected electrons from the anode can account for the deviation. The required secondary emission ratios are in substantial agreement with those reported for barium oxide.

THE effect of space charge on the current passing between an electron-emitting cathode and another electrode, when current flows under the influence of an accelerating field insufficient to cause saturation, is well known. The exactitude of the relation for the current $I = PV^{3/2}$, where V is the applied voltage and P a constant determined by the charge-to-mass ratio of the electron and the geometry of the system, has been verified many times for pure metal emitters.

In 1935 H. Nelson[1] observed that tubes with oxide cathodes show a small but consistent deviation from this relation whenever the applied voltage exceeds approximately ten volts. Recent measurements confirm his observations.

When the voltage applied to an oxide-cathode diode is increased beyond ten volts, the current is found to be less than predicted by the above relation. The current-voltage relation for a typical diode is shown in Figure 1. A two-thirds-power scale is used for the current so that a straight line characteristic is obtained if the current is determined solely by space charge arising from electrons emitted by

* Decimal Classification: R131 × R138.1.

† Presented at the Symposium on Electron Emission sponsored by the Division on Electron Physics of the American Physical Society in collaboration with the Panel on Electron Tubes of the Research and Development Board at New York, N. Y. on January 30-31, 1951.

[1] H. Nelson, RCA Victor Division, unpublished report.

the cathode. Below ten volts the characteristic is a straight line within the limits of experimental error; at ten volts a marked deviation occurs and persists to much higher voltages.

Many deviations from the normal space-charge relationship have been observed with oxide cathodes. These deviations have almost invariably been functions of time and of the past history of the tube. Almost all of them are difficult to reproduce with any precision. In contrast, the present effect is extremely stable and reproducible. Provided a tube is not operated under unusual or extreme conditions, curves such as shown in Figure 1 can be repeated with an accuracy of one per cent or better over a period of weeks. Even severe overheating results

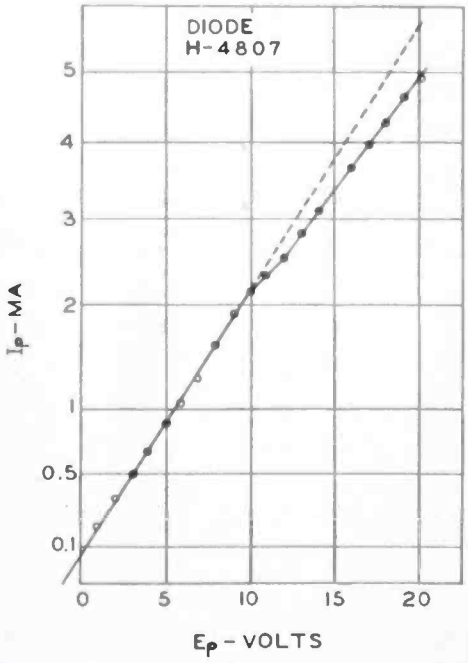

Fig. 1—Ten-volt effect in a diode.

in only small changes in the magnitude of the deviation from the space charge line. The magnitude of the deviation varies slightly from tube to tube but the point of onset, approximately ten volts, is independent of tube geometry or materials.

Irregularities in the *I-V* characteristics of tubes with oxide cathodes have frequently been attributed to the release of ions or molecules from the anode by electron bombardment. When these particles reach the cathode, they may cause either a change in the total emission, or a change in the cathode impedance, or both. The effect of a change in emission on the *I-V* characteristics of a tube is very slight unless the decrease is great enough so that the current through the tube becomes emission limited. The near parallelism of the measured *I-V* characteristics with the 3/2 power law above ten volts indicates that emission limitation is not a likely explanation of the effect. However, a small

increase of cathode impedance at ten volts could readily produce the effect observed. Since the present effect occurs only with applied voltages greater than ten volts, it is conceivable that 10 electron-volts is the energy necessary to cause ionization or the release of a particle from the anode. The effect of ions on the cathode can be eliminated by operating a diode under such conditions that ions cannot cross from anode to cathode. This can be accomplished by operating a diode as a high-frequency rectifier under class C conditions. Then positive ions originating at the anode can be accelerated toward the cathode only during the period when the anode is positive with respect to the cathode. Since the time of transit of a charged particle is a function of its charge-to-mass ratio and since this ratio for ions is much smaller than for electrons, it is possible to choose an operating frequency such that all ions having less than a given ratio cannot cross the interelectrode space but are returned to the anode during the inverse cycle. This method was used with frequencies as high as six hundred megacycles and with spacings such that no particle having a charge-to-mass ratio less than one one-hundredth of that of an electron could cross from anode to cathode. The ten-volt break was always observed.

In these high-frequency measurements it is impossible to observe the *I-V* characteristic during each cycle. The average current is observed as the amplitude of the high-frequency signal is varied. The ten-volt break is readily detected in a plot of average current versus peak applied voltage and this directly indicates that ions are not responsible because none can cross from anode to cathode. The possibility of the effect being due to neutral particles may be eliminated by computing the average current using the low-frequency *I-V* characteristic. The exact agreement of the computed and the measured values indicates that the characteristic observed at low frequency is valid at the high frequency. The transit time of neutral particles is at least equal to that of ions of equal mass as it is extremely improbable that a neutral could be released from the anode with significantly more energy than that possessed by the impinging electron. Hence, any effect by neutrals would be averaged over many cycles and would result in changing the *I-V* characteristic below as well as above the ten-volt point with the result that the average current computed using the low-frequency *I-V* characteristic would be in error.

To determine whether the effect originates within or at the surface of the cathode, measurements have been made on diodes, some with probes inside the coating and others with probes immediately outside of the cathode coating. Measurements of probe potential indicate whether the excess voltage drop in the tube is occurring on the anode or cathode side of the probe. The results with a platinum probe wire

imbedded in the oxide coating are shown by the solid lines in Figure 2. The diode *I-V* characteristic is shown in the lower half of the figure. The characteristic has been plotted as $V^{3/2}$ versus I, so that a common current scale could be used for the two parts of the figure. The solid curve in the upper half of the figure shows the probe potential with

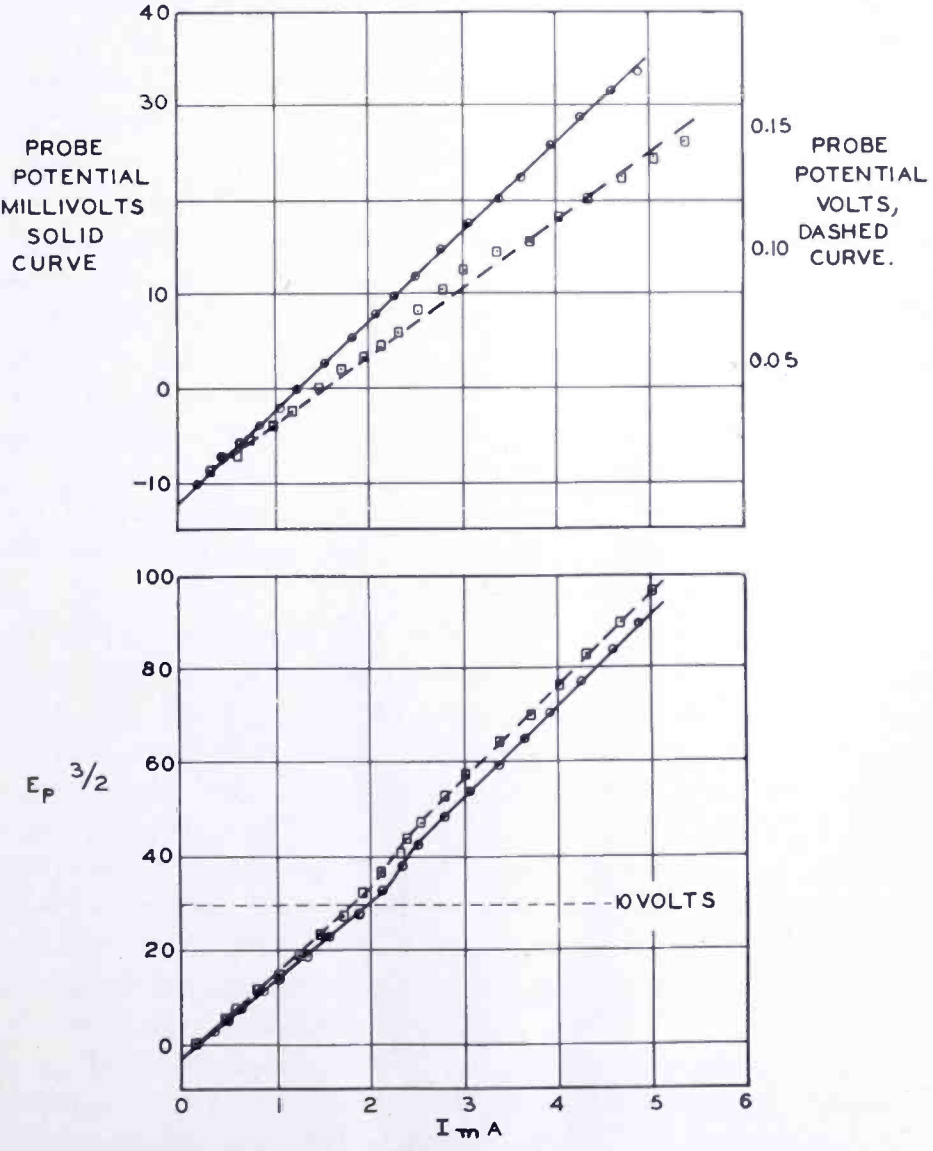

Fig. 2—Variation of anode and cathode-probe potentials with current. Solid curve—probe embedded in oxide coating. Dashed curve—probe .002 inch from cathode surface.

respect to the cathode base metal as a function of current. This clearly indicates that the irregularity in the *I-V* characteristic is occurring on the anode side of the probe.

The dashed curves in Figure 2 were obtained with a diode having an emitting filamentary probe 0.001 inch in diameter located 0.002 inch

from the cathode surface. Since these measurements were made in a rather widely-spaced (2-millimeter) diode with low applied voltages, the electron velocities in the vicinity of the probe were substantially thermal and the zero-current point on the probe *I-V* characteristic may be used as a measure of the space potential. The fact that the probe potential measured with respect to cathode is a linear function of the diode current indicates that the ten-volt break in the diode *I-V* characteristic is due to an effect occurring between the probe and the anode or at the surface of the anode, and that the cathode is not directly responsible.

The evidence that the excess voltage drop does not occur within or at the surface of the cathode is also supported by measurements in a tube having a rotating anode constructed so that the same portion of the anode may be used to collect electrons either from an oxide cathode or from a tungsten filament. With the anode in its initial position, the *I-V* characteristic obtained with the tungsten filament satisfied the 3/2 power law and the characteristic with the oxide cathode showed the ten-volt departure. Upon rotating the anode it was found that any portion of the anode which had been exposed to the heated oxide cathode showed the typical ten-volt break whether operated with the oxide cathode or the tungsten filament.

Further examination of the effect was made by varying anode temperature. With a nickel anode the magnitude of the deviation increased by less than 5 per cent for anode temperatures up to 1600°K. This change was completely reversible. At approximately 1600°K the deviation increased rapidly and irreversibly by about 50 per cent and a slight curvature of the characteristic below 10 volts appeared. No further change was obtained below the melting point of nickel, 1725°K. With a tantalum anode the results were similar for temperatures below 1600°K. When the anode was heated above 1600°K the effect disappeared and the normal 3/2 power characteristic was observed. Allowing the anode to cool resulted in the gradual reappearance of the effect, the initial characteristic being restored in approximately 1000 seconds. The vapor pressure of barium oxide given by Blewett[2] et al indicates that this is almost exactly the period to transfer one monolayer of barium oxide from cathode to anode.

The preceding experiments suggest that the ten-volt effect is due to the presence of barium oxide on the anode. If this conjecture is correct, then the irreversible change occurring with the nickel anode

[2] J. P. Blewett, H. A. Leibhafsky, and E. F. Hennelly, "The Vapor Pressure and Rate of Evaporation of Barium Oxide", *Jour. Chem. Phys.*, Vol. 7, p. 478, July 1939.

is caused by the formation of a barium silicate layer on the anode. These compounds are known to form gradually on nickel cathodes.[3] At 1660°K, the liquid phase first appears on the BaO-SiO_2 phase diagram, and a rapid reaction is therefore probable. The elimination of the effect on tantalum is due to the reduction of barium oxide by the tantalum, as in the well-known batalum getter.

It may be concluded from the foregoing that the effect is associated with the anode and that it is probably due to a layer of barium oxide. The high-frequency measurements require that any mechanism ex-

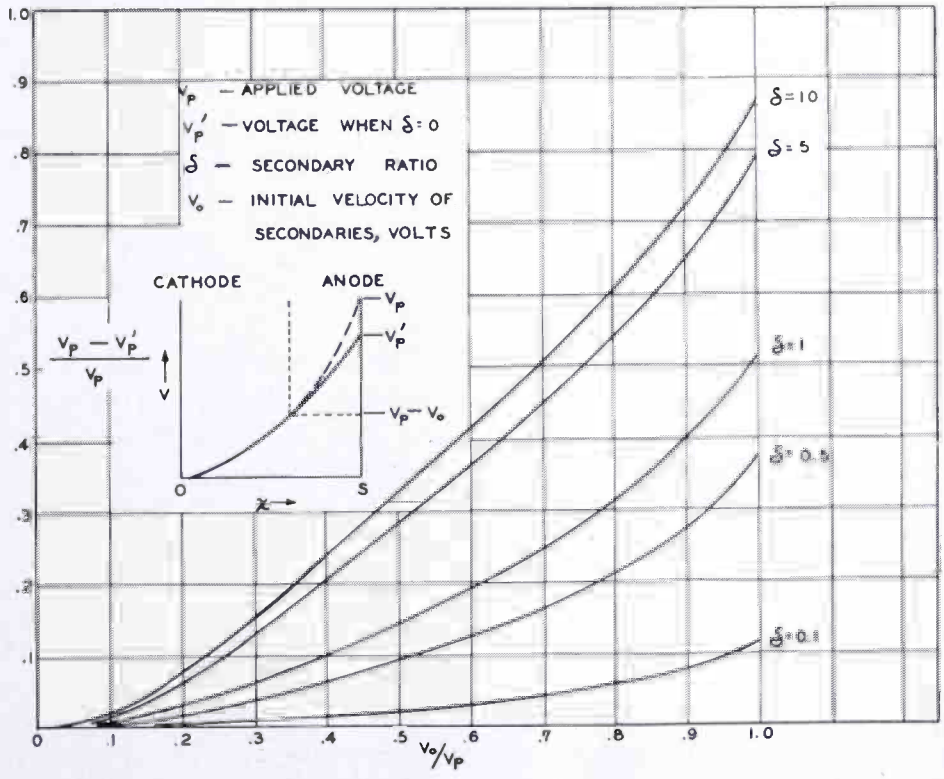

Fig. 3—The computed increase in anode voltage required to maintain constant current in a diode as a function of secondary initial velocity with the secondary emission ratio as a parameter.

plaining the effect have a time constant of 10^{-9} second or less. Secondary emission from the anode seems the only mechanism likely to fulfill these requirements.

The effect of secondary electrons and reflected primaries from the anode on the space charge in a diode has been analyzed. Because of the slight amount of data available on secondary yields at low primary velocities and because of the obvious difficulties in handling the general case, the treatment is restricted to secondaries having a single initial

[3] A. S. Eisenstein, "Oxide Coated Cathodes", Section of ADVANCES IN ELECTRONICS, Vol. I, Academic Press, New York, 1948.

velocity normal to the anode surface and making one transit. The inset in Figure 3 shows the conditions for the analysis. The space potential (V) is plotted as a function of distance (x) from the cathode. The potential is proportional to the four-thirds power of the distance, as shown by the solid curve in the figure. If secondaries are released by the anode with a velocity V_o (expressed in volts), they will move toward the cathode until they reach a point having a potential $V_p - V_o$ and then return to the anode. If the current through the diode is to be maintained constant, the additional space charge due to the secondaries must be compensated for so that the potential distribution near the cathode is not disturbed. This can be accomplished only by increasing the anode potential from V'_p to V_p. Figure 3 shows the increase of anode potential necessary for various values of the secondary emission ratio (δ) and initial velocity (V_o). It may be seen that rather modest yields of low velocity secondaries or even smaller numbers of reflected primaries can produce quite noticeable shifts in the I-V characteristic of a diode. If, as is likely, secondaries produce tertiaries, even smaller yields are sufficient to produce the observed shifts.

Since it is known that almost all secondary electrons have energies of a few volts or less,[4] by choosing a reasonable secondary velocity the measured deviations from the space charge line may be used to determine the approximate secondary yield as a function of primary velocity. The secondary emission ratio determined in this manner is proportional to the square root of the difference between the primary energy and a constant and is in tolerably good agreement with the values for barium oxide given by Bruining[5] over the range from ten to forty volts primary energy.

The well-known effect of secondary electrons in tetrodes has been used to verify the marked increase of secondary yield as the primary energy is raised above ten volts. A typical family of plate current versus plate voltage curves for a tetrode is shown in Figure 4. The effect of secondaries or reflected primaries is noticeable even at voltages as low as two or three volts, but a marked break in plate current occurs when the plate voltage is increased beyond ten volts, whenever the screen is sufficiently positive to collect the secondaries from the plate.

Additional evidence of the marked increase in numbers of secondaries when the applied potential is increased beyond ten volts was obtained by operating a tetrode with increased heater power so that

---

[4] R. Kollath, "The Secondary Emission of Solid Bodies", *Phys. Zeits.*, Vol. 38, p. 202, 1937.

[5] H. Bruining, "Secondary Emission—Part III", *Physica*, Vol. 5, p. 913, December 1938.

the first grid emits thermionically. Figure 5 shows the plate current as a function of plate voltage. The cathode is biased positively with respect to the first grid so that cathode and grid currents of the same order of magnitude are obtained. The plate current exhibits the ten-

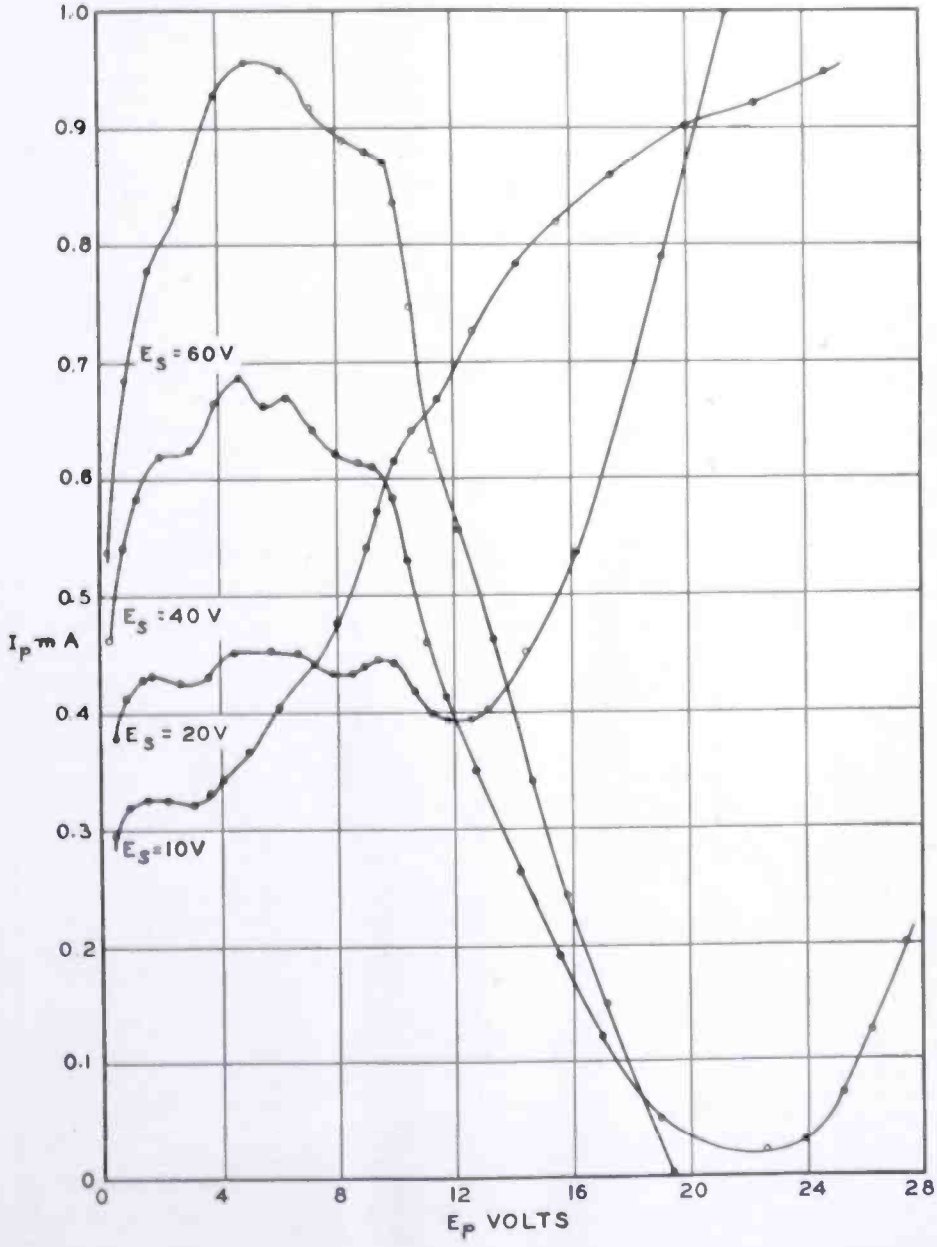

Fig. 4—Plate characteristics of a tetrode with screen voltage as a parameter.

volt break when the plate is struck by ten-volt electrons from either the grid or the cathode and the effect of each velocity group is independent of the other. The difference between the onset of cathode current and the measured cathode bias is due to contact potential

which is large in this case because of the abnormally high cathode temperature.

Some evidence as to the relative importance of reflected primaries and true secondaries has been obtained. The circuit employed is shown in Figure 6. In this circuit the control-grid, screen, and anode voltages vary sinusoidally, but with fixed ratios, for any one

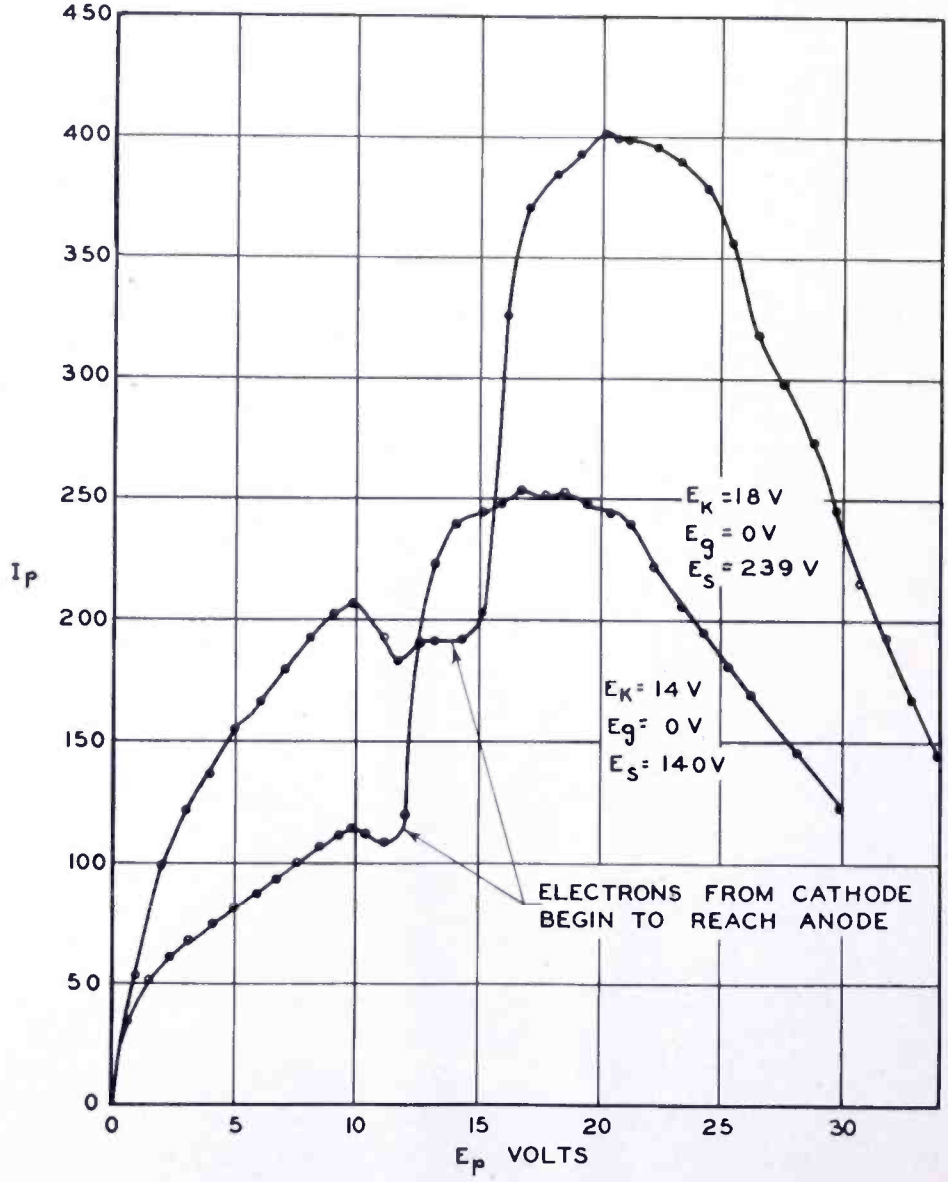

Fig. 5—Ten-volt effect with electrons of two velocity classes.

experimental curve. The upper experimental curve in Figure 6 shows the results with the plate always positive with respect to the screen. As the plate voltage increases beyond ten volts, the plate current shows the normal deviation. When the screen also exceeds ten volts the

plate current rises due to collection of secondaries from the screen. The lower curve shows the effect with the screen always positive with respect to the plate. When the screen voltage exceeds ten volts the plate current falls due to excess space charge caused by secondaries from the screen and when the plate voltage exceeds ten volts the usual deviation occurs.

The curvature of the characteristic below ten volts is of particular interest. It seems likely that this is due to reflected electrons which, having substantially primary energy, can return to the virtual cathode. In the tetrode these electrons produce μ times the effect of

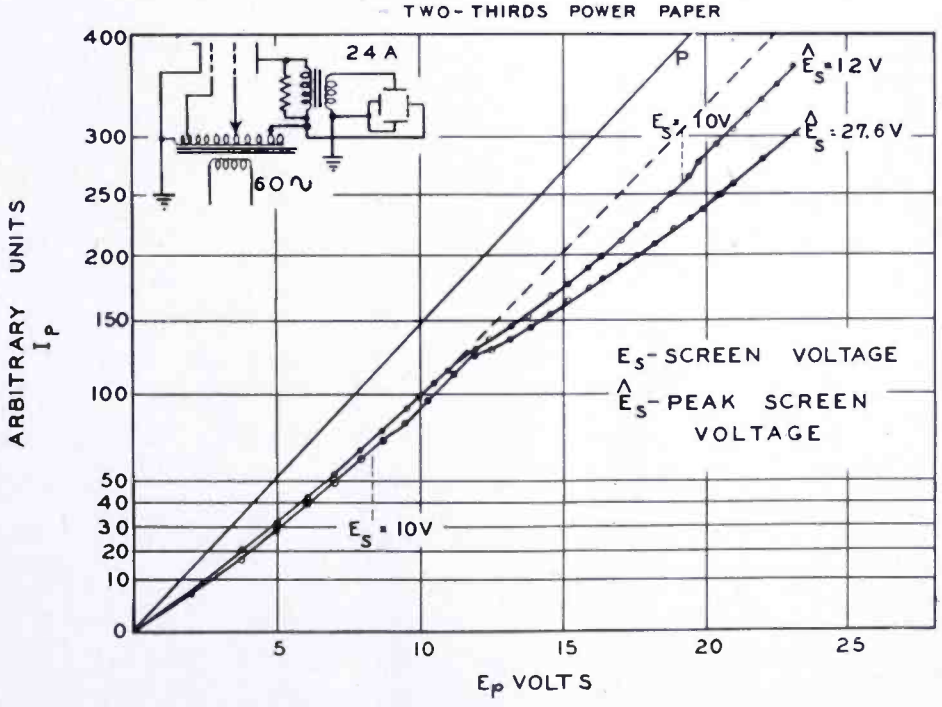

Fig. 6—Screen and anode ten-volt effect in a tetrode.

true secondaries, which are confined to the screen-plate region. Bruining[5] has measured the yields of both reflected primary and secondary electrons from barium oxide as a function of primary velocity. As a matter of definition he considered electrons leaving the barium oxide surface with substantially primary energy to be reflected electrons, and those with lower energies to be true secondaries. He finds that below seven volts the number of reflected electrons exceeds the number of true secondaries. In view of the above considerations, it may be assumed that the curvature below ten volts is due solely to reflected electrons. If this assumption is correct, it should be possible to choose a straight line representing the true perveance of the tube in the absence of reflected electrons,

so that the discrepancy between this line and the experimental points can be accounted for by Bruining's data for the yield of reflected electrons. The straight line P in Figure 6 has been so chosen. The procedure used to check the true perveance line P below ten volts may be applied above ten volts to ascertain the I-V characteristic of the tube with reflected primaries, but in the absence of true secondaries. The dashed line in Figure 6 has been obtained in this manner. It may then be concluded that the remaining deviation between the dashed line and the experimental points is due to true secondaries. While the yield of reflected electrons becomes small compared with the yield of secondaries at the higher primary energies, the high initial velocities of the reflected electrons permit them to reach the potential minimum where they produce an effect comparable with that produced by the larger number of true secondaries, which are confined to the screen-anode space.

In summary, the small, stable deviations from the 3/2 law found in tubes with oxide cathodes are due to a layer of extraneous material on the anode. Secondary electrons from this layer increase the charge in the interelectrode space, depress the potential minimum, and reduce the space current below that predicted by the 3/2 law. Evaporation experiments and secondary yield data indicate that the layer consists of barium oxide evaporated from the cathode. The apparent sudden onset of the effect is then explained by the rapid rise of secondary yield of barium oxide in the neighborhood of 10 volts.

DIRECT-READING NOISE-FACTOR MEASURING SYSTEMS*

By

R. W. Peter

Research Department, RCA Laboratories Division.
Princeton, N. J.

Summary—*For investigation and optimum adjustment of low-noise amplifiers, it is highly desirable to have an instrument which indicates continuously the noise factor of an amplifier under test. A new type of direct-reading noise-factor measuring system has been developed for the ultra-high-frequency range. Its principle and construction are described after giving a survey of earlier systems and their disadvantages.*

The new noise-factor meter uses a noise source (a saturated diode or a gas discharge tube) as a calibrated power source. The noise source is switched on and off by a relay. The direct-current component of the rectified amplifier output is displayed on a cathode-ray oscilloscope. Either the scope is calibrated to read noise factor directly, or the noise source output is adjusted by a calibrated attenuator for a certain power output ratio. Instead of the cathode-ray oscilloscope, a current-ratio meter in conjunction with a selector switch can be used to read the noise factor directly from a dial.

Introduction

IN CONNECTION with the development of low-noise-factor (or noise figure) traveling-wave-tube amplifiers, it was felt necessary to have an instrument which would indicate continuously the noise factor of an amplifier under test. This would show the effect of changing the different variables (voltages, magnetic field, radio-frequency coupling, etc.) and permit them to be adjusted for lowest noise factor in a short time, a procedure which is otherwise extremely time consuming for this type amplifier with its many variables.

As no entirely satisfactory method of measuring noise factors continuously at microwave frequencies was available, several systems were investigated and a new one was developed which is based on a square-wave pulsed noise source.

The meter built for the super-high-frequency (SHF) range incorporates a gas-discharge noise source. For lower frequencies a noise diode would be used, e.g., the Bendix TT-1 coaxial diode up to 3000 megacycles or the 5722 diode up to several hundred megacycles.

This paper describes the principle and the design of a new direct-

* Decimal Classification: R273.1.

reading noise-factor measuring system after giving a short survey of the known systems.

Noise Factor—Definition and Standard Measuring Techniques

The noise factor of an amplifier is a measure of the noise power added to the original signal by the amplifier. It is here defined[1] as the ratio between the noise-to-signal power ratio at the output, N_b/S_b, and at the input, N_a/S_a, i.e.,

$$F = \frac{N_b/S_b}{N_a/S_a}, \tag{1}$$

where the N_a and S_a are "available" noise and signal powers respectively and the input noise power, N_a, is fixed at

$$N_a = kT_oB \doteq 0.004 \times B \text{ micromicrowatts.} \tag{2}$$

kT_oB is the noise power delivered to an impedance matched to the source at room temperature, T_o. B is the effective frequency bandwidth, in megacycles, $k = 1.38 \times 10^{-23}$ joule per degree, and $T_o = 290°\text{K}$.

To determine the noise factor, one can measure the gain $G_1 = S_b/S_a$, at a frequency f_1, and the noise-power output, N_b, of the amplifier. The noise-power input, N_a, is computed from the integrated frequency response of the amplifier,

$$B = \frac{1}{G_1}\int_0^\infty G\,(F)\,df. \tag{3}$$

An application of this method is discussed in the next paragraph. It is difficult, however, to obtain an accurate absolute measurement of the output noise power. G_1 or B may change between gain and noise measurement. The gain measurement can be eliminated by adding a known amount of signal power to the noise input and observing the increase in power output.

Two different kinds of calibrated signal power are used for this purpose:

(1) Sinusoidal, i.e., single-frequency power from a signal generator (signal-source method).

[1] For the original definition of the noise factor see D. O. North, "The Absolute Sensitivity of Radio Receivers", *RCA Review*, Vol. VI, No. 3, p. 332-343, January 1942.

(2) Power from a noise source with a continuous frequency spectrum of constant amplitude ("white" noise) over the considered band (noise-source method).

The noise-source method has many advantages over the signal-source method so that, at present, it is widely used. Its features are:

(1) Radio-frequency powers of similar spectral distribution are compared. A determination of the effective frequency bandwidth, B, therefore, is not necessary. This is an important point because B may change during adjustment of the amplifier for minimum noise figure.

(2) The available noise sources deliver power of such magnitude that powers of similar amplitude are compared. Insertion of large and calibrated attenuation and careful shielding are not necessary.

(3) For the complete radio-frequency spectrum there exist noise sources which are more stable than a signal generator with attenuator.

A saturated diode works satisfactorily as a noise source[2] up to several hundred megacycles. By special constructions, in which the diode is made part of the transmission system, its frequency range has been extended up to 3000 megacycles[3,4]. Since Mumford[5] found that a gaseous discharge represents a stable noise generator at microwave frequencies, this type has replaced the diode in all frequency bands for which waveguides are practical[6].

When properly made, the gas discharge noise source exhibits practically no insertion loss when not fired, i.e., it acts as an almost perfect transducer. The fired noise source represents a broadband termination for the waveguide. The spectral distribution of the noise-power output is flat over the useful waveguide band, contrary to diode arrangements where transit time reduces the noise output with increasing frequency.

The relative noise temperature of the argon-gas noise source standard used by the author is 15.5 ± 0.25 decibels above room temperature at 6975 megacycles.† For a commercial 15-watt fluorescent lamp (T-8

[2] R. W. Slinkman, "Temperature-Limited Noise Diode Design", *Sylvania Technologist*, Vol. 2, No. 4, p. 6, October 1949.

[3] R. Kompfner, J. Hatton, E. E. Schneider and L. A. G. Dresel, "The Transmission-Line Diode as Noise Source at Centimeter Wavelengths", *Jour. Inst. Elec. Eng.*, Vol. 93, Part IIIA, No. 9, p. 1436-1442, March-May, 1946.

[4] H. Johnson, "A Coaxial-Line Diode Noise Source for U-H-F", *RCA Review*, Vol. VIII, No. 1, p. 169-185, March 1947.

[5] W. W. Mumford, "A Broad-Band Microwave Noise Source", *Bell Sys. Tech. Jour.*, Vol. 28, p. 608, October 1949.

[6] H. Johnson, "Gaseous Discharge Noise Sources for S-H-F", unpublished report, August 1950.

† Recent unpublished measurements by J. E. Sees and H. Corbett at the Naval Research Laboratories.

bulb, 18 inches long) with mercury-argon gas filling, 16.2 ± 0.5 decibels was obtained at 3000 megacycles. Values were found to be practically independent of temperature.*

The procedure of measuring the noise figure of an amplifier with a calibrated noise (or signal) source consists of measuring the relative power output of the amplifier while the noise (or signal) source is operating (P_b) and while it is shut off (N_b). This measurement is

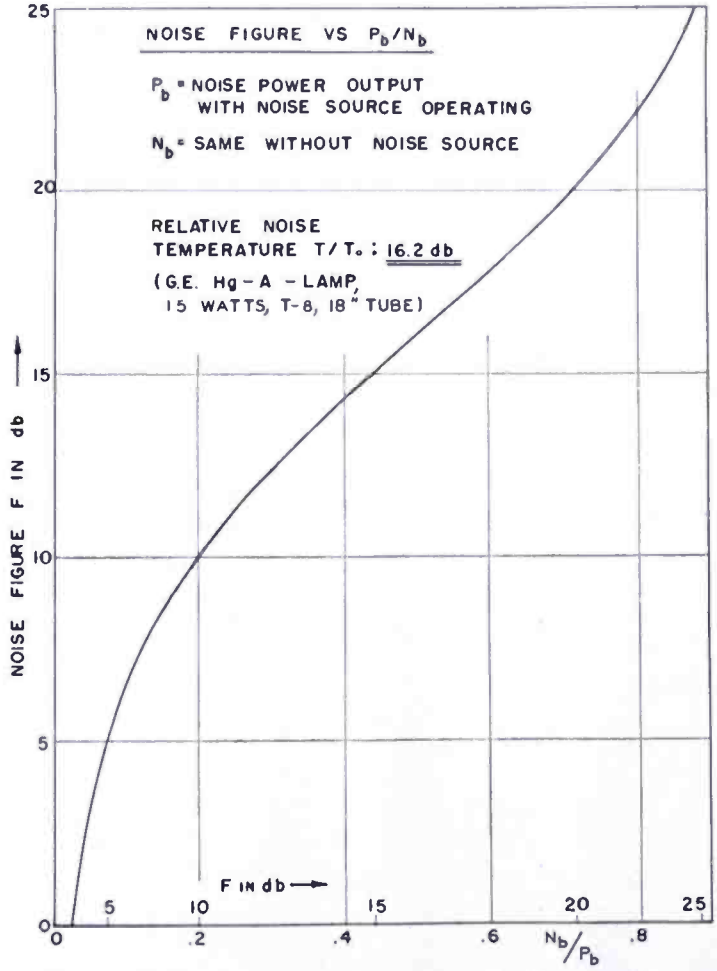

Fig. 1—Plot of noise figure versus N_b/P_b (Equation (4)).

made with a square-law detector which adds linearly amounts of power of different frequencies, or with a linear detector of which the output is proportional to the square root of the measured power.

Looking backward from the amplifier input, the noise-source impedance must be the same in both measurements. The noise factor is

* Mercury-argon fluorescent lamps are reported to have appreciable noise temperature versus operating temperature coefficients under normal operating conditions. With the particular tube used in this apparatus, however, the dissipated power per unit volume can be held low enough to assure a negligibly small change between cold and operating temperature. For other frequency ranges and other conditions, special tubes without mercury may be desirable (see reference 6).

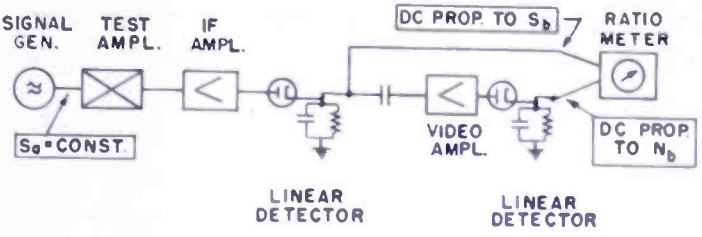

Fig. 2—Noise measuring system used by Herold.

then computed from Equation (4) which follows directly from Equation (1):

$$F = \frac{P_a/N_a - 1}{P_b/N_b - 1}, \tag{4}$$

where $P_a = N_a + S_a$, total input power (noise and signal),

$P_b = N_b + S_b$, total output power.

In case of a gas discharge noise source,

$$P_a/N_a = T/T_o \tag{5}$$

is the relative noise temperature. T represents the temperature of the electron gas. Equation (4) is plotted for a relative noise temperature of 16.2 decibels in Figure 1. The abscissa shows a nomographic representation of Equation (4) which is used later.

Direct-Reading Noise-Factor Meters — Earlier Proposals

According to the foregoing, a direct-reading noise-factor meter must continuously supply the results of two measurements. These measurements can be made in principle either simultaneously or in rapid repeated succession, with storage of the measured data in between. There exist proposals for both types of noise-factor meters. An unpublished arrangement, originated and used about 10 years ago by E. W. Herold,† is representative of the first group where the two measurements are performed simultaneously (see Figure 2).

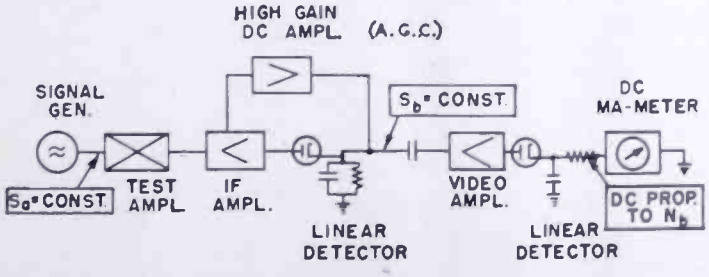

Fig. 3—Noise measuring system used by Richmond.

† RCA Laboratories Division, Princeton, N. J.

A relatively large constant continuous-wave signal applied to the amplifier yields a rectified current proportional to the gain, if the output signal-to-noise ratio is chosen large enough. The noise later is amplified separately to about the amplitude of the signal. The ratio of the two rectified currents is proportional to the square-root of the noise figure and may be read directly on a ratio meter. Linear detectors are used. Figure 3 shows a modification of this circuit which incorporates an automatic gain control (AGC) to hold the total gain for the signal constant. The noise-power output, in this case, is proportional to the noise factor. An arrangement of this type was used by M. Richmond[‡] but has not been published.

This method, with either variation, requires an absolute calibration to read noise factor. Its accuracy is limited by the stability of video amplifier, signal generator and effective bandwidth, B.

The proposal of Clayton et al[7] belongs to the second group, i.e., the two measurements are performed in succession (Figure 4). The signal

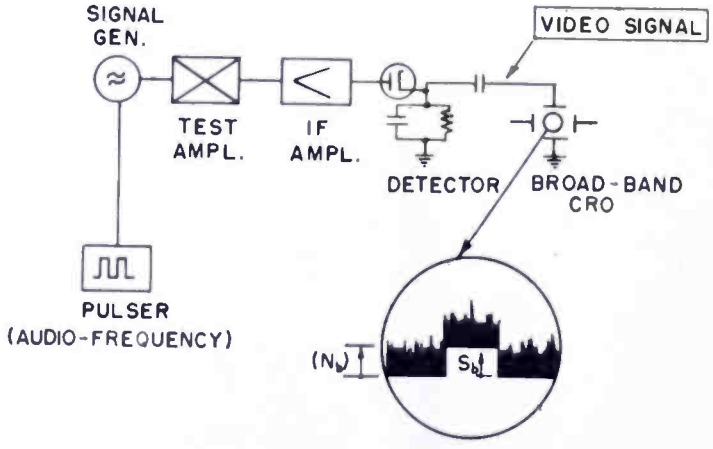

Fig. 4—Noise measuring system used by Clayton et al.[7]

generator is pulsed at an audio frequency rate and the total video output of the amplifier is displayed on a broadband cathode-ray oscilloscope after detection with a square-law detector. The signal-pulse amplitude is adjusted to equal the subjectively estimated average noise amplitude and yields a "visual" noise figure, from which the actual noise figure can be computed. The accuracy depends on subjective quantities and is stated to be within ± 1 decibel.

A New Direct-Reading Noise-Factor Meter

As the earlier noise-factor meters basically use the signal-source

[‡] Formerly RCA Laboratories Division, Princeton, N. J.

[7] R. J. Clayton, J. E. Houldin, H. R. L. Lamont and W. E. Willshaw, "Radio Measurements in the Decimetre and Centimetre Wavebands", *Jour. Inst. Elec. Eng.*, Vol. 93, Part III, No. 22, p. 97-125, March 1946.

method, they inherently have its previously discussed disadvantages. The new noise-factor meter is based on the noise-source method and therefore avoids those difficulties.

Figure 5 shows one version of the system, which belongs to the second group, where the two measurements are made in succession. Its essential difference from Clayton's system is that direct-current amplitudes are compared instead of video and direct-current signals. This makes the measurement independent of subjective judgment, and the quantities can be measured on meters. As will be discussed later, a possible modification (shown dotted, on Figure 5) uses a gated AGC system to hold the peak of the pulse at constant value.

Actually, this meter simply speeds up the conventional two-step measuring procedure explained earlier. A noise source whose impedance is independent of whether or not it is fired, is pulsed at a slow rate

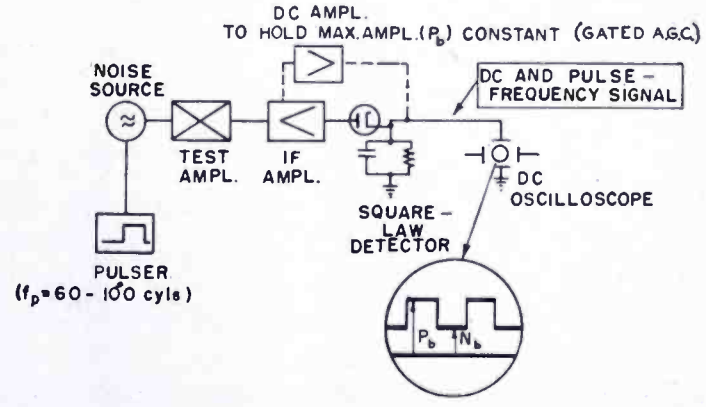

Fig. 5—Noise-factor meter based on the noise-source method.

($f_p = 60$ to 100 cycles per second), i.e., fired and switched off periodically. The output of the amplifier is rectified in a square-law detector and fed through a low-pass filter, of which the cutoff frequency, f_c, is chosen high enough to transmit the pulses undistorted, i.e.,

$$f_c \geqq 10 \times f_p. \tag{6}$$

It is important for the choice of f_p that f_c is negligible compared to the intermediate-frequency bandwidth, B, i.e.,

$$10\, f_p \leqq f_c \ll B. \tag{6a}$$

From the two pulse amplitudes, P_b and N_b, the noise figure can be evaluated or "read" in three different ways:

(1) Direct current plus pulse-frequency output are displayed on a direct-current cathode-ray oscilloscope and the total noise-power input, P_a, is adjusted until $P_b/N_b = 2$ (see Figure 5).

In this case

$$F = P_a/N_a - 1 = S_a/N_a. \tag{7}$$

This method, of course, is only applicable if the noise figure is small enough, i.e., $F \leqq (S_a/N_a)$ maximum. For a saturated diode noise source, Equation (7) becomes

$$F = S_a/N_a = \frac{eIR}{2kT_o} = 20IR, \tag{8}$$

where I is the diode current, in amperes, and R is the diode noise-source impedance, in ohms. F is proportional to I. If a gas discharge noise source is used, the noise-power input must be adjusted with a calibrated series attenuator. The relative noise output, in decibels, of the noise source with $L = 10 \log b$ decibels series attenuation,[8] is

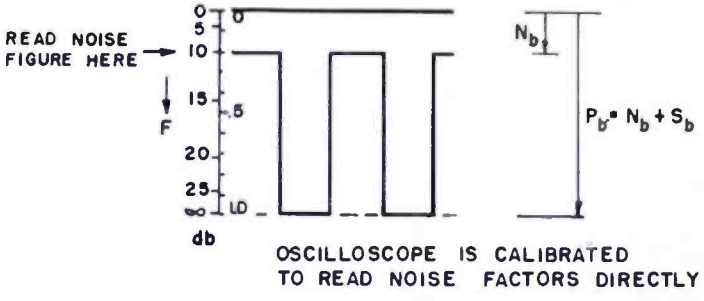

Fig. 6 — Method of calibration of scope permitting direct reading of noise factor.

$$F = S_a/N_a = \frac{1}{b}(T/T_o - 1) + 1, \tag{9}$$

where T/T_o is the actual relative noise temperature of the source. For the fluorescent lamp noise source with $T/T_o = 41.7$ (i.e., 16.2 decibels),

$$F = \frac{40.7}{b} + 1. \tag{10}$$

(2) A second way of measuring the noise figure is to hold the relative input power, P_a/N_a, constant, and measure the ratio of the output power, P_b/N_b, from the display on a cathode-ray oscilloscope. The noise figure, then follows from Equation (4) or Figure 1, and the screen of the scope may be calibrated to read noise factor directly in decibels (see Figure 6). A direct-current amplifier with a gated AGC may be used to hold the

[8] E. W. Herold and L. Malter, "Some Aspects of Radio Reception at Ultra-High Frequency, Part III", *Proc. I. R. E.*, Vol. 31, No. 9, p. 509, September 1943.

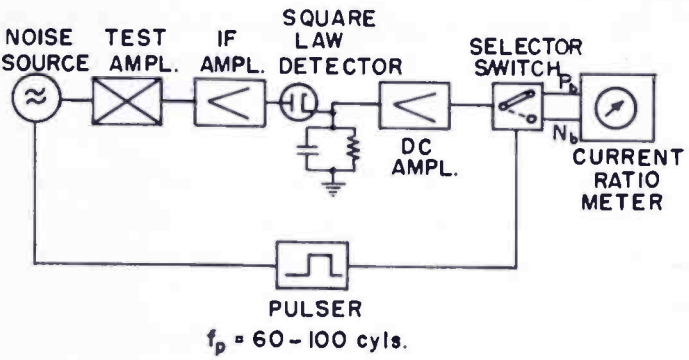

Fig. 7 — Method of reading noise factor from current-ratio meter by employing synchronous selector switch.

maximum amplitude constant as indicated in Figure 5 in dotted lines.

(3) A third way of reading the noise factor is shown in Figure 7. Again P_a/N_a is constant. The two currents proportional to P_b and N_b are fed separately into the two inputs of a ratio meter by means of a switch which is coupled to the pulser. A direct-current amplifier multiplies the direct current and the pulse-current output of the square-law detector up to the required value for the meter. The meter is calibrated with the curve of Figure 1 to read noise figure directly. It is important to note that the amplifier instability does not affect the meter reading.

In general, it can be said that in many cases reading the noise figure from the cathode-ray oscilloscope is preferable because it allows one to observe any unwanted distortion of the output-signal by oscillation, hum modulation, etc.

A noise-factor meter of this type was built for the 2500- to 4000-megacycle range to measure noise figures of traveling-wave tube amplifiers. It was operated with a direct-current scope. Most of the time the first of the above mentioned methods was used, as the noise figures to be measured were well below 16 decibels.

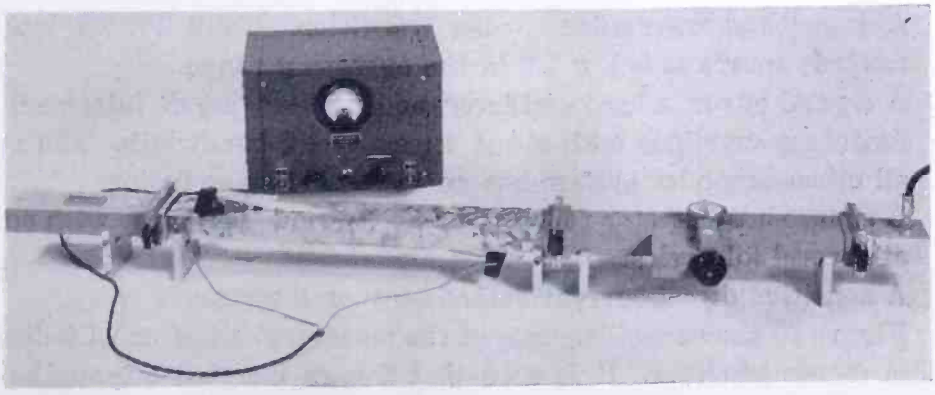

Fig. 8—Noise source with pulser and calibrated attenuator used in noise-factor meter.

The system, in principle, is the one of Figure 5. A picture of the noise source with pulser and attenuator is shown in Figure 8. The complete direct-reading noise-factor meter is seen in Figure 9. It consists of:

A broad-band gas discharge noise source with a 15-watt mercury-argon lamp mounted at a 10-degree angle in an S band waveguide and terminated on one side. Its relative noise temperature is 16.2 ± 0.5 decibels above 290°K.

A pulser to switch the noise source on and off 60 or 80 times per second or to run it continuously.

A variable calibrated waveguide attenuator which introduces a maximum voltage-standing-wave ratio (VSWR) of 1.1.

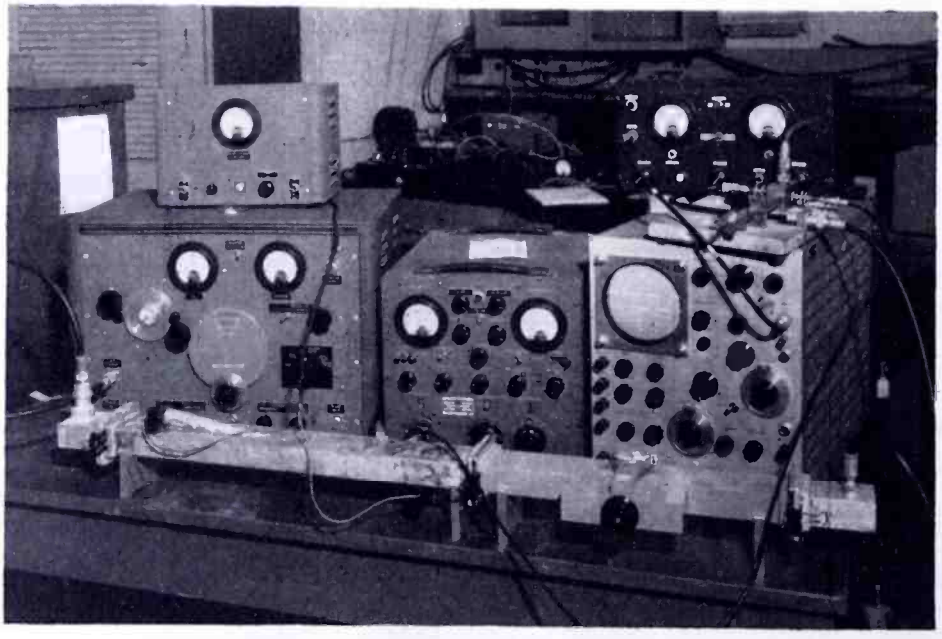

Fig. 9—Complete direct-reading noise-factor meter.

A broadband waveguide-to-coax transition. Total VSWR looking towards source is below 1.2 in the operating range.

A crystal mixer, a local oscillator, and a 30-megacycle intermediate-frequency amplifier with about 7 megacycles bandwidth. The over-all mixer-amplifier system has an 11-decibel noise factor.

A square-law detector followed by an R-C low-pass filter with cutoff at several kilocycles.

A sensitive direct-current cathode-ray oscilloscope.

Figure 10 shows oscillograms of the measurement of an 11.9-decibel noise factor amplifier. It is seen that for an inserted attenuation of $L = 4.2$ decibels, $P_c/N_c = 2$. According to Equation (10) this yields a noise figure, F, of 11.9 decibels.

Some design factors and details of this system will be discussed in the following sections.

Pulsed Gas Discharge Noise Source

About 500 volts direct current are necessary to ignite the 15-watt fluorescent lamp easily without using a heated cathode. An adjustable

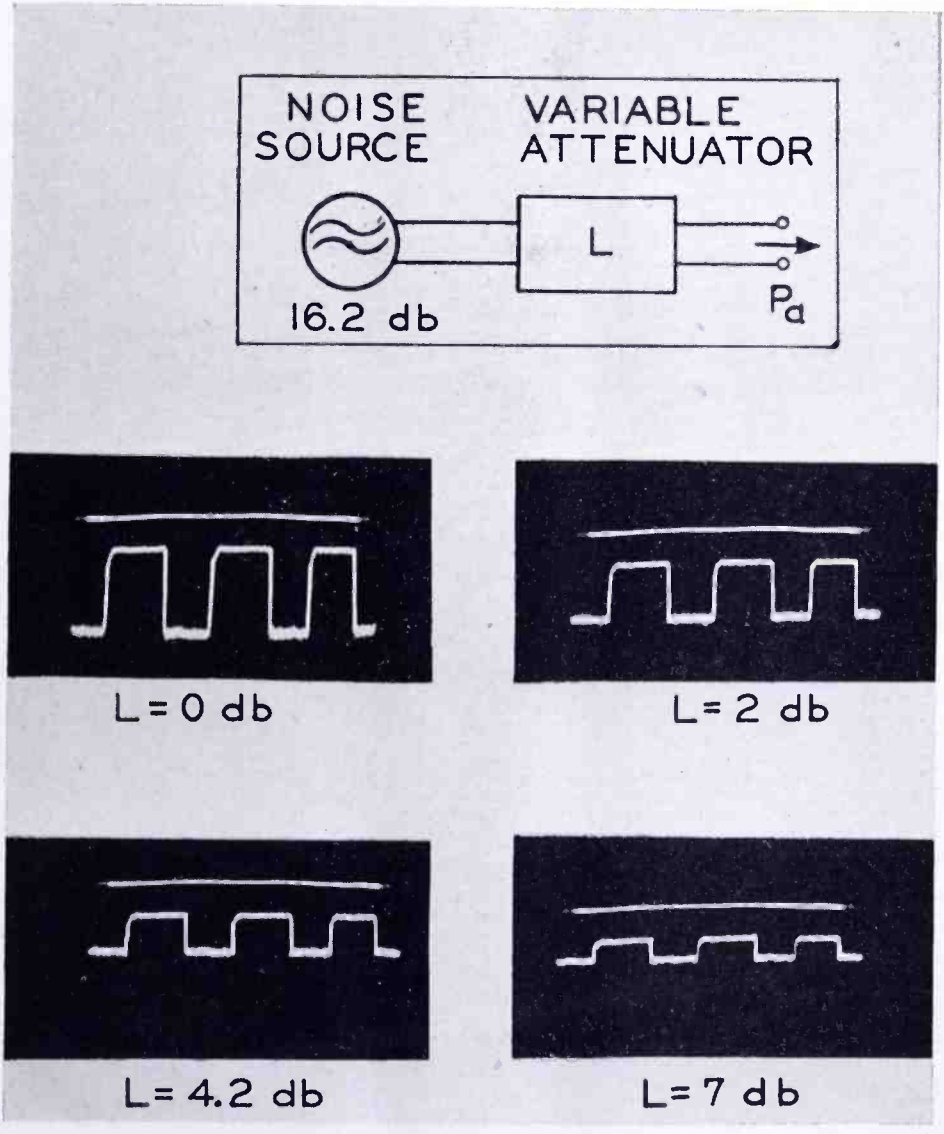

Fig. 10—Output of noise-factor meter for different noise-power input, P_a.

resistor limits the direct current to the required 75 milliamperes. A mechanical vibrator, the 276-E relay, was chosen to switch the lamp on and off at a rate of either 60 or 80 cycles. The principal circuit is shown in Figure 11.

It was found that once the discharge is established, it sets in again

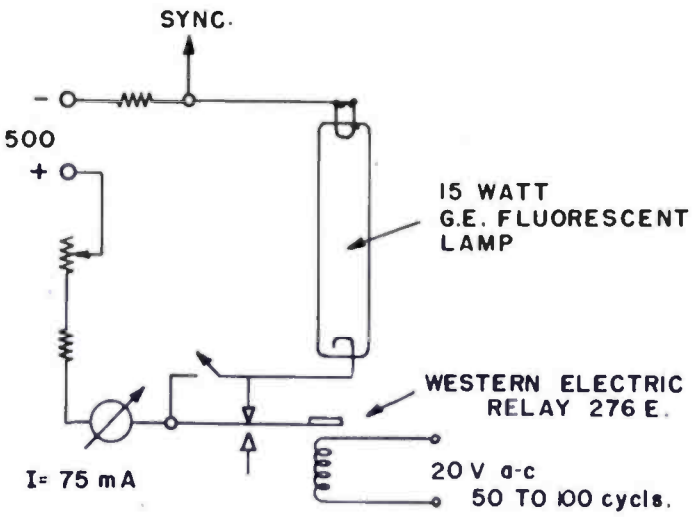

Fig. 11 — Simplified schematic of noise-source pulser.

after a short interruption, so that sharp pulses are obtained (see oscillograms in Figure 10). To start the discharge initially, however, may take as long as a second. A small current first sets in, which, after a certain delay, jumps to the steady value. Under certain special conditions, small plasma oscillations in the audio-frequency range have been observed superimposed on the pulse amplitude.

The 276E relay is balanced for 60 cycles. It runs stably enough, however, up to 90 cycles. To separate any 60-cycle hum component from the pulsed signal output, an R-C generator was designed to drive

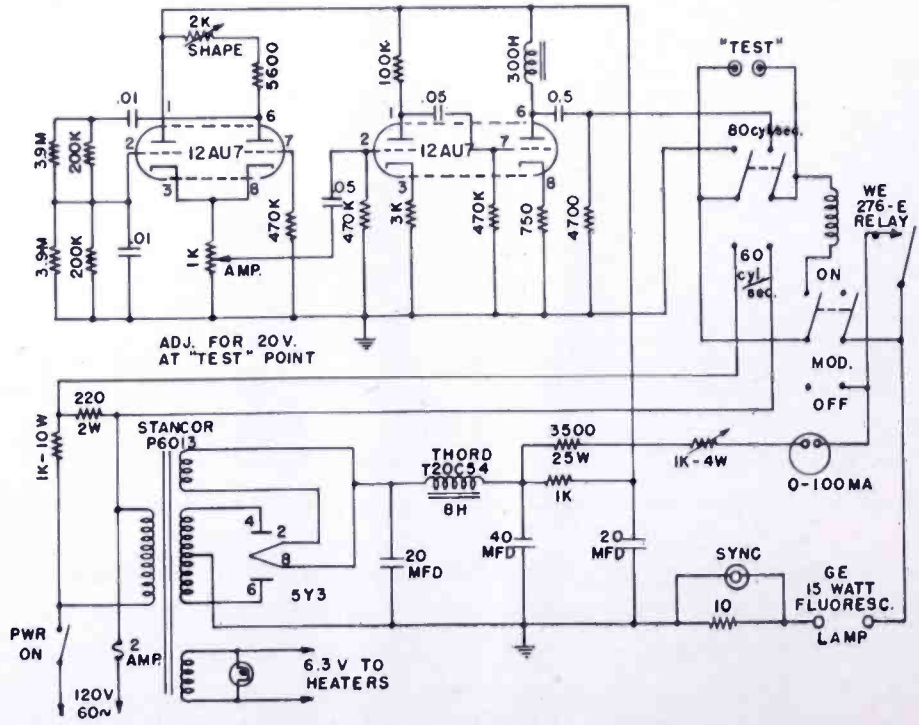

Fig. 12—Schematic of noise-source pulser.

the relay at 80 cycles. The detailed noise-source pulser circuit is shown in Figure 12.

Square-Law Detector

The 6AL5 diode-detector of a standard 30-megacycle intermediate-frequency amplifier with 7-megacycle video bandwidth is run as a square-law detector. The detector current output is linear to single-frequency signal-power input up to a level of 5 microamperes. As the maximum amplitude of random noise exceeds the peak value of the alternating-current signal with which the detector is calibrated, the detector current is kept below 3 microamperes for noise-power measurements.

Noise-Factor Measuring Circuit with Current-Ratio Meter

In cases where it is desirable to read the noise figure directly from a meter scale, the arrangement of Figure 7 can be used.

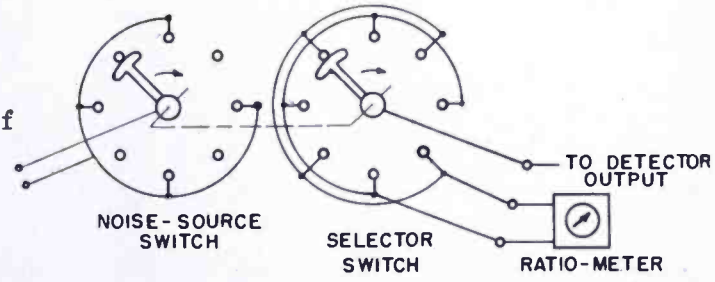

Fig. 13—Diagram of a selector switch.

Two rotating switches mounted on a common axis provide a suitable pulser and synchronous selector (Figure 13). The minimum allowed switching frequency is determined by the time constant of the circuit and meter.

Acknowledgment

The author wishes to thank E. W. Herold and H. Johnson for many valuable discussions and suggestions, and R. Hughes for his contribution in the design and construction of the noise-source pulser.

RCA TECHNICAL PAPERS†

First Quarter, 1951

Any request for copies of papers listed herein should be addressed to the publication to which credited.

"All New 250-Watt AM Transmitter, R. J. Newman, *Broadcast News* (March-April) 1951
"An Automatic Nonlinear Distortion Analyzer", H. F. Olson and D. F. Pennie, *RCA Review* (March) 1951
"Application of Transformer RCA-225T1 in Deflection System for Wide-Angle Large-Screen Kinescopes", *RCA Application Note AN-149*, RCA Tube Department, Harrison, N. J. (March 1) 1951
"Cathodoluminescence of Zinc Orthosilicate with Manganese Activator", S. Larach and R. E. Schader, *Jour Appl. Phys.* (March) (Letter to the Editor) 1951
"Coaxial Line Triple-Tuned UHF Tuner", M. Braverman, *RCA Licensee Bulletin LB-816* (January 17) 1951
"Columbate Dielectrics", C. Wentworth, *RCA Licensee Bulletin LB-825* (March 28) 1951
"Dark Adaptation", Albert Rose, *Jour. Opt. Soc. Amer.* (March) (Letter to the Editor) 1951
"Design of Mobile Two Way Radio Communication Equipment at 152-174 Mc.", R. A. Beers, W. A. Harris and A. D. Zappacosta, *Broadcast News* (January-February) 1951
"Efficient Deflection and High-Voltage Circuits for Kinescopes Such as RCA-14EP4 and RCA-17CP4", *RCA Application Note AN-148*, RCA Tube Department, Harrison, N. J. (January 15) 1951
"Electron Bombardment Induced Conductivity in Germanium Point Contact Rectifiers", A. R. Moore and F. Hermon, *Rev. Sci. Instr.* (February) 1951
"Filter Design Simplified", B. Sheffield, *Audio Eng.* (March) 1951
"Flat Reflector for UHF System", T. Roylston, *Electronics* (March) .. 1951
"A Flexible TV Audio System", W. L. Lyndon, *Broadcast News* (January-February) 1951
"The Heteronull", Clarence A. West, *CQ* (February) 1951
"Horizontal Pulling", J. R. Meagher, *Rad. and Tele. News* (March) .. 1951
"Image Gradation Graininess and Sharpness in Television and Motion Picture Systems, Part I—Image Structure and Transfer Characteristics", O. H. Schade, *Jour. S.M.P.T.E.* (February) 1951
"Installation of Theater Television Equipment", E. Stanko and C. Y. Keen, *Jour. S.M.P.T.E.* (March) 1951
"Investigation of Ultra-High-Frequency Television Transmission and Reception in the Bridgeport, Connecticut Area", R. F. Guy, *RCA Review* (March) 1951
"Locked-in Oscillator for TV Sound", M. S. Corrington, *Electronics* (March) 1951
"Long Line Stabilization of UHF Oscillators", S. Fisher, *RCA Licensee Bulletin LB-817* (January 29) 1951
"Los Angeles to San Francisco Miscrowave Relay", B. W. Southwell, *Tele-Tech* (February) 1951
"Low-Noise Miniature Pentode for Audio Amplifier Service", D. P. Heacock and R. A. Wissolik, *Tele-Tech* (February) 1951
"Low-Reflection Films Produced on Glass in a Liquid Fluosilicic Acid Bath", S. M. Thomsen, *RCA Review* (March) 1951

† Report all corrections or additions to RCA Review, Radio Corporation of America, RCA Laboratories Division, Princeton, N. J.

"Manufacture of an RCA Developmental Three-Gun Tri-Color Kinescope", *RCA Licensee Bulletin LB-822* (February 28) 1951
"A Modern Frequency Measuring Installation", H. A. Taylor and E. C. Rundquist, *Electronics* (March) 1951
"New Broadcast Lightweight Pickup and Tone Arm", L. J. Anderson and C. R. Johnson, *Audio Eng.* (March) 1951
"New Editing Machine for Professional Tape Recordings", D. C. Yarnes, *Tele-Tech* (January) 1951
"New Limiting Amplifier, BA-6A", G. A. Singer, *Broadcast News* (March-April) 1951
"New Senior VoltOhmyst WV-97A", John Cornell, *RCA Rad. Serv. News* (January-March) 1951
"A Noise Inversion Circuit for Improved Noise Immunity in Television Receivers", J. Avins, *RCA Licensee Bulletin LB-823* (March 23) .. 1951
"An Objective for Use in the Electron Microscopy of Ultra-Thin Sections", J. Hillier, *Jour. Appl. Phys.* (February) 1951
"On the Sharpening of Microtome Knives for Ultra-Thin Sectioning", J. Hillier, *Rev. Sci. Instr.* (March) 1951
"Open-Field Test Facilities for Measurement of Incidental Receiver Radiation", C. G. Seright, *RCA Review* (March) 1951
"Particle-Size Distribution of Tungsten and Molybdenum Powders", A. D. Power and I. M. Kakascik, Section of THE PHYSICS OF POWDER METALLURGY, McGraw-Hill Book Company, Inc., New York, N. Y. 1951
"Permanent-Magnet Electron Microscope", J. H. Reisner and S. M. Zollers, *Electronics* (January) 1951
"Photo-Luminescence Efficiency of ZnS:Cu Phosphors as a Function of Temperature", R. H. Bube, *Phys. Rev.* (February) 1951
"Principles of the Electrical Rating of High-Vacuum Power Tubes", E. E. Spitzer, *Proc. I.R.E.* (January) 1951
"Projection Kinescope 7NP4 for Theater Television", L. E. Swedlund and C. W. Thierfelder, *Jour. S.M.P.T.E.* (March) 1951
"Properties of Some Wide-Band Phase-Splitting Networks", D. G. C. Luck, *Proc. I.R.E.* (March) (Letter to the Editor) 1951
"The RCA PT-100 Theater Television Equipment", R. V. Little, Jr., *Jour. S.M.P.T.E.* (March) 1951
"The Selective Electrostatic Storage Tube", J. Rajchman, *RCA Review* (March) 1951
"Shortwave Radio Propagation Correlation with Planetary Positions", J. H. Nelson, *RCA Review* (March) 1951
"Signal Strength Analyzer", R. W. George, *Electronics* (January) .. 1951
"Some Prospects in the Field of Electronics", V. K. Zworykin, *Jour. Frank. Inst.* (January) 1951
"Television Service. Part XI — Automatic-Gain-Control Troubles", John R. Meagher, *RCA Rad. Serv. News* (January-March) 1951
"Television Totem Pole", Frank G. Kear and O. B. Hanson, *Electronics* (February) 1951
"Ultra-Thin Sections for the Electron Microscopy of Tissues", J. Hillier, *Transactions of the New York Academy of Sciences* (February) 1951
"An Unobtrusive Dynamic Pressure Microphone", H. F. Olson and J. Preston, *RCA Licensee Bulletin LB-818* (February 1) 1951
"Use of New Low-Noise Twin Triode in Television Tuners", R. M. Cohen, *RCA Licensee Bulletin LB-824* (March 28) 1951
"Use of New Low-Noise Twin Triode in Television Tuners", R. M. Cohen, *RCA Review* (March) 1951
"A Versatile Video Special Effects System", E. M. Gore, *Broadcast News* (March-April) 1951
"Video Relay Switching — Part II", C. R. Monro, *TV Eng.* (January) 1951
"Video Relay Switching — Part III", C. R. Monro, *TV Eng.* (February) 1951

NOTE—Omissions or errors in these listings will be corrected in the yearly index.

Correction:

Some errors have been discovered in the paper entitled "Transient Response of Filters", by Murlan S. Corrington, which appears in the September 1949 issue.

page 417 — Equation (30), first integral. The integrand is $\alpha x - B(x)$.

page 417 — Equation (31), first integral. The integrand is $\alpha x + B(x)$.

page 418 — Last line. Add a minus sign in front of the integral in the braces.

page 419 — First integral. Change the sign of the coefficient to plus.

Following line. Change the sign of sin α to plus.

Sixth line of integrals. Change the sign of sin α to plus.

Eighth line of integrals. Change the sign of α^2 to plus.

Ninth line. Change the denominator of $A_2\alpha^2$ from 2 to 2!

Tenth line. Change the sign of α^3 to minus.

page 422 — Second line of Equation (50). In the second pair of brackets change all numbers in the denominators to the corresponding factorials.

Third line. Change the sign of sin α to minus.

All of the numerical tables and the curves are correct as given.

AUTHORS

JOHN B. ATWOOD attended Washington and Jefferson College in 1924-25 and transferred to Cornell University where he obtained the M.E. degree in 1930 and the M.S.E. degree in 1937. Previously he had been active in amateur radio from 1922 to 1929 and also studied radio engineering at Carnegie Institute of Technology. Before joining the operating staff of RCA Communications, Inc. in 1936, he was employed by the Bell Telephone Laboratories in the Radio Systems Department. In 1937, he transferred to the Research and Advanced Development of RCA Communications, Inc. and since 1942 has been a member of the Communications Research Section of RCA Laboratories Division. Mr. Atwood is a member of Tau Beta Pi and a Senior Member of the Institute of Radio Engineers.

ARTHUR H. BENNER received the B.S. degree in Electrical Engineering from the University of Kansas in 1944, the M.S. degree in 1948, and the Ph.D. degree in 1951 from Pennsylvania State College. From 1944 to 1946, he served as an officer in the U. S. Army Signal Corps. From 1946 to 1949 he was a research engineer with the Ordnance Research Laboratory, State College, Pa., and from 1949 through 1950 he was associated with the Radio Propagation Laboratory at Pennsylvania State College. At present, he is a member of the Advanced Development Engineering Section of the Engineering Products Department. Dr. Benner is a Member of the Institute of Radio Engineers, Sigma XI, Tau Beta Pi, and the American Institute of Electrical Engineers.

ROBERT W. BYLOFF received the B.S. degree in Electrical Engineering from Massachusetts Institute of Technology in 1943. He served with the United States Marine Corps as a radar officer in the Pacific during World War II. In 1946 Mr. Byloff joined the Audio-Video Engineering group of the National Broadcasting Company where he is engaged in the design of components and systems for radio broadcasting and television.

JOHN E. DILLEY was graduated from Drexel Institute of Technology in 1943 with the degree of B.S. in Electrical Engineering. From 1943 to 1946 he served with the U. S. Army Signal Corps. In 1946 he joined the staff of RCA Laboratories Division in Princeton, N. J. Mr. Dilley is an Associate Member of the Institute of Radio Engineers.

L. E. FLORY received the B.S. degree in Electrical Engineering from the University of Kansas in 1930. He was a member of the Research Division of RCA Manufacturing Co., Camden, N. J. from 1930 to 1942. During this time he was engaged in research on television tubes and related electronic problems, particularly in the development of the iconoscope. In 1942 he transferred to the RCA Laboratories Division at Princeton, N. J., where he continued to work on electronic tubes and special circuit problems, including electronic computers, infrared image tubes and sensory devices. Since 1949 he has been in charge of work on storage tubes and industrial television. Mr. Flory is a Member of Sigma XI and a Senior Member of the Institute of Radio Engineers.

H. E. GIHRING received the B.S. degree in Electrical Engineering from Washington University in 1926. From 1926 to 1928, he served as Electrical Assistant in the Signal Corps. In 1929, he joined the Technical and Test Department of RCA. In 1930, he was transferred to Camden in the newly formed Broadcast Transmitter Section, and from 1930 to 1935 he was assigned to propagation and antenna work. In 1936, he was transferred to New York for a year to work on the Empire State television transmitter installation, and from 1937 to 1940, he was engaged in television transmitter development. In 1940, he was assigned to the supervision of the Television Transmitter Group which expanded into radar activities until 1944. From 1944 to the present time, he has been engaged in television transmitter and antenna work in a supervisory capacity. Mr. Gihring is a Senior Member of the Institute of Radio Engineers.

LOUIS MALTER received the B.S. degree from the College of the City of New York in 1926 and the M.A. and PhD. degrees in Physics from Cornell University in 1931 and 1936, respectively. He taught Physics at the College of the City of New York from 1926 to 1928. He was with the Acoustic Research and Photophone Divisions of Radio Corporation of America from 1928 to 1930, and during the Summer of 1931. From 1933 to 1942 he was with RCA Manufacturing Company at Camden, N. J., and from 1942 to 1943 with RCA Laboratories Division at Princeton, N. J. From 1943 to 1946, he was in charge of the Special Development Division of RCA Manufacturing Company at Lancaster, Pa. From May 1946 to December 1947 he was in charge of the Vacuum Tube Research Section of the Naval Research Laboratory, Washington, D.C. In December 1947 he returned to the RCA Laboratories where he is now engaged in research on gaseous electronics. Dr. Malter is a Fellow of the American Physical Society, a Senior Member of the Institute of Radio Engineers, a Member of the American Association for the Advancement of Science, and a Member of Sigma Xi.

HARWICK JOHNSON received his B.S. degree in Electrical Engineering from the Michigan College of Mining and Technology and his M.S. and Ph.D. degrees from the University of Wisconsin. From 1938 to 1942 he was a research fellow and teaching assistant in the Department of Electrical Engineering at the University of Wisconsin. Since 1942 he has been associated with RCA Laboratories Division at Princeton, N. J. Dr. Johnson is a Senior Member of the Institute of Radio Engineers, a Member of Tau Beta Pi, Gamma Alpha and Sigma Xi.

R. M. MATHESON received the A.B. degree from Cornell University in 1938 and the M.A. degree the following year. He attended graduate school at Princeton University in 1939 and 1940, holding a research assistantship during the latter year. From 1941 to 1946 he served in the U. S. Army Air Force, being released from active duty as a Captain. Prior to joining RCA in 1947, Mr. Matheson served as secretary to the Panel on Electron Tubes of the Joint Research and Development Board.

LEON S. NERGAARD received the B.S. degree in Electrical Engineering from the University of Minnesota in 1927, the M.S. degree from Union College in 1930, and the Ph.D. degree from the University of Minnesota in 1935. From 1927 to 1930, he was in the research laboratory and vacuum-tube engineering department of the General Electric Company; from 1930 to 1933 a teaching assistant in the department of physics at the University of Minnesota; from 1933 to 1942 in the research and development laboratory of the RCA Manufacturing Company; and since 1942 at the RCA Laboratories Division in Princeton, N. J. He is a Member of Sigma Xi, the American Physical Society, the American Association for the Advancement of Science, and a Senior Member of the Institute of Radio Engineers.

ROLF W. PETER received the M.S. degree in Electrical Engineering in 1944, and the Ph.D. degree in Radio Engineering in 1948 from the Swiss Federal Institute of Technology in Zurich, Switzerland. From 1946 to 1948 he was Assistant Professor of Radio Engineering at the Swiss Federal Institute of Technology. In 1948 he joined the RCA Laboratories Division in Princeton, N. J., where he has been engaged in research on traveling-wave tube amplifiers. Dr. Peter is a Member of Sigma Xi and an Associate Member of the Institute of Radio Engineers.

WINTHROP SEELEY PIKE received the B.A. degree in Physics in 1941 from Williams College. He served with U. S. Army Signal Corps during World War II as radar officer and later as project officer in charge of the Signal Corps Moon Radar project. In 1946 he joined the research staff of RCA Laboratories Division at Princeton, N. J., where he has worked on sensory aids for the blind, storage tube applications, color television and industrial television. Mr. Pike is a Member of the Institute of Radio Engineers, Sigma Xi, and the American Guild of Organists.

LOUIS M. SEEBERGER received the B.S. degree in Electrical Engineering from the University of California at Berkeley in 1943. From 1942 to 1943 he was employed by the Alameda County Sheriff's office as an operator and maintenance engineer for KPDA. From 1943 to 1945 he was a member of the Signal Corps, U. S. Army and was commissioned in 1944. As a radar officer, he attended the Harvard Graduate School and the Massachusetts Institute of Technology from 1944 to 1945. In 1946 he joined the Radio Corporation of America and participated in the development of the Teleran System of Air Navigation. Since 1948, he has been engaged in advanced circuit development for the Graphechon storage tube as a member of the Advanced Development Section of the Engineering Products Department. Mr. Seeberger is an Associate Member of the Institute of Radio Engineers.

ROLAND W. SMITH received the B.S. degree from Western Kentucky State College in 1939, and the M.S. degree in Physics from Northwestern University in 1942. He was with the Central Scientific Company in Chicago during the period 1939-1940. From 1942 to 1947 he did research in photoconductors at Northwestern for the Office of Scientific Research and Development. In 1947 he joined the Research Department of RCA Laboratories Division at Princeton, N. J. Mr. Smith is a Member of the American Physical Society and Sigma Xi.

WILLIAM M. WEBSTER studied physics at Rensselaer Polytechnic Institute and at Union College as a Navy V-12 student. He received a B.S. degree in physics in 1945. He was released from active duty in 1946 and joined the RCA Laboratories Division, Princeton, in October of that year. He is currently enrolled in the Graduate School of Princeton University on a part-time basis. Mr. Webster is an associate member of the Institute of Radio Engineers.